

Utah State University

DigitalCommons@USU

All Graduate Theses and Dissertations

Graduate Studies

5-2014

Electron Transfer and Substrate Reduction in Nitrogenase

Karamatullah Danyal
Utah State University

Follow this and additional works at: <https://digitalcommons.usu.edu/etd>



Part of the [Biochemistry Commons](#)

Recommended Citation

Danyal, Karamatullah, "Electron Transfer and Substrate Reduction in Nitrogenase" (2014). *All Graduate Theses and Dissertations*. 2181.

<https://digitalcommons.usu.edu/etd/2181>

This Dissertation is brought to you for free and open access by the Graduate Studies at DigitalCommons@USU. It has been accepted for inclusion in All Graduate Theses and Dissertations by an authorized administrator of DigitalCommons@USU. For more information, please contact digitalcommons@usu.edu.



ELECTRON TRANSFER AND SUBSTRATE REDUCTON IN NITROGENASE

by

Karamatullah Danyal

A dissertation submitted in partial fulfillment
of the requirements for the degree

of

DOCTOR OF PHILOSOPHY

in

Biochemistry

Approved:

Lance C. Seefeldt
Major Professor

Scott A. Ensign
Committee Member

Alvan C. Hengge
Committee Member

Sean J. Johnson
Committee Member

Korry Hintze
Committee Member

Mark R. McLellan
Vice President for Research and
Dean of the School of Graduate Studies

UTAH STATE UNIVERSITY

Logan, Utah

2014

Copyright © Karamatullah Danyal 2014
All Rights Reserved

ABSTRACT

Electron Transfer and Substrate Reduction in Nitrogenase

by

Karamatullah Danyal, Doctor of Philosophy

Utah State University, 2014

Major Professor: Dr. Lance C. Seefeldt
Department: Chemistry and Biochemistry

Population growth over the past ~50 years accompanied by the changes in dietary habits due to economic growth have markedly increased the demand for fixed nitrogen. Aided by biological nitrogen fixation, the Haber-Bosch process has been able to fulfill these demands. However, due to its high temperature and pressure requirements, Haber-Bosch is an expensive process. Every year, approximately 2% of the total energy expenditure by man is used to manufacture fixed nitrogen. Biological systems, on the other hand, produce ammonia at ambient temperature and pressure with much higher efficiency than the Haber-Bosch process. Research in the field of biological nitrogen fixation could prove valuable in understanding the mechanism of the enzyme responsible, nitrogenase. This could eventually allow researchers to mimic the enzyme and fix nitrogen at standard temperature and pressure, which would lead to greater availability of fixed nitrogen and a better standard of living for mankind.

As part of this research, nitrogenase of *Azotobacter vinelandii* was studied to understand the order of events in reduction of substrates and the conformational changes in the enzyme responsible for its ability to reduce said substrates at room temperature and pressure. This knowledge was used to study variant forms of nitrogenase that could be activated using controlled external reductants. This freedom from the biological reductant of nitrogenase opens the door for further research into the understanding and development of enzyme mimics that can reduce substrates at room temperature and pressure.

(191 pages)

PUBLIC ABSTRACT

Electron Transfer and Substrate Reduction in Nitrogenase

by

Karamatullah Danyal, Doctor of Philosophy

Utah State University, 2014

Major Professor: Dr. Lance C. Seefeldt
Department: Chemistry and Biochemistry

The reduction of nitrogen to ammonia by the industrial Haber-Bosch process is considered one of the major scientific breakthroughs of the last century. It is considered to be responsible for approximately one third of the world's current population. This growth over the past 50 or so years accompanied by the changes in dietary habits due to economic growth have markedly increased the demand for fixed nitrogen in the form of fertilizer. The Haber-Bosch process and biological nitrogen fixation has been able to fulfil this demand. However, this industrial process is costly due to its high temperature and pressure requirements. Every year, approximately 2% of the total global energy is used to manufacture fixed nitrogen (ammonia). Microorganisms like the diazotrophs though, can fix nitrogen at a fraction of the cost. Research in the field of biological nitrogen fixation could prove valuable in understanding the mechanism of the enzyme responsible, nitrogenase which could eventually allow researchers to mimic the enzyme

and fix nitrogen at room temperature and pressure. In the current climate of energy awareness, this should be a high priority.

Nitrogenase, the enzyme responsible for nitrogen fixation in nature, has two component proteins that associate and dissociate multiple times to reduce nitrogen. This was studied to understand the order of events in association and dissociation such as; electron transfer, ATP hydrolysis, and phosphate release. When the two components associate, they induce movements within the enzyme complex. These movements, called conformational changes, are responsible for the ability of the enzyme to reduce nitrogen at room temperature and pressure. The conformational changes, and their effect on the reduction of substrates was also studied. This knowledge was used to find and study modified forms of one half of nitrogenase that could be activated using controlled external reductants. This freedom from the association and dissociation events opens the door for further research into the understanding and development of enzyme mimics that can reduce substrates at room temperature and pressure.

ACKNOWLEDGMENTS

I would like to thank first and foremost my loved ones. Mom and Dad (Ammi and Abbu) for being an inspiration in both the desire to learn and the work ethic that goes hand in hand with this desire. Also for the constant unwavering support and love that you have provided me throughout my life. Listening to me whine about an enzyme that you didn't know much about and reminding me that all I can do is my best and even if I don't achieve that I still have your love. My wife, who seems to be the personification of love and support and patience towards my imbalanced life that leaves less time for her than nitrogenase. Hibba, your love and support have meant everything to me and I stand indebted to you for the rest of my life. I am thankful to my sister Bano and my brothers Anser, Ahsan and Jerry who have always been there to talk with me and brighten my day each and every time. May Allah bless you and yours for all eternity. Finally, I am thankful to the Almighty Allah for granting me my childhood wish of becoming a student of nature and science and blessing me with the best support system in the world in the form of my family.

There are people at work who have been amazing over the past seven years. First and foremost, my professor Dr. Seefeldt, you have been the coolest person to work with. I have loved coming to work, enjoyed every experiment I have done and reveled in the glory of scientific research because of the environment you nurture in your lab. Your support and guidance have always made me better than I was and I hope to maintain this relationship after I leave. My supervisory committee members, I know it can be hard when you have to be on a committee for seven years, but I thank you all for all your help

and guidance and above all your encouragement year round. Thank you all for your open door policy especially Dr. Johnson whom I have constantly bothered with structure related questions over the past seven years.

I would like to thank my friends James, Brad, Simon, Boyd, Kasia, Ashwini, Ameya, Sudipta, Nimesh, AJ and the numerous others that deserve to be thanked. Some of you I worked with, some of you were buddies at or after work. In this group I would like to specially thank James Danford who has been and continues to be my best friend. I would also like to thank Simon Duval for being a great friend to me over the past two years both in the lab and outside. I am lucky to have known and been friends with you all.

Finally, I would like to thank the departmental and university administration (thank you Geri and Margaret) for setting up a great scientific research environment here at Utah State University.

Karamatullah Danyal

CONTENTS

	Page
ABSTRACT.....	iii
PUBLIC ABSTRACT	v
ACKNOWLEDGMENTS	vii
LIST OF FIGURES	xi
ABBREVIATIONS	xv
CHAPTER	
1. INTRODUCTION	1
Iron Protein	5
MoFe Protein	8
Trapping Inhibitors and Substrates on Nitrogenase During Turnover.....	11
MoFe-Fe Protein Complex	20
Iron Protein Cycle	22
MoFe Protein Cycle	28
References.....	30
2. CONFORMATIONAL GATING OF ELECTRON TRANSFER FROM Fe PROTEIN TO MoFe PROTEIN.....	43
Abstract.....	43
References.....	50
3. ELECTRON TRANSFER WITHIN NITROGENASE: EVIDENCE FOR A DEFICIT SPENDING MECHANISM.....	53
Abstract	53
Introduction.....	54
Materials and Methods.....	58
Results.....	60
Discussion.....	68
References.....	77

4.	TEMPERATURE INVARIANCE OF THE NITROGENASE ELECTRON TRANSFER MECHANISM.....	84
	Abstract.....	84
	Introduction.....	85
	Materials and Methods.....	89
	Results and Analysis.....	92
	Discussion.....	102
	References.....	105
	Appendix: Supporting Information.....	110
5.	ELECTRON TRANSFER PRECEDES ATP HYDROLYSIS DURING NITROGENASE CATALYSIS.....	123
	Abstract.....	123
	Introduction.....	124
	Results.....	127
	Discussion.....	132
	Materials and Methods.....	140
	References.....	144
6.	UNCOUPLING NITROGENASE: CATALYTIC REDUCTION OF HYDRAZINE TO AMMONIA BY A MoFe PROTEIN IN THE ABSENCE OF Fe PROTEIN-ATP.....	149
	Abstract.....	149
	References.....	157
7.	SUMMARY AND FUTURE DIRECTIONS	159
	Conformational Changes in Nitrogenase.....	160
	Electron Transfer Event in Nitrogenase.....	169
	Kinetic Isotope Effect in the Fe Protein Cycle	174
	References.....	179
	APPENDIX.....	185
	CURRICULUM VITAE.....	189

LIST OF FIGURES

Figure		Page
1-1	Nitrogen cycle.....	1
1-2	Molybdenum based nitrogenase	3
1-3	Derivative EPR spectra of Fe protein	6
1-4	Nitrogenase complexes	7
1-5	P Cluster of the MoFe protein.....	9
1-6	FeMo-cofactor.....	11
1-7	Derivative EPR spectra of MoFe protein in resting state and during turnover.....	12
1-8	EPR spectra of nitrogenase trapped during reduction of protons and propargyl alcohol.....	13
1-9	EPR spectra of nitrogenase trapped during reduction of acetylene and propargyl alcohol.....	14
1-10	EPR spectra of nitrogenase trapped during reduction of N ₂ , diazene, and hydrazine.....	16
1-11	EPR spectra of nitrogenase trapped during turnover with high and low CO	17
1-12	Alternating (A) vs. distal (D) pathway of N ₂ reduction.....	19
1-13	Movement of the [4Fe-4S] cluster	22
1-14	Electron transfer in nitrogenase	25
1-15	The Fe protein cycle.....	27
1-16	The MoFe protein cycle	29
2-1	Representation of complexes between Fe protein and MoFe protein.....	44
2-2	Stopped-flow oxidation of Fe ^{red} within the [Fe ^{red} (MgATP) ₂ : MoFe] complex	46

2-3	Log of the rate constants for oxidation of Fe^{red} within the $[\text{Fe}^{\text{red}}(\text{MgATP})_2; \text{MoFe}]$ complex as a function of osmolyte concentration.....	48
3-1	Nitrogenase proteins and electron transfer between metal clusters.....	56
3-2	P-cluster in the oxidized and reduced states	58
3-3	Electron transfer from the Fe protein to MoFe proteins monitored by stopped-flow spectroscopy	61
3-4	Electron transfer from Fe protein to MoFe proteins with the nucleotide analog $\beta\gamma$ -methylene ATP	64
3-5	Electron transfer from Fe protein to MoFe proteins with the nucleotide analog MgADP-AlF_4^-	65
3-6	Electron transfer from Fe protein to apo-MoFe proteins	66
3-7	Osmotic pressure effects on electron transfer reactions from Fe protein to MoFe protein	67
3-8	Models for nitrogenase mechanism.....	75
4-1	Events proposed as occurring at the interface of the MoFe protein and the Fe protein as the latter delivers an electron to the former.....	87
4-2	Temperature-response stopped-flow traces for oxidation of Fe^{red} within $[\text{Fe}^{\text{red}}(\text{MgATP})_2; \text{MoFe}]$ complex in H_2O and D_2O buffers	94
4-3	Semi-logarithmic plot of the observed rate constants, k_{obs} for D_2O and H_2O	95
4-4	Temperature dependence of absorbance changes ΔA	97
4-5	Plot of the solute-dependent osmotic effect on nitrogenase	99
4-S1	Mathcad spreadsheet chart.....	111
4-S2	Semi-logarithmic plot of k_{obs} vs. inverse temperature	113
4-S3	Temperature profile of the optical change in the Fe protein in the presence of the MoFe protein.....	114
4-S4	Temperature-response stopped-flow traces for oxidation of Fe^{red} within $[\text{Fe}^{\text{red}}(\text{MgATP})_2; \text{MoFe}]$ complex in HEPES buffer for H_2O and D_2O	115

4-S5	Temperature dependence of absorbance changes ΔA in HEPES buffer	116
4-S6	Temperature dependence of absorbance changes ΔA of truncated traces	117
4-S7	pH dependence of ET kinetic traces for reaction carried out in HEPES at 5°C...118	
4-S8	pH/pD dependence of absorbance changes ΔA , in HEPES buffer at 5°C	119
4-S9	Plot of the solute-dependent osmotic effect on Nitrogenase	120
4-S10	Semi-logarithmic plot of the rate constant vs. inverse temperature for the re-reduction of Fe^{ox} to Fe^{red}	121
4-S11	Temperature dependence of absorbance changes ΔA_{Dr}	122
5-1	Order of events in nitrogenase complex	125
5-2	Kinetics of key nitrogenase catalytic steps	128
5-3	Time course for key steps in nitrogenase cycle	130
5-4	Model of nitrogenase order of events	133
5-5	Thermodynamic Fe-protein cycle	135
6-1	MoFe protein metal clusters and key amino acid residues	151
6-2	Hydrazine reduction to ammonia as a function of time	154
7-1	Osmotic pressure effects on phosphate release.....	161
7-2	$\log k$ vs. molality of 1°ET vs. Pi release	162
7-3	Protein-Protein docking geometries in AMPPCP and ADP bound Fe:MoFe complex.....	163
7-4	Interactions of surface residues between Fe and MoFe protein.....	165
7-5	α -64 ^{Tyr} , β -98 ^{Tyr} , and β -99 ^{Phe} in mesh representation.....	167
7-6	Time course analysis of the reduction of hydrazine to ammonia by α -64 ^{His} , β -98 ^{His} , and β -99 ^{His} variant of the MoFe protein.....	168

7-7	Reduction of hydrazine to ammonia by α -64 ^{His} , β -98 ^{His} , and β -99 ^{His} variant of the MoFe protein with increasing hydrazine concentration.....	169
7-8	Percent maximum EPR signal intensity comparison of P cluster, M cluster, and the [4Fe-4S] cluster of the Fe protein	172
7-9	Lowe-Thorneley model of electron transfer and substrate binding in nitrogenase	173
7-10	VFQ analysis of the early E states in α -195 ^{Gln} MoFe protein.....	175
7-11	Kinetics of key nitrogenase catalytic steps in H ₂ O and D ₂ O at 25°C	177
7-12	VFQ analysis of α -195 ^{Gln} MoFe protein with acetylene in D ₂ O.....	178

ABBREVIATIONS

7-meG	7-methylguanine
^{32}P -ATP	Radioactively labeled ATP on the α phosphate
ADP	Adenosine diphosphate
AMPPCP	$\beta\gamma$ -methylene Adenosine Triphosphate
ATP	Adenosine Triphosphate
Apo-MoFe protein	FeMo-cofactor deficient MoFe protein
DTPA	Diethylene triamine pentaacetic acid
EDTA	Ethylenediaminetetraacetic acid
EGTA	Ethylene glycol tetraacetic acid
E_m	Midpoint potential
E_n	MoFe protein reduced by n electrons (n=1-8)
ENDOR	Electron nuclear double resonance
EPR	Electron paramagnetic resonance
ET	Electron transfer
F cluster	[4Fe-4S] cluster of the iron protein
Fe Protein	Iron protein
FeMo-cofactor	Iron-molybdenum cofactor
HEPES	4-[2-hydroxyethyl]-1-piperazineethanesulfonic acid
K_m	Michaelis constant
k_{Pi}	Rate of phosphate release
k_{ET}	Rate of electron transfer

k_{Diss}	Rate of dissociation
k_{ATP}	Rate of ATP hydrolysis
M cluster	Iron-molybdenum cofactor (FeMo-cofactor)
MDCC	N-[2-(1-maleimidyl) ethyl]-7-(diethylamino) coumarin-3-carboxamide
M^N	FeMo-cofactor in the dithionite reduced state
MOPS	3-(N-morpholino) propanesulfonic acid
MoFe protein	Molybdenum iron protein
M^{OX}	Oxidized FeMo-cofactor
M^R	FeMo-cofactor reduced beyond M^N
NHE	Normal hydrogen electrode
P cluster	[8Fe-8S] cluster of MoFe protein
PBP	Phosphate binding protein
P^{1+}	P cluster in the one electron oxidized state
P^{2+}	P cluster in the two electron oxidized state
P^{3+}	P cluster in the three electron oxidized state
Pi	Inorganic phosphate
P^N	P cluster in the dithionite reduced state
PNPase	Purine nucleoside phosphorylase
P^{ox}	Oxidized P cluster
RFQ	Rapid freeze quench
SDS-PAGE	Sodium dodecyl sulfate polyacrylamide gel electrophoresis
sKIE	secondary kinetic isotope effect

SF	Stopped-flow
UV-Vis	Ultra violet-visible
VFQ	Viscogen freeze quench

CHAPTER 1

INTRODUCTION*

Due to its seemingly endless presence in many biomolecules such as proteins and nucleic acids, the importance of nitrogen (N_2) is undeniable. However, only the reduced form of nitrogen can be used for growth and development of organisms. Consequently, despite its abundance in our atmosphere (~80%), it represents the limiting nutrient for growth.¹ There are many oxidation states of nitrogen (+5 to -3) and the conversion of one state to the other follows a cyclic path known as the nitrogen cycle (**Figure 1-1**).

Nitrogen fixation, the conversion of nitrogen (N_2) to ammonia (NH_3), is of particular interest in nitrogenase research. There are three known ways in which N_2 is converted to NH_3 .

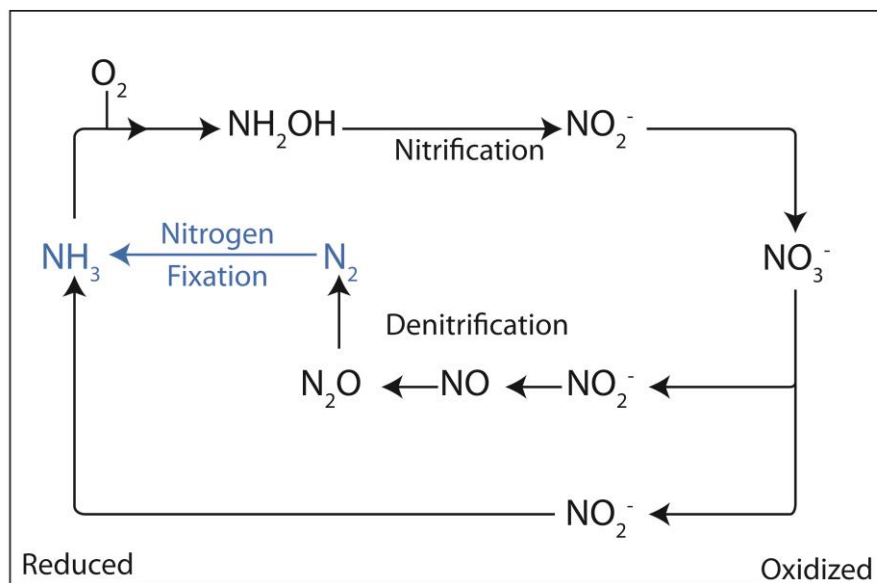


Figure 1-1: Nitrogen Cycle. Nitrogen Fixation (highlighted in blue) is the focus of this research

*Parts of this chapter are coauthored by Karamatullah Danyal, Zhi-Yong Yang, and Lance C. Seefeldt (2011) *Methods Mol. Biol.* 766, 191-205. Copyright 2011 Springer Science and Business Media. Reprinted with permission.

Approximately 1% of the 3×10^{14} gallons of total nitrogen fixed every year comes from lightning strikes². The industrial process developed by Fritz Haber in 1908 and commercialized by Carl Bosch is now used to produce approximately half of the total nitrogen fixed every year.^{3,4} In the Haber-Bosch process hydrogen and nitrogen react at high temperature and pressure ($\sim 450^\circ\text{C}$; 200 atmospheres) over iron based catalysts to produce ammonia for fertilizers.^{5,6} Biological nitrogen fixation by microbes called diazotrophs is responsible for the remainder of the nitrogen fixation on our planet. A common feature in all diazotrophs is the presence of a metalloenzyme responsible for the reduction of nitrogen to ammonia, called nitrogenase (**Figure 1-2**).

Nitrogenase enzymes are classified according to the metal composition of their active site cofactor, which is known to contain molybdenum and iron (MoFe), vanadium and iron (VFe), or iron only (FeFe).^{7,8} Out of these forms of the enzyme, the molybdenum containing enzyme (MoFe), isolated from *Azotobacter vinelandii* is the enzyme of choice for most researchers. This is due to the established behavior of the enzyme and genetic tractability of *Azotobacter vinelandii*. All known nitrogenases include a smaller component protein called dinitrogenase reductase, also known as the iron (Fe) protein.⁹

Until recently the Fe protein was the only known redox active agent with the ability to transfer electrons to the larger component (MoFe protein) in a way that the latter can reduce substrates.¹⁰⁻¹³ It contains a [4Fe-4S] cluster and transfers the electrons to the MoFe protein in a MgATP dependent manner. The MoFe protein contains the P cluster and the M cluster. The P cluster is an [8Fe-7S] metal cluster and is known to be the immediate electron acceptor from the Fe protein. It also serves as an intermediate in

the overall electron transfer from the Fe protein to the MoFe protein (**Figure 1-2**).² The M cluster also known as the FeMo-cofactor is the active site of nitrogenase where substrate binding and reduction occur [7Fe-9S-Mo-C-homocitrate].^{14,15} The general N_2 reduction reaction catalyzed by the Fe-MoFe complex is presented in eq 1:¹⁶

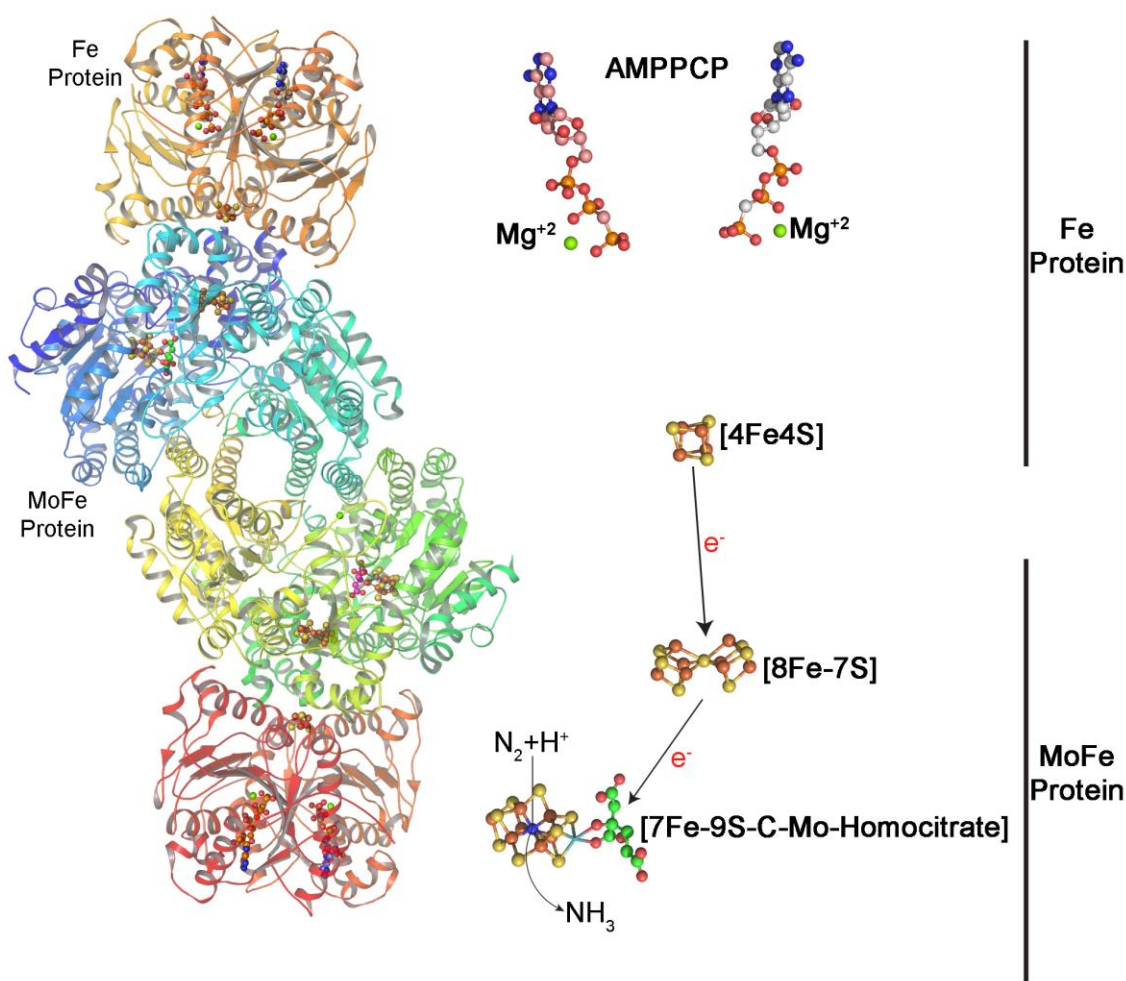


Figure 1-2: Molybdenum based nitrogenase. Representation of MoFe and Fe protein of nitrogenase. (Left) MoFe and Fe protein complex with the two catalytic halves (PDB ID 2AFK). (Right) Clusters of nitrogenase with the direction of electron flow.

The accepted mechanism of nitrogenase enzyme proposes that the Fe protein, in its reduced and MgATP bound state (reduced by ferredoxin), binds to one side ($\alpha\beta$ -unit) of the MoFe protein. The immediate consequence of this binding is the electron transfer and hydrolysis of the two MgATP molecules to two MgADP molecules.^{17,18} The order of the two events is unknown.¹⁹⁻²⁵ Two possible pathways about the electron transfer events have been proposed. In one pathway the binding of the Fe protein to the MoFe protein initiates electron transfer from the Fe protein to the P cluster.²⁶ In the other pathway, however, the binding initiates electron transfer from the P to the M cluster within the MoFe protein followed by the reduction of the P cluster from the Fe protein.²⁷ A distance of approximately 30Å separates the Fe protein [4Fe-4S] cluster and FeMo-cofactor.²⁸ The P cluster acts as a mediator in the electron transfer pathway and transfers electrons to the FeMo-cofactor.

It has now been nearly twenty years since the structure of the molybdenum containing nitrogenase was solved.^{28,29} This was followed by structures of many variants of nitrogenase.³⁰⁻³² Important information such as the positions of the clusters inside the protein as well as their arrangement and interactions with the protein, was obtained due to these efforts. These structures have, however, re-emphasized several key questions about the enzyme, some of which have been the main target of my research. In the remainder of this chapter we will take a greater look at the two protein components in nitrogenase, the role of nucleotides in electron transfer, and substrate binding and reduction on the enzyme in the presence of the Fe protein.

Iron Protein:

The homodimeric Fe protein of nitrogenase is the most common redox-active agent that can transfer electrons to the MoFe protein for substrate reduction and is the only reductant for substrate reduction to the wild-type/unaltered MoFe protein.⁹ This protein is also important in the biosynthesis and insertion of FeMo-cofactor as well as the maturation of the P cluster into an [8Fe-7S] cluster from two [4Fe-4S] clusters.³³

Binding of one ATP to each monomer of the Fe protein prior to complex formation and electron transfer is required for the two events to occur. The two ATP molecules bind to the Fe protein sequentially with the second ATP binding with higher affinity due to cooperative binding.^{34,35} Binding of MgATP to the Fe protein causes the E_m for the [4Fe-4S]^{2+/1+} redox couple to shift by -120 mV from -300 mV to -420 mV.^{36,37} The same potential change occurs when the Fe protein binds MgADP though no electron transfer to the MoFe protein takes place.

Upon binding MgATP, the Fe protein undergoes conformational changes.³⁸ The major consequence of these conformational changes is the outwardly movement of the [4Fe-4S] cluster by ~5 Å. The movement of this iron sulfur cluster ligated by four cysteine residues allows for a distance shortening between it and the P cluster of the MoFe protein.²⁸

The Fe protein [4Fe-4S] cluster is paramagnetic in the as-isolated state in the presence of dithionite and is in the 1+ oxidation state with 3Fe²⁺ and 1Fe³⁺.³⁹⁻⁴¹ In this oxidation state, the [4Fe-4S] cluster exhibits a mixed spin state with an S = 1/2 and S = 3/2 (**Figure 1-3**). This results in an EPR spectrum with features centered in the g = 2 region and g = 4.3 region. The g = 2 (S=1/2) region signal is rhombic in lineshape, with

g values of 2.04, 1.94, and 1.89 while the $S = 3/2$ signal has inflections around $g \approx 5$.³⁹

The proportions of the two spin states can be changed by the addition of either glycerol or urea to the sample prior to freezing.³⁹ Adding glycerol shifts the spin equilibrium in favor of $S = 1/2$, while adding urea shifts the spin equilibrium in favor of $S = 3/2$.⁴²

The addition of nucleotides (MgATP or MgADP) change the lineshape of the $[4\text{Fe-4S}]^{1+}$ EPR spectrum. Adding MgADP results in subtle changes to the lineshape, whereas adding MgATP results in a shift in the lineshape from rhombic to largely axial (**Figure 1-3**).^{43,44}

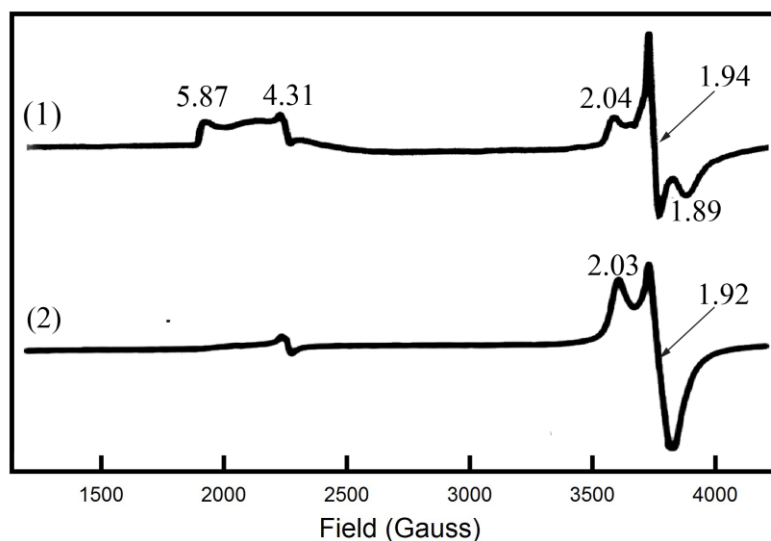


Figure 1-3: Derivative EPR spectra of Fe protein. Trace 1 shows the EPR spectrum of Fe protein ($70 \mu\text{M}$) in the as-isolated state. Spectral conditions were 9.44 GHz microwave frequency, 1.26 modulation amplitude, and 15 mW microwave power at 12 K. Trace 2 shows the Fe protein in the presence of MgATP (7.5 mM) under the same spectra conditions as trace 1.

The oxidized $[4\text{Fe-4S}]^{2+}$ cluster is diamagnetic and therefore is silent in the EPR.⁴⁵ The 1+ oxidation state can be reduced to an all ferrous state (0 oxidation state) by

treating the Fe protein with low potential electron mediators like Ti-citrate or reduced flavodoxin.⁴⁶⁻⁴⁸ The $[4\text{Fe-4S}]^0$ state has 4Fe^{2+} , and a spin $S = 4$ state that can be observed in the parallel mode of an EPR spectrometer. The parallel mode spectrum shows a single inflection centered at $g = 16.4$.⁴⁶⁻⁴⁸

Complex formation between Fe and MoFe protein leads to ATP hydrolysis, electron transfer, phosphate release and the eventual dissociation of the Fe protein from the MoFe protein.^{10,49} Crystallographic evidence supports the Fe protein rolling over the surface of the MoFe protein during these events (**Figure 1-4**).²⁹ During these movements the $[4\text{Fe-4S}]$ cluster of the Fe protein moves towards and eventually away from the MoFe protein. This implies that conformational changes are taking place while Fe and MoFe protein are in complex. This is supported by the change in EPR signal of the Fe protein upon binding with 2MgATP molecules from rhombic to axial.⁴³ Further support for the rolling motion is presented in chapters 2,3,4 and 7 where these conformational changes have been studied for the different events in the iron protein cycle.

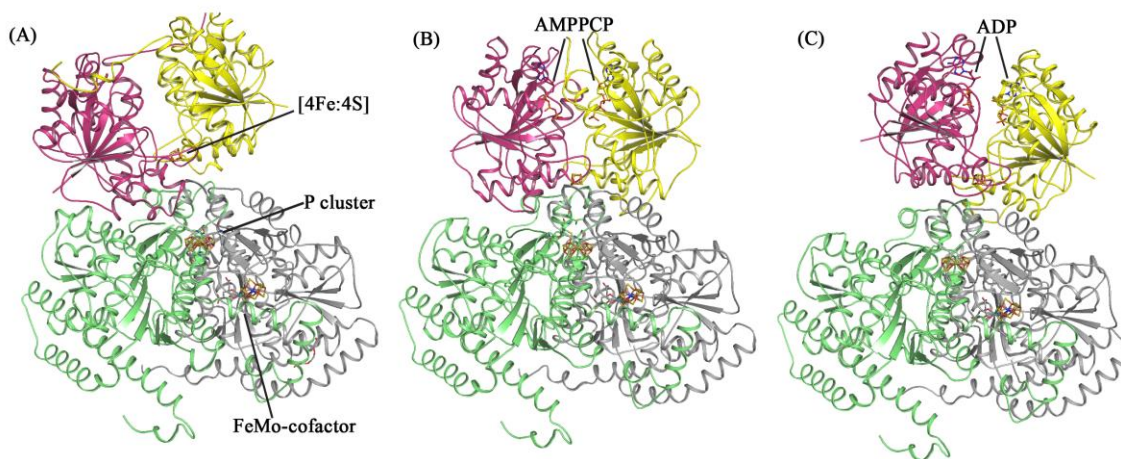
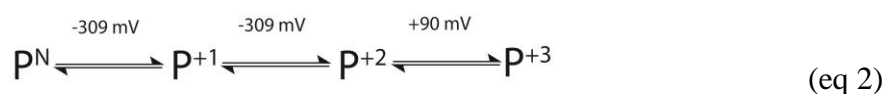


Figure 1-4: Nitrogenase complexes. Representation of the Fe protein in complex with the MoFe protein under differing conditions: (A) nucleotide free (PDB ID 2AFH), (B) $\beta\gamma$ -methylene ATP bound (PDB ID 2AFK), and (C) ADP bound form (PDB ID 2AFI).²⁹

MoFe protein

The $\alpha_2\beta_2$ heterotetrameric MoFe protein with two catalytic halves contains a P cluster and an M cluster in each half. From the X-ray crystal structure of nitrogenase complexed with the Fe protein (PDB ID 1G21) we know that the P cluster (**Figure 1-5**) lies between the M cluster and the Fe protein (**Figure 1-2**).^{28,50} This represents the strongest evidence for the argument that the P cluster behaves as a capacitor that receives and stores the electrons from the Fe protein and donates them to the M cluster. A general lack of direct evidence demonstrating redox changes in the P cluster during catalysis has hindered the proper assignment of the redox role of the P cluster. Therefore, a conclusive statement about the order of transfer of electrons could not be made. Some redox properties of the P cluster, such as its different oxidation states, are known.⁵¹⁻⁵³ It is also known that the P cluster undergoes conformational changes upon chemical oxidation to the P^{ox} state.³⁰ As determined by Mössbauer spectroscopy, under dithionite reduced conditions, the P cluster is an all ferrous iron sulfur cluster. This is known as the P^N state of the P cluster (eq 2).^{54,55}



A suggested P^R state (1e⁻ reduction beyond the P^N state) has never been observed. This is consistent with all Fe atoms being in the ferrous state in P^N . The P^N state, under the influence of the midpoint potentials of different mediators, can be oxidized sequentially to the P^{+1} , P^{+2} , and the P^{+3} oxidation state.⁵¹⁻⁵³ Since it is not possible to reverse the P^{+3} state to P^{+2} in vitro, it is assumed that this state is biologically irrelevant. This has led researchers to propose an electron transfer model involving only the $P^{+1/N}$ and the $P^{+2/+1}$ redox couple. These two redox couples of the P cluster transfer either 1e⁻ or

$2e^-$ from the P cluster to the M cluster. The P^N state is EPR silent, while the P^{+1} and the P^{+2} states are EPR active. As described above the P cluster can be oxidized from the resting state to three additional states called P^{1+} , P^{2+} , and P^{3+} . The P^{+1} state is a mixed spin system of $S = 1/2$ and $S = 5/2$, with a rhombic signal with $g = 2.06, 1.95,$ and 1.82 and minor inflections at $g = 6.67$ and 5.3 . The P^{2+} oxidation state does not have a signal in perpendicular mode EPR. It has a parallel mode signal with $g = 11.8$. This is due to a non-Kramer system integer spin $S \geq 3$. The P^{3+} oxidation state has a mixed spin $S = 7/2$ and $S = 1/2$ state with a signal with $g = 2.0$, and signals at $g = 10.4$ and 7.2 .^{53,56} Even though the P^{+1} and P^{+2} states of the P cluster are paramagnetic, they have proven to be difficult to observe in nitrogenase turnover samples. This has led to a general lack of knowledge about the role of the P cluster during enzyme turnover.

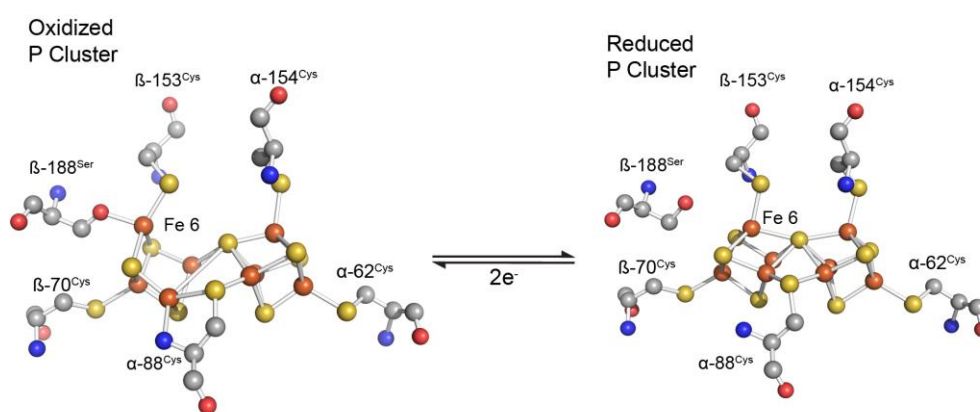


Figure 1-5: P cluster of the MoFe protein. The reduced form of the P cluster (right) shows the structure of the P cluster [8Fe-7S] intact with ligands such as $\alpha\text{-}62^{\text{Cys}}$, $\alpha\text{-}88^{\text{Cys}}$, $\alpha\text{-}154^{\text{Cys}}$, and $\beta\text{-}153^{\text{Cys}}$, $\beta\text{-}70^{\text{Cys}}$ bound to the P cluster. $\beta\text{-}188^{\text{Ser}}$ is also shown with the reduced P cluster. The oxidized P cluster (left) shows the conformational changes that the P cluster goes through upon oxidation. The Fe 6 of the P cluster moves away from the S1 by $\sim 1 \text{ \AA}$ and binds to the $\beta\text{-}188^{\text{Ser}}$. The $\alpha\text{-}88^{\text{Cys}}$ backbone nitrogen ligates with the Fe 5 of the P cluster as well. These newly formed ligations stabilize the new oxidation state of the cluster.

Two models for the role of the P cluster in nitrogenase catalysis can be hypothesized. One in which the Fe protein donates an electron to the P cluster reducing it beyond its all ferrous state to a super reduced state and the P cluster then reduces the FeMo-cofactor. A second in which upon Fe protein binding, the P cluster, in its P^N state, donates an electron to the M cluster, thereby creating a deficit of electrons in itself. This deficit can then be back-filled by the Fe protein restoring the P^N oxidation state of the P cluster. The deficit spending model also explains the lack of any spectroscopic evidence due to the immediate back-filling by the Fe protein.^{27,57}

The M cluster (also known as FeMo-cofactor) [7Fe-9S-Mo-C-Homocitrate] is composed of two cubane substructures bridged by three sulfides.¹⁵ One of the two sub-clusters is a [4Fe-4S] cluster while the other is a [3Fe-4S-Mo] cluster. The homocitrate is bound to the molybdenum atom via two oxo ligands. The cofactor is bound to the protein by α -442^{His} and α -275^{Cys} via the molybdenum and iron(**Figure 1-6**).¹⁴

The FeMo-cofactor is the active site in nitrogenase where substrate reduction takes place.¹⁰ It can be reduced beyond the resting state when the Fe protein binds in the presence of ATP. The M^N cluster is reduced to the M^R state (**Figure 1-7**), which is an integer spin $S \geq 1$ EPR silent, diamagnetic state.⁵⁸ As the electron transfer from the Fe protein to the MoFe protein is not synchronized, it is likely that the M^R state contains more than one oxidation state of the FeMo-cofactor. The P-cluster remains silent under turnover conditions, consistent with it remaining in the P^N , EPR silent state.⁵⁹

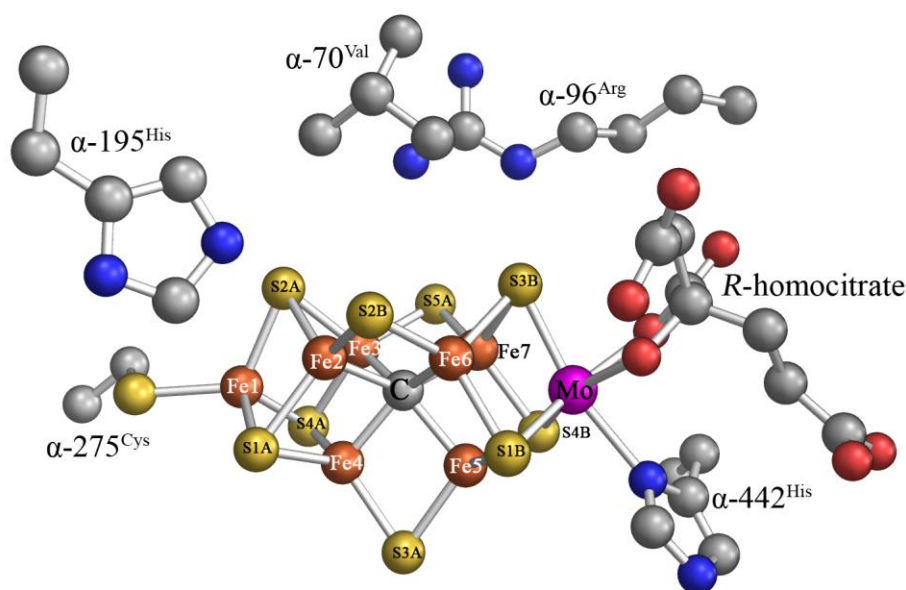


Figure 1-6: FeMo-cofactor. Structure of the FeMo-cofactor with *R*-homocitrate and α -70^{Val}, α -96^{Arg}, α -195^{His}, α -275^{Cys}, α -442^{His} amino acids. The individual atoms of the cofactor are labeled.

Trapping inhibitors and substrates on nitrogenase during turnover.

The EPR spectrum of the M cluster in the resting state of the MoFe protein does not show any changes upon addition of substrates or inhibitors, indicating a lack of changes to the redox state or electronic properties of the M-cluster or P cluster which has been interpreted as a lack of binding of these compounds to the M^N oxidation state.⁶⁰ Under turnover conditions, with the M cluster reduced to the M^R state, it is possible to trap a number of different substrates and inhibitors on FeMo-cofactor, yielding a substrate-FeMo-cofactor complex that is EPR active.^{61,62} Given that only paramagnetic states can be observed, these trapped states must arise from FeMo-cofactor in the M^N oxidation state or even number of electron reduced states.⁶³ Turnover conditions require

both Fe protein and MoFe protein, ATP, $MgCl_2$, an ATP-regeneration system, and the substrate that is being trapped under anaerobic conditions. The ATP regeneration system commonly used includes phosphocreatine and creatine phosphokinase. Following mixing of all of the components, the samples are frozen in liquid nitrogen.

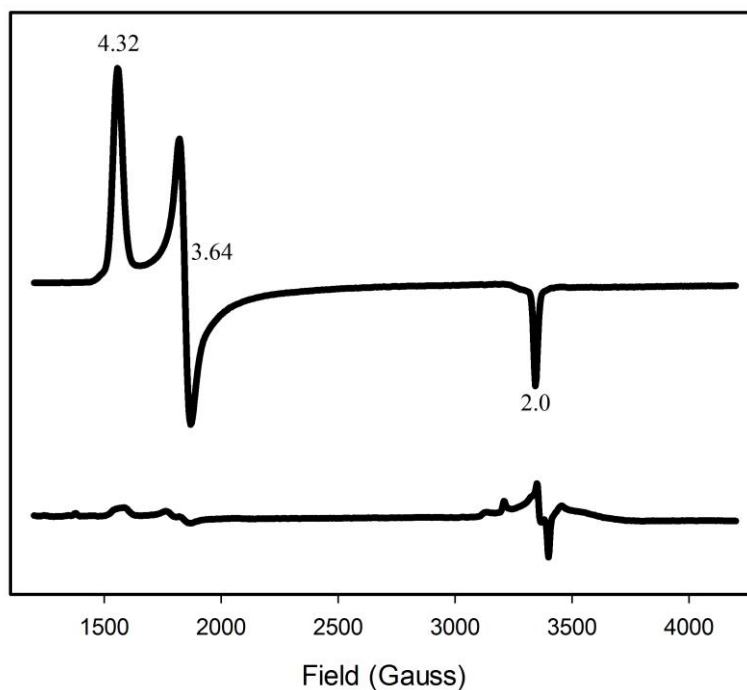


Figure 1-7: Derivative EPR spectra of MoFe protein in resting state and during turnover. Trace 1 shows the EPR spectrum of the MoFe protein ($50\mu M$) in its as-isolated state. Spectral conditions were 9.65 GHz microwave frequency, 1.26 modulation amplitude, and 1.0 mW microwave power at 4.8 K. Trace 2 shows the EPR spectrum of MoFe protein ($50\mu M$) and Fe protein ($70\mu M$) during turnover (30 seconds of turnover prior to freeze quenching the sample) under the same spectral conditions.

Proton. Protons can be trapped bound to FeMo-cofactor in the wild-type MoFe protein, but the EPR signals are of low intensity.⁶⁴ If the valine at position α -70 is

substituted by an isoleucine, a much stronger EPR signal is observed (**Figure 1-8**, trace 1).⁶⁵ The new rhombic signal arises from an $S = 1/2$ spin state of FeMo-cofactor, with g values of (2.14, 2.00, 1.96). This state is trapped for the MoFe protein under steady-state turnover in argon atmosphere. Use of ^1H and ^2H ENDOR spectroscopy reveals that the bound intermediate is associated with one or more Fe atoms and likely represents two bound hydrides. More recent analysis using ^{95}Mo has revealed that the intermediate is not bound to Mo, but rather to one or more Fe atoms.^{65,66}

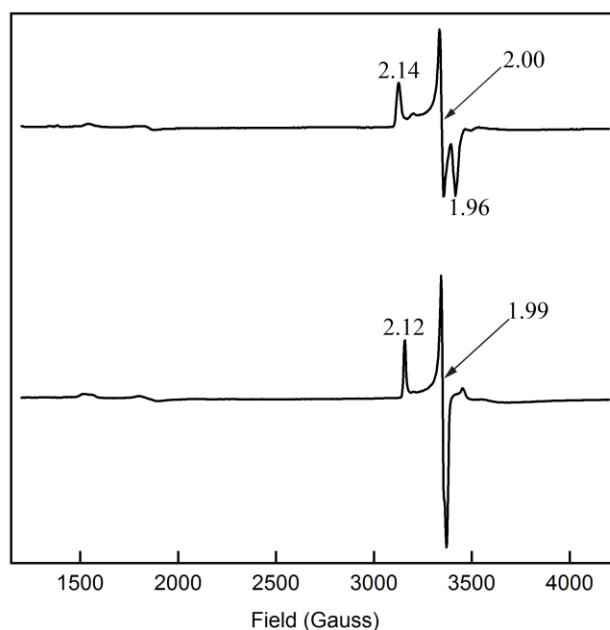


Figure 1-8: EPR spectra of nitrogenase trapped during reduction of protons and propargyl alcohol. The top trace shows the EPR spectrum of the α -70^{lle} MoFe protein trapped during proton reduction. Turnover was created by mixing 100 μM MoFe protein with 50 μM Fe protein with MgATP and a MgATP regeneration system. Spectral conditions were 9.65 GHz microwave frequency, 1.26 modulation amplitude, and 2 mW microwave power at 8 K. The lower trace shows the α -70^{Ala} MoFe protein trapped during turnover with propargyl alcohol. Spectral conditions were 9.64 GHz microwave frequency, 2.0 mW microwave power, and 1.26 mT modulation amplitude at 5 K.

Alkynes. The non-physiological substrate propargyl alcohol ($\text{HC}\equiv\text{C}-\text{CH}_2\text{OH}$) is reduced to allyl alcohol ($\text{H}_2\text{C}=\text{CH}-\text{CH}_2\text{OH}$) in the α -70^{Val-Ala} and α -70^{Val-Thr} variant MoFe protein.⁶⁷ When trapped during turnover with propargyl alcohol, a new $S = 1/2$ spin state spectrum is observed (**Figure 1-8**, trace 2)(**Figure 1-9**, trace 1). Other non biological and alkyne substrates have also been trapped on FeMo-cofactor (e.g., CS_2 and acetylene (**Figure 1-9**, trace 2)).^{68,69}

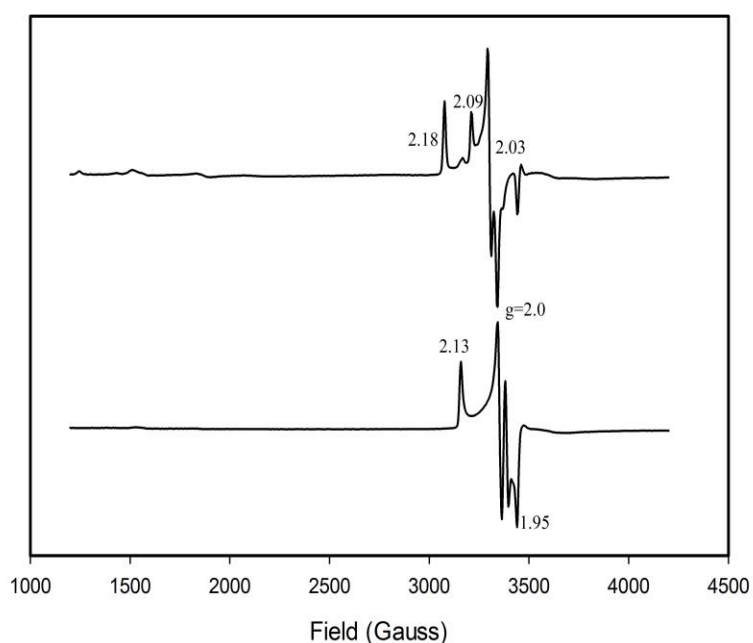


Figure 1-9: EPR spectra of nitrogenase trapped during reduction of acetylene and propargyl alcohol. The top trace shows the EPR spectrum of the α -70^{Thr} MoFe protein trapped during propargyl alcohol reduction. Turnover was created by mixing 50 μM MoFe protein with 50 μM Fe protein with MgATP and a MgATP regeneration system. Spectral conditions were 9.64 GHz microwave frequency, 1.26 modulation amplitude, and 2 mW microwave power at 4.8 K. The lower trace shows the α -195^{Gln} MoFe protein trapped during turnover with acetylene. Spectral conditions were 9.65 GHz microwave frequency, 2.0 mW microwave power, and 1.26 mT modulation amplitude at 8 K.

Dinitrogen. An intermediate derived from N_2 can be trapped on the wild-type MoFe protein.^{70,71} This is achieved by mixing Fe and MoFe protein (with an ATP regeneration system) with a full atmosphere of N_2 and allowing a steady-state to be achieved before rapidly freezing in a liquid N_2 frozen slurry of hexane. The trapped state reveals a novel $S = 1/2$ EPR spectra with g values 2.08, 1.99, 1.97 (**Figure 1-10**, trace 1).^{70,71} $^{14}N_2$ and $^{15}N_2$ have been used as substrates coupled with the appropriate ENDOR spectroscopy to show that the N derived from N_2 is bound to FeMo-cofactor in this trapped state. The presence of a second N atom has not been confirmed, but the current model is for this intermediate to represent an N_2 bound end-on to one or more Fe atoms of FeMo-cofactor.⁷⁰

Diazene. The stepwise reduction of a N_2 bound to FeMo-cofactor is proposed to proceed through a partially reduced intermediate at the level of reduction of diazene ($HN=NH$).^{72,73} Diazene can be reduced by nitrogenase and can be trapped bound to FeMo-cofactor.⁷⁴ Both the wild-type and α -195^{Gln} MoFe protein can be trapped under turnover conditions with diazene or methyldiazene by rapidly freezing 30 s after initiating the reaction. In the wild-type protein, the signal is similar to the N_2 wild-type bound state with $g = 2.06$, and 1.98 with a minor inflection at $g = 4.25$ (**Figure 1-10**, trace 2). On the other hand, in the α -70^{Ala}/ α -195^{Gln} variant of the MoFe protein, the diazene trapped state shows an $S = 1/2$ spin state with $g = 2.07$ and 2.01. (**Figure 1-10**, trace 3).^{74,75}

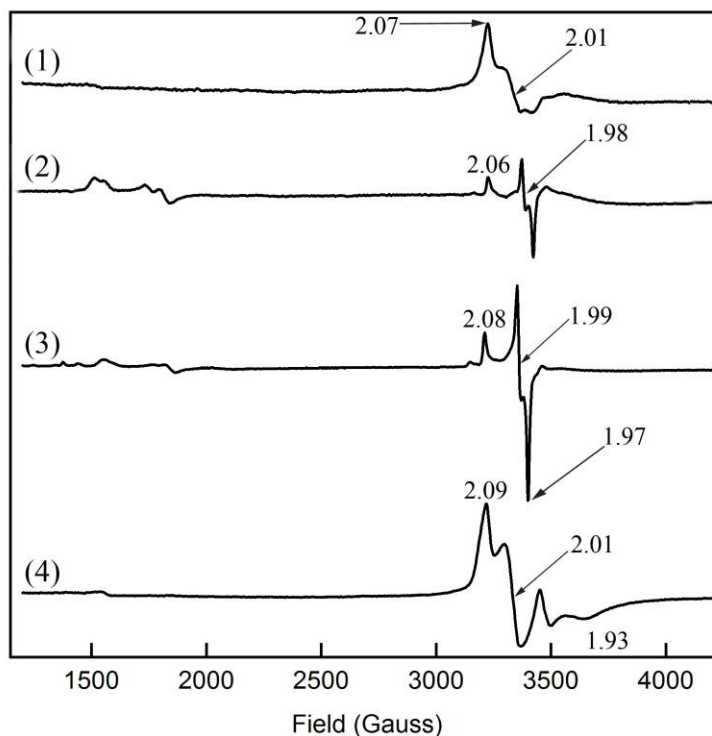


Figure 1-10: EPR spectra of nitrogenase trapped during reduction of N_2 , diazene, and hydrazine. Trace 1 shows the wild type MoFe protein trapped during turnover with 1 atm of N_2 . Spectral conditions were 9.65 GHz microwave frequency, 1.26 modulation amplitude, and 1 mW microwave power at 4.7 K. Trace 2 shows the wild-type MoFe protein trapped during turnover with diazene, while trace 3 shows the α -70^{Ala}/ α -195^{Gln} MoFe protein trapped during turnover with diazene. Trace 4 shows the α -70^{Ala}/ α -195^{Gln} MoFe trapped during turnover with hydrazine. In all cases, turnover conditions were achieved with 75 μ M MoFe protein, 50 μ M Fe protein, and MgATP including a regenerating system. Spectral conditions were 9.65 GHz microwave frequency, 1.26 modulation amplitude, and 20 mW microwave power at 8 K.

Hydrazine. Hydrazine (H_2N-NH_2) is a substrate for nitrogenase, being reduced to two ammonia molecules.⁷⁶ It is proposed that during the reduction of N_2 , an intermediate

is bound to FeMo-cofactor that is at the level of reduction of hydrazine.⁷⁷ It is possible to trap a hydrazine derived intermediate on FeMo-cofactor. This is best achieved in a MoFe protein variant with the α -195^{His} substituted by a glutamine. Trapping this variant MoFe protein during steady-state turnover with 50 mM hydrazine by rapidly freezing results in a $S = 1/2$ spin state with EPR signals at $g = 2.09, 2.01,$ and 1.93 . The intensity of the signals can be increased by also substituting the α -70^{Val} by an alanine in the α -195^{Gln} background (**Figure 1-10**, trace 4).⁷⁸

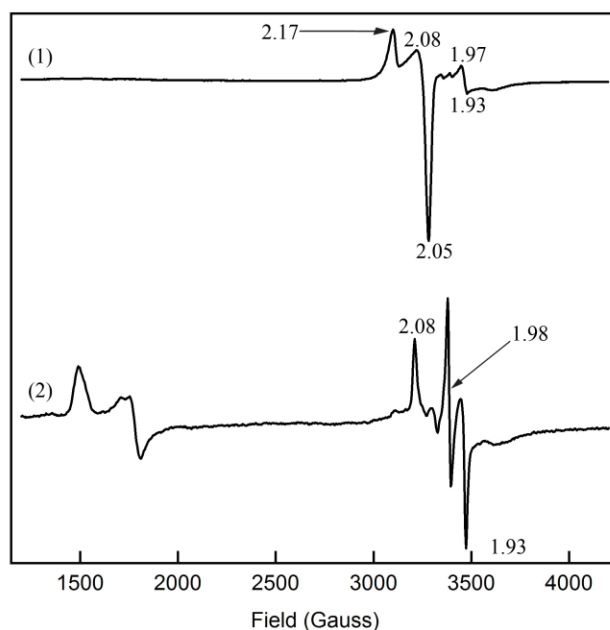


Figure 1-11: EPR spectra of nitrogenase trapped during turnover with high and low CO. Trace 1 shows the Hi-CO EPR signal observed when MoFe protein (50 μ M) and Fe protein (40 μ M) are trapped during turnover under 0.5 atm CO. Trace 2 shows the Lo-CO EPR signal when nitrogenase is trapped under turnover with 0.08 atm CO. Analysis was conducted at 9.44 GHz microwave frequency, 1 mW microwave power, and 0.84 mT (8.4 G) modulation amplitude at 12.8 K for the Hi-CO while the Lo-CO sample was obtained at 9.44GHz microwave frequency, 20mW microwave power and 0.84mT (8.4 G) modulation amplitude at 13 K.

Carbon monoxide. The inhibitor CO can also be trapped bound to FeMo-cofactor.⁶⁰ Two known signals for the binding of CO to the FeMo-cofactor have been observed.^{79,80} One signal (**Figure 1-11**, trace 1) is known as the hi-CO signal since it is achieved at 0.5 atm or higher partial pressure of CO, while the other signal is known as the lo-CO signal (**Figure 1-11**, trace 2) since it is trapped under lower CO concentrations (0.08 atm partial pressure of CO).^{80,81} The hi-CO signal has been assigned to two CO molecules bound to FeMo-cofactor, while the lo-CO signal has been assigned to one CO molecule bound.⁶⁰ The hi-CO signal exhibits an axial EPR signal with $g = 2.17, 2.06$, while the lo-CO sample exhibits a rhombic EPR signal with $g = 2.09, 1.97, 1.93$.⁸⁰

During catalysis of N_2 to ammonia, the MoFe protein of nitrogenase goes through eight separate electron reductions by the Fe protein (eight iron protein cycles).⁴⁹ Different substrates bind at different electronic states (E states) and get reduced by the enzyme.⁸² Nitrogen reduction begins at the E_4 state and results in the first ammonia molecule being produced at E_7 and the second one being produced at E_8 .⁸²

The turnover trapped states of nitrogenase have had a tremendous impact on our understanding of the reduction of substrates on the enzyme. By trapping the turnover trapped states of diazene, hydrazine and dinitrogen and evaluating the electronic states of the cofactors it can be stated that during its reduction of nitrogen, nitrogenase undergoes an alternating mechanism in which intermediates such as diazene and hydrazine are produced (**Figure 1-12**).^{60,65,70,71,74,78,81}

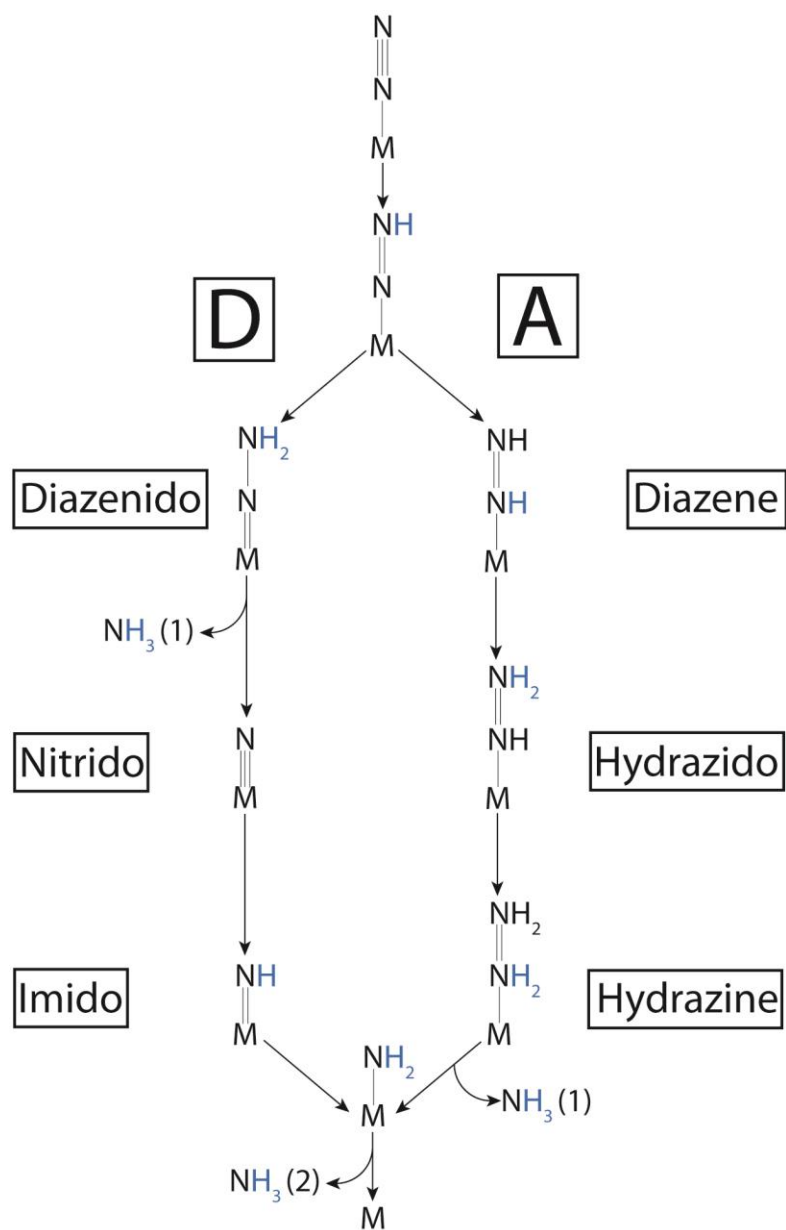


Figure 1-12: Alternating (A) vs. distal (D) pathway of N_2 reduction. Here M specifies FeMo-cofactor (No individual metals are specified). Straight arrows indicate the addition of H^+/e^- to the substrates.⁸²

MoFe-Fe Protein Complex

The initiation of nitrogenase catalytic cycle (docking of Fe protein to the MoFe protein) is followed by a series of events of which only a few are known and understood.¹⁰ From studies conducted by examining the effects of salts on the formation of Fe-MoFe complex and from the use of cross-linking agents, important interface residues were identified.^{2,83-86} These residues play a role in the docking of the Fe protein to the MoFe protein. These studies also provided evidence for the interface residues on the Fe protein being near the [4Fe-4S] cluster.^{84,85} The nitrogenase enzyme complex forms transiently between the MoFe protein and the Fe protein. X-ray crystallography has revealed structures for the Fe-MoFe complex nucleotide free and with MgADP, β,γ -Methylene adenosine 5'-triphosphate, and MgADP+AlF₄ bound to the Fe protein.²⁹ The 127^{Leu- Δ} variant of the Fe protein binds to the MoFe protein in the absence of any nucleotides and creates a stable and tight complex. This Fe protein is capable of binding ATP though does not hydrolyze it. This has allowed the examination of many properties of the complex. When the 127^{Leu- Δ} protein is in complex with the MoFe protein, the E_m of its [4Fe-4S] cluster changes by a value of -200mV resulting in a reduction potential of -620 mV. Nitrogenase complex structures of the 127^{Leu- Δ} Fe protein both in the presence and absence of ATP have been obtained. The P cluster's E_m is shifted by -80 mV in complex. Similar E_m shift has been observed in the [Fe₂MgADP+AlF₄]:[MoFe] complex as well.^{28,37}

The crystal structure of the 127^{Leu- Δ} variant of the Fe protein in complex with MoFe protein in the presence of ATP has been obtained. When the Fe protein from this complex is compared to the crystal structure of as-isolated Fe protein many details about

the nature of the changes in the Fe protein in complex become evident. The comparison of the two structures shows that significant conformational changes are observed in the switch I and II regions (segments of Fe protein homologous to other nucleotide binding protein e.g. Ras P-21 and myosin) of the Fe protein.¹⁷ This movement in the switch I and II regions of the Fe protein results in the forward movement of the [4Fe-4S] cluster towards the P cluster. Though these movements observed in complex cannot be specified to only the binding of ATP they inform us of possible changes occurring during the electron transfer event.²⁸

The nucleotide free, β,γ -Methylene adenosine 5'-triphosphate, and MgADP+AlF₄ bound complex crystal structures show the extent of the conformational changes and the motion of the Fe protein over the surface of the MoFe protein (**Figure1-13**).^{29,50} The overall area of this rolling motion of Fe protein over the surface of the MoFe protein has an area of $\sim 2000 \text{ \AA}^2$. During this motion the Fe protein hydrolyses the ATP, transfers the electron and dissociates from the MoFe protein after releasing the phosphate. The [4Fe-4S] cluster of the Fe protein moves towards and eventually away from the P cluster of the MoFe protein. (**Figures 1-5 and 1-13**).

The [4Fe-4S] cluster of the Fe protein is situated away from the P cluster when there are no nucleotides bound to it. It moves closer and occupies almost the same position in both the AMPPCP and the ADP-AlF₄ bound form. Finally the cluster moves away in the opposite direction from the nucleotide free form in the ADP bound form. This movement of the cluster in conjunction with the rolling motion has been studied for the electron transfer event and the phosphate release event (Chapters 2 and 7).

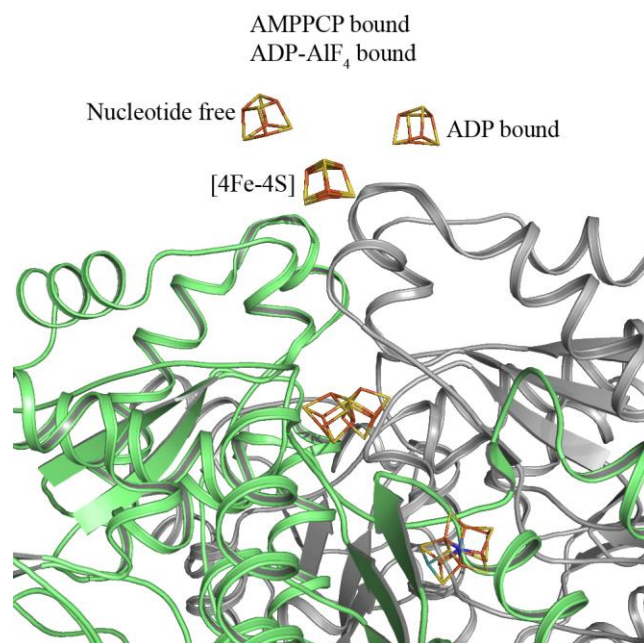


Figure 1-13: Movement of the [4Fe-4S] cluster. Movement of the nucleotide free, AMPPCP($\beta\gamma$ -methylene ATP), ADP-AlF₄, and ADP bound [4Fe-4S] cluster relative to the P cluster of the MoFe protein shows the cluster starting from a farther distance from the P cluster in the nucleotide free form and moving closer by ~ 5 Å in the AMPPCP and ADP-AlF₄ bound form followed by a movement away in the ADP bound form.²⁹

Iron Protein Cycle

As noted earlier the Fe protein reduces the MoFe protein while it is transiently associated in the form of a complex (2Fe:1MoFe). This event is coupled to an ATP hydrolysis event which is followed by phosphate release and dissociation of the Fe protein from the MoFe protein. The combination of association, conformational changes, ATP hydrolysis, electron transfer, phosphate release and dissociation is known as the Fe protein cycle. The order of all the events within this cycle was unknown. It was known that upon binding 2MgATP molecules the reduced iron protein undergoes conformational

changes.⁴³ This is followed by the binding of the activated Fe protein to the MoFe protein. The order of events at this point became unclear. After the binding of the Fe protein to the MoFe protein 2ATP molecules are hydrolyzed. It was also known that an electron is transferred from the Fe protein to the MoFe protein during this time as well. A number of studies have attempted to determine the order of these two (ATP hydrolysis and electron transfer) events in the Fe protein cycle. This was attempted by monitoring phosphate release with quench flow or by observing change in fluorescence using MDCC labeled phosphate binding protein, proton production using pH indicators or by monitoring heat release utilizing stopped-flow calorimetry.^{19–21,24,25} All of these approaches are problematic. Using quench flow to study phosphate release does not establish a difference between the released phosphate vs phosphate still bound to the Fe protein. Heat and pH changes in the overall system are difficult to attribute to a specific step in the iron protein cycle. This is especially complicated by the conformational changes in the protein. The stopped-flow fluorometric approach utilizing MDCC-PBP clearly identifies the rate of phosphate release.¹⁹ This rate is faster than the rate of dissociation, however, it does not help in determining when the ATP hydrolysis event takes place.

ATP hydrolysis can occur independent of electron transfer, however, electron transfer seems to require ATP.^{10,87} There is evidence stating that the two events might not be coupled to each other at all. Experiments conducted with $2e^-$ reduced Fe protein show that the stoichiometry of the electrons transferred to the MoFe protein changes from $1e^-/2ATP$ molecules to $2e^-/2ATP$ molecules.¹⁰ This suggests that ATP binding but not hydrolysis might be needed for electron transfer. Another study using 127^{Leu} deletion

variant of the Fe protein shows electron transfer from the Fe protein to the MoFe protein in the absence of ATP. The crystal structure of this protein shows conformational changes within the Fe protein similar to the ATP bound form of the wild type Fe protein.²⁸ Evidence presented in chapter 3 using β -188^{Ser-Cys} variant of the MoFe protein also supports this argument.

However, contrary evidence also exists. ITC studies showing the ATP hydrolysis event taking place prior to electron transfer suggest that not only ATP binding but also its hydrolysis has to occur prior to electron transfer.²⁵

The order of ATP hydrolysis relative to electron transfer is not the only mystery in the Fe protein cycle. The P cluster's positioning between the [4Fe-4S] cluster of the Fe protein and the M cluster of the MoFe protein suggests a role for the P cluster in the electron transfer from the Fe protein to the M cluster of the MoFe protein. This is supported by selective mutagenesis (around the P cluster) studies that show either reduction in or complete lack of enzymatic activity and serve as evidence for the role of P cluster. Variant proteins such as β -188^{Ser-Gly} and β -153^{Cys-Ser} show reduction in protein activity due to these mutations around the P cluster.^{51,88} All of this serves as evidence supporting the role of the P cluster during electron transfer. The order of electron transfer from the [4Fe-4S] cluster of the Fe protein to the P cluster and eventually to the M cluster is uncertain.

Prior to research presented in chapter 3 two hypothesis for the order of electron transfer existed. One states that the P cluster must be reduced first by the Fe protein to an as of yet unidentified so called P super reduced state. This super reduced P cluster can then transfer the electron to the M cluster (**Figure 1-14-A**). Another hypothesis states that

upon Fe protein binding the P cluster transfers the electron to the M cluster resulting in a deficit of an electron on the P cluster fulfilled, eventually, by the [4Fe-4S] cluster of the Fe protein (**Figure 1-14-B**).

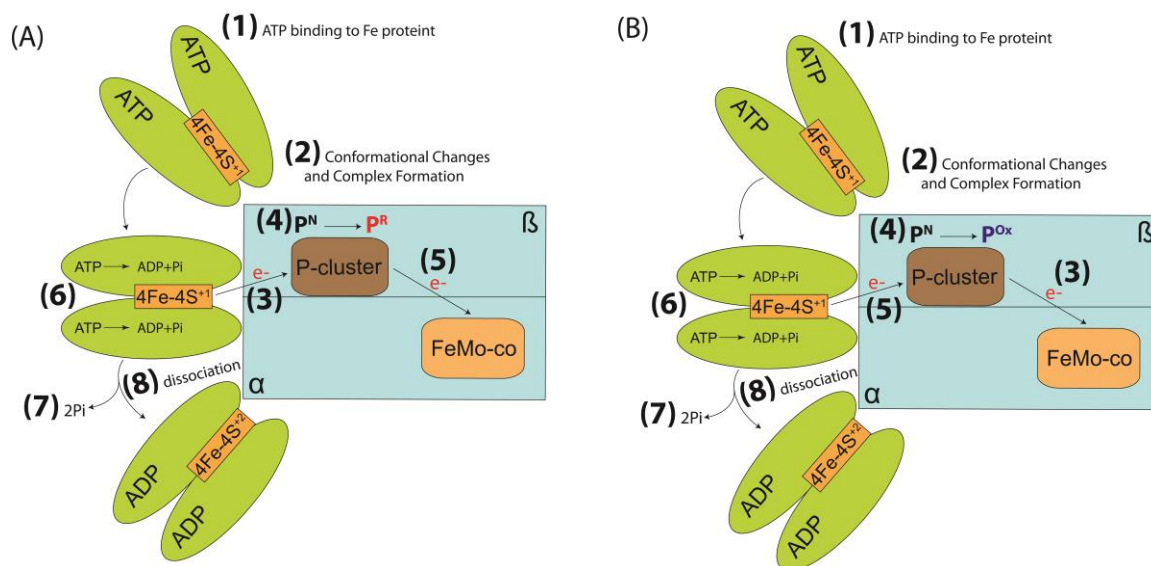


Figure 1-14: Electron transfer in nitrogenase. (A) shows the P cluster super reduction model of electron transfer with the electron from Fe protein being received by the P cluster first (step 4) while (B) shows the electron transfer event from the P cluster to the M cluster occurring first (Step 4).

The order of ATP hydrolysis relative to electron transfer was also unknown. This resulted in a lack of knowledge about whether it was the binding or hydrolysis of ATP that provided the energy for the electron transfer event. If ATP hydrolysis was occurring prior to electron transfer then the energy from the event could be responsible for the electron transfer. However, if ATP hydrolysis followed the electron transfer event then the binding of ATP rather than the hydrolysis would result in the transfer of an electron from Fe protein to the MoFe protein.^{20,21,24,25}

In **figure 1-15**, a scheme showing the true electron transfer event and ATP hydrolysis order is shown based on work presented in chapter 5. It shows that the ATP hydrolysis event (70 s^{-1}) is slower than and thus follows electron transfer which is a faster event at $\sim 140 \text{ s}^{-1}$.

Fe protein bound to two MgATP molecules associates with the MoFe protein. This binding/association event between the two proteins creates conformational changes within the MoFe protein between the P and the M cluster (unpublished). This conformational change is accompanied by the transient association of the β -188^{Ser} residue and the P cluster which leads to the lowering of the P cluster reduction potential. This allows the P cluster to reduce the FeMo-cofactor. The electron transfer event between the P and the M clusters generates an electron deficit at the P cluster. This deficit is fulfilled by the Fe protein's $[4\text{Fe-4S}]^{+1}$ cluster. The rate constant of this series of events is $\sim 140 \text{ s}^{-1}$ (Chapter 3).²⁷

The oxidation of the $[4\text{Fe-4S}]$ cluster of the Fe protein is followed by the hydrolysis of ATP at the two sites on the Fe protein (70 s^{-1}) (Chapter 5). Upon hydrolysis the protein goes through another set of conformational changes (Chapter 7) which results in the release of inorganic phosphate from the Fe protein (30 s^{-1}). The dissociation of the Fe protein from the MoFe protein (6 s^{-1}) follows the release of phosphate. Upon dissociation the Fe protein releases the two MgADP molecules and gets re-reduced. This regenerates the Fe protein for another iron protein cycle.

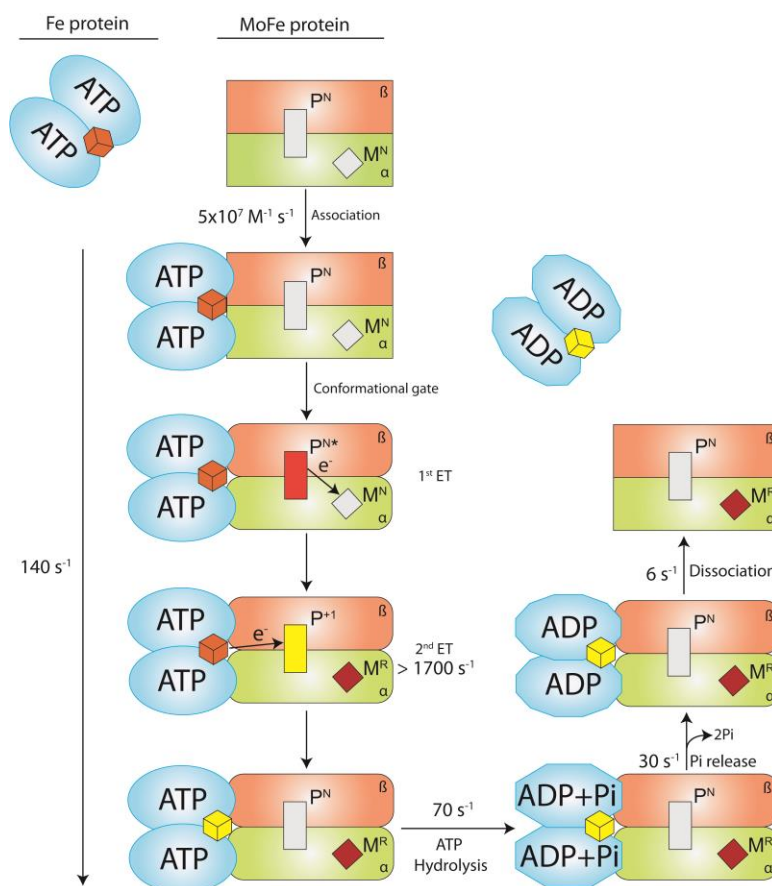
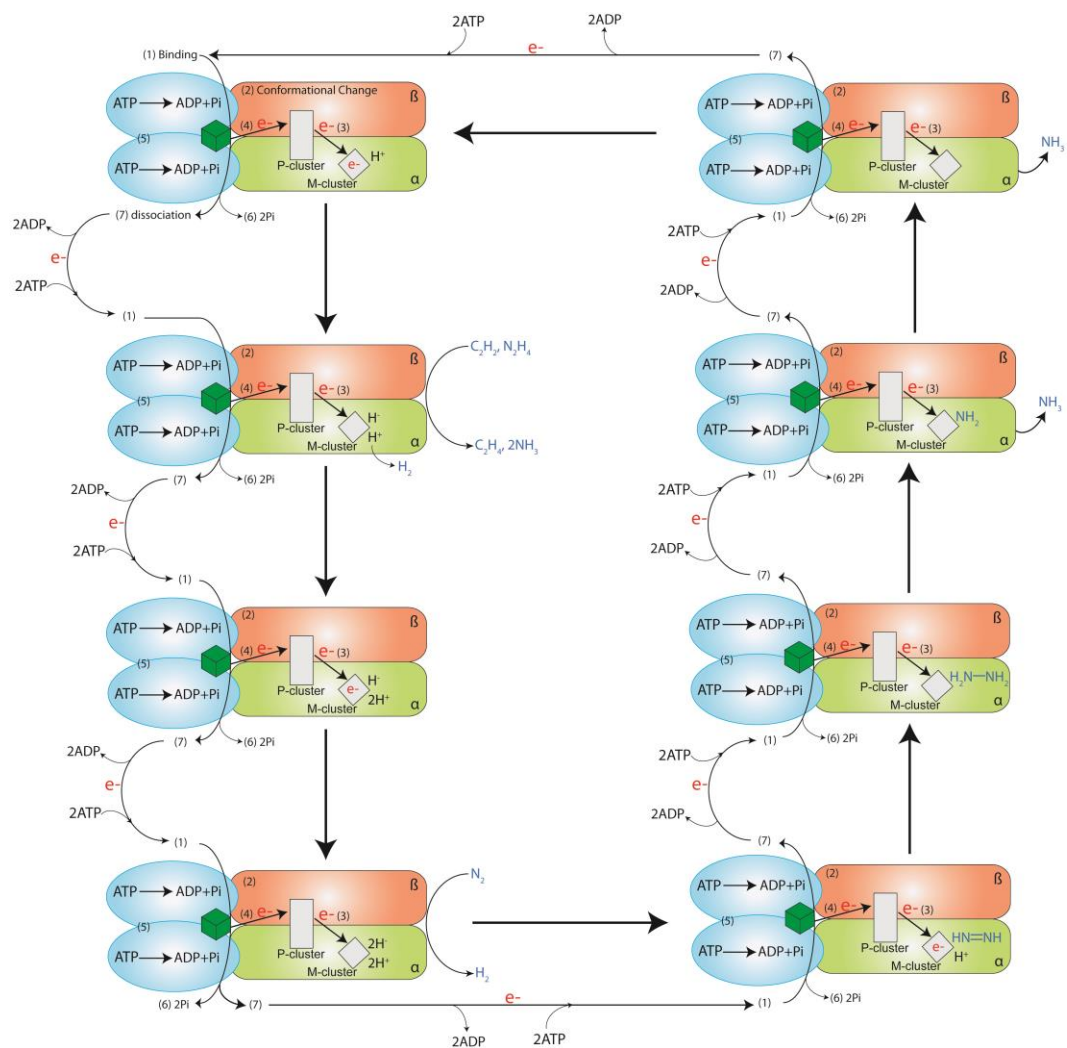


Figure 1-15: The Fe protein cycle. Fe protein is shown as (blue ovals) with the two oxidation states of the [4Fe-4S] cluster (+1 (orange cube) or +2 (yellow cube)) binding to MoFe protein (α subunit red and β subunit green) with the P cluster (rectangle, grey P^N , red activated P^{N*} and yellow P^{+1} states) and the M cluster (diamond, grey M^N and maroon M^R state). Starting from the top left with the association of the Fe protein with the MoFe protein and ending at top right with the dissociation of the oxidized Fe protein from the reduced MoFe protein the scheme shows a complete Fe protein cycle. First order rate constant (k, s^{-1}) values for 25°C are shown. Conformational changes in the Fe protein and MoFe protein are denoted by changes in shape of the ovals or rectangles.

MoFe Protein Cycle

The MoFe protein cycle is an eight state cycle in which the MoFe protein is reduced for substrate reduction via successive single electron reductions (E states) each as a result of a Fe protein cycle and each coupled to proton transfer.^{49,51,82} Different substrates bind at different E states and are subsequently reduced.⁸² Acetylene undergoes two electron reductions by binding at E₂ once sufficient electrons have been accumulated in the form of hydrides bound to the cofactor. Hydrazine binds to E₁ and is subsequently reduced in the next two electron transfer steps. Nitrogen binds at the E₄ state and is reduced in multiple steps until its release in the form of ammonia (**Figure 1-16**).

There are four major questions in the field of nitrogenase. Other than understanding the biosynthesis of the clusters of nitrogenase, three major questions are regarding the mechanism. These include understanding the role of ATP binding and hydrolysis in the electron transfer event (Chapter 5), the role of the P cluster in the electron transfer event (Chapter 3) and the mechanism of substrate reduction at the active site (FeMo-cofactor) (Chapter 6). The work presented in this dissertation is aimed at contributing to the understanding of these open questions about the nitrogenase mechanism.



Scheme 1-16: The MoFe protein cycle. Shows eight consecutive steps of the MoFe protein reduction with substrates entering and departing at different steps (Blue). Fe protein is shown as a homodimer with two blue ovals and a cube [4Fe-4S] cluster. MoFe protein is shown as rectangles (Red and green) prior to conformational changes and rounded edge after conformational changes. Each of the eight steps includes an iron protein cycle. Alternating mechanism of reduction is used for the depiction of nitrogen reduction.

REFERENCES

- (1) Ferguson, S. J. (1998) Nitrogen cycle enzymology. *Curr. Opin. Chem. Biol.* 2, 182–193.
- (2) Igarashi, R. Y., and Seefeldt, L. C. (2003) Nitrogen fixation: the mechanism of the Mo-dependent nitrogenase. *Crit. Rev. Biochem. Mol. Biol.* 38, 351–384.
- (3) Finan, T. M., Layzell, D. B., O’Brian, M. R., and Newton, W. E. (Eds.). (2002) Nitrogen fixation: global perspectives. *Proc. Int. Congr., 13th.* CABI Publishing, Willingford, UK.
- (4) Haber, F., and Le Rossignol, R. (1908) The ammonia equilibrium under pressure. *Z. Elektrochem. Angew. P* 14, 181–196.
- (5) Newton, W. E. (2000) Nitrogen fixation, in *Encyclopedia of Chemical Technology*, 1-46, John Wiley & Sons, Hoboken, NJ.
- (6) Haber, F. The production of ammonia from nitrogen and hydrogen. *Naturwissenschaften* 10, 1041–1049.
- (7) Eady, R. R., Robson, R. I., Richardson, T. H., Miller, R. W., and Hawkins, M. (1987) The vanadium nitrogenase of *Azotobacter chroococcum*: purification and properties of the VFe protein. *Biochem. J.* 244, 197–207.
- (8) Siemann, S., Schneider, K., Dröttboom, M., and Müller, A. (2002) The Fe-only nitrogenase and the Mo nitrogenase from *Rhodobacter capsulatus*. *Eur. J. Biochem.* 269, 1650–1661.
- (9) Georgiadis, M. M., Komiya, H., Chakrabarti, P., Woo, D., Kornuc, J. J., and Rees, D. C. (1992) Crystallographic structure of the nitrogenase iron protein from *Azotobacter vinelandii*. *Science* 257, 1653–1659.

- (10) Burgess, B. K., and Lowe, D. J. (1996) Mechanism of molybdenum nitrogenase. *Chem. Rev.* *96*, 2983–3012.
- (11) Danyal, K., Inglet, B. S., Vincent, K. A., Barney, B. M., Hoffman, B. M., Armstrong, F. A., Dean, D. R., and Seefeldt, L. C. (2010) Uncoupling nitrogenase: catalytic reduction of hydrazine to ammonia by a MoFe protein in the absence of Fe protein-ATP. *J. Am. Chem. Soc.* *132*, 13197–13199.
- (12) Roth, L. E., Nguyen, J. C., and Tezcan, F. A. (2010) ATP- and iron-protein-independent activation of nitrogenase catalysis by light. *J. Am. Chem. Soc.* *132*, 13672–13674.
- (13) Roth, L. E., and Tezcan, F. A. (2012) ATP-Uncoupled, six-electron photoreduction of hydrogen cyanide to methane by the molybdenum–iron protein. *J. Am. Chem. Soc.* *134*, 8416–8419.
- (14) Einsle, O., Tezcan, F. A., Andrade, S. L. A., Schmid, B., Yoshida, M., Howard, J. B., and Rees, D. C. (2002) Nitrogenase MoFe-protein at 1.16 Å resolution: a central ligand in the FeMo-cofactor. *Science* *297*, 1696–1700.
- (15) Spatzal, T., Aksoyoglu, M., Zhang, L., Andrade, S. L. A., Schleicher, E., Weber, S., Rees, D. C., and Einsle, O. (2011) Evidence for interstitial carbon in nitrogenase FeMo cofactor. *Science* *334*, 940.
- (16) Simpson, F. B., and Burris, R. H. (1984) A nitrogen pressure of 50 atmospheres does not prevent evolution of hydrogen by nitrogenase. *Science* *224*, 1095–1097.
- (17) Howard, J. B., and Rees, D. C. (1994) Nitrogenase: a nucleotide-dependent molecular switch. *Ann. Rev. Biochem.* *63*, 235–264.

- (18) Seefeldt, L. C., and Dean, D. R. (1997) Role of nucleotides in nitrogenase catalysis. *Acc. Chem. Res.* *30*, 260–266.
- (19) Lowe, D. J., Ashby, G. A., Brune, M., Knights, H., Webb, M. R., and Thorneley, R. N. F. (1995) ATP hydrolysis and energy transduction by nitrogenase, in *Nitrogen Fixation: Fundamentals and Applications* (Tikhonovich, I. A., Provorov, N. A., Romanov, V. I., and Newton, W. E., Eds.), pp 103–108. Springer, Netherlands.
- (20) Hageman, R. V., and Burris, R. H. (1978) Nitrogenase and nitrogenase reductase associate and dissociate with each catalytic cycle. *Proc. Natl. Acad. Sci. U.S.A.* *75*, 2699–2702.
- (21) Eady, R. R., Lowe, D. J., and Thorneley, R. N. F. (1978) Nitrogenase of *Klebsiella pneumoniae*: a pre-steady state burst of ATP hydrolysis is coupled to electron transfer between the component proteins. *FEBS Lett.* *95*, 211–213.
- (22) Wilson, P. E., Nyborg, A. C., and Watt, G. D. (2001) Duplication and extension of the Thorneley and Lowe kinetic model for *Klebsiella pneumoniae* nitrogenase catalysis using a mathematica software platform. *Biophys. Chem.* *91*, 281–304.
- (23) Lanzilotta, W. N., Fisher, K., and Seefeldt, L. C. (1996) Evidence for electron transfer from the nitrogenase iron protein to the molybdenum–iron protein without MgATP hydrolysis: characterization of a tight protein–protein complex. *Biochemistry* *35*, 7188–7196.
- (24) Imam, S., and Eady, R. R. (1980) Nitrogenase of *Klebsiella pneumoniae*: reductant-independent ATP hydrolysis and the effect of pH on the efficiency of coupling of ATP hydrolysis to substrate reduction. *FEBS Lett.* *110*, 35–38.

- (25) Thorneley, R. N., Ashby, G., Howarth, J. V., Millar, N. C., and Gutfreund, H. (1989) A transient-kinetic study of the nitrogenase of *Klebsiella pneumoniae* by stopped-flow calorimetry. Comparison with the myosin ATPase. *Biochem. J.* 264, 657–661.
- (26) Ma, L., Brosius, M. A., and Burgess, B. K. (1996) Construction of a form of the MoFe protein of nitrogenase that accepts electrons from the Fe protein but does not reduce substrate. *J. Biol. Chem.* 271, 10528–10532.
- (27) Danyal, K., Dean, D. R., Hoffman, B. M., and Seefeldt, L. C. (2011) Electron transfer within nitrogenase: evidence for a deficit-spending mechanism. *Biochemistry* 50, 9255–9263.
- (28) Chiu, H.-J., Peters, J. W., Lanzilotta, W. N., Ryle, M. J., Seefeldt, L. C., Howard, J. B., and Rees, D. C. (2001) MgATP-bound and nucleotide-free structures of a nitrogenase protein complex between the Leu 127 Δ -Fe-protein and the MoFe-protein. *Biochemistry* 40, 641–650.
- (29) Tezcan, F. A., Kaiser, J. T., Mustafi, D., Walton, M. Y., Howard, J. B., and Rees, D. C. (2005) Nitrogenase complexes: multiple docking sites for a nucleotide switch protein. *Science* 309, 1377–1380.
- (30) Peters, J. W., Stowell, M. H. B., Soltis, S. M., Finnegan, M. G., Johnson, M. K., and Rees, D. C. (1997) Redox-dependent structural changes in the nitrogenase P-cluster. *Biochemistry* 36, 1181–1187.
- (31) Sørli, M., Christiansen, J., Lemon, B. J., Peters, J. W., Dean, D. R., and Hales, B. J. (2001) Mechanistic features and structure of the nitrogenase α -Gln¹⁹⁵ MoFe protein. *Biochemistry* 40, 1540–1549.

- (32) Sarma, R., Barney, B. M., Keable, S., Dean, D. R., Seefeldt, L. C., and Peters, J. W. (2010) Insights into substrate binding at FeMo-cofactor in nitrogenase from the structure of an α -70^{lle} MoFe protein variant. *J. Inorg. Biochem.* *104*, 385–389.
- (33) Lee, C. C., Blank, M. A., Fay, A. W., Yoshizawa, J. M., Hu, Y., Hodgson, K. O., Hedman, B., and Ribbe, M. W. (2009) Stepwise formation of P-cluster in nitrogenase MoFe protein. *Proc. Natl. Acad. Sci. U.S.A.* *106*, 18474–18478.
- (34) Cordewener, J., Haaker, H., Ewijk, P. V., and Veeger, C. (1985) Properties of the MgATP and MgADP binding sites on the Fe protein of nitrogenase from *Azotobacter vinelandii*. *Eur. J. Biochem.* *148*, 499–508.
- (35) Lanzilotta, W. N., Parker, V. D., and Seefeldt, L. C. (1999) Thermodynamics of nucleotide interactions with the *Azotobacter vinelandii* nitrogenase iron protein. *Biochim. Biophys. Acta.* *1429*, 411–421.
- (36) Lanzilotta, W. N., Ryle, M. J., and Seefeldt, L. C. (1995) Nucleotide hydrolysis and protein conformational changes in *Azotobacter vinelandii* nitrogenase iron protein: defining the function of aspartate 129. *Biochemistry.* *34*, 10713–10723.
- (37) Lanzilotta, W. N., and Seefeldt, L. C. (1997) Changes in the midpoint potentials of the nitrogenase metal centers as a result of iron protein–molybdenum-iron protein complex formation. *Biochemistry.* *36*, 12976–12983.
- (38) Lanzilotta, W. N., Parker, V. D., and Seefeldt, L. C. (1988) Electron transfer in nitrogenase analyzed by marcus theory: evidence for gating by MgATP. *Biochemistry* *37*, 399–407.

- (39) Lindahl, P. A., Day, E. P., Kent, T. A., Orme-Johnson, W. H., and Münck, E. (1985) Mössbauer, EPR, and magnetization studies of the *Azotobacter vinelandii* Fe protein. Evidence for a $[4\text{Fe-4S}]^{1+}$ cluster with spin $S = 3/2$. *J. Biol. Chem.* 260, 11160–11173.
- (40) Hagen, W. R., Dunham, W. R., Braaksma, A., and Haaker, H. (1985) On the prosthetic group(s) of component II from nitrogenase: EPR of the Fe-protein from *Azotobacter vinelandii*. *FEBS Lett.* 187, 146–150.
- (41) Hagen, W. R., Eady, R. R., Dunham, W. R., and Haaker, H. (1985) A novel $S = 3/2$ EPR signal associated with native Fe-proteins of nitrogenase. *FEBS Lett.* 189, 250–254.
- (42) Lindahl, P. A., Gorelick, N. J., Münck, E., and Orme-Johnson, W. H. (1987) EPR and Mössbauer studies of nucleotide-bound nitrogenase iron protein from *Azotobacter vinelandii*. *J. Biol. Chem.* 262, 14945–14953.
- (43) Zumft, W. G., Palmer, G., and Mortenson, L. E. (1973) Electron paramagnetic resonance studies on nitrogenase. II. Interaction of adenosine 5'-triphosphate with azoferredoxin. *Biochim. Biophys. Acta.* 292, 413–421.
- (44) Orme-Johnson, W. H., Hamilton, W. D., Jones, T. L., Tso, M.-Y. W., Burris, R. H., Shah, V. K., and Brill, W. J. (1972) Electron paramagnetic resonance of nitrogenase and nitrogenase components from *Clostridium pasteurianum* W5 and *Azotobacter vinelandii* OP. *Proc. Natl. Acad. Sci. U.S.A* 69, 3142–3145.
- (45) Thorneley, R. N., and Ashby, G. A. (1989) Oxidation of nitrogenase iron protein by dioxygen without inactivation could contribute to high respiration rates of *Azotobacter* species and facilitate nitrogen fixation in other aerobic environments. *Biochem. J.* 261, 181–187.

- (46) Angove, H. C., Yoo, S. J., Burgess, B. K., and Münck, E. (1997) Mössbauer and EPR evidence for an all-ferrous Fe₄S₄ cluster with S= 4 in the Fe protein of nitrogenase. *J. Am. Chem. Soc.* *119*, 8730–8731.
- (47) Watt, G. D., and Reddy, K. R. N. (1994) Formation of an all ferrous Fe₄S₄ cluster in the iron protein component of *Azotobacter vinelandii* nitrogenase. *J. Inorg. Biochem.* *53*, 281–294.
- (48) Lowery, T. J., Wilson, P. E., Zhang, B., Bunker, J., Harrison, R. G., Nyborg, A. C., Thiriot, D., and Watt, G. D. (2006) Flavodoxin hydroquinone reduces *Azotobacter vinelandii* Fe protein to the all-ferrous redox state with a S = 0 spin state. *Proc. Natl. Acad. Sci.* *103*, 17131–17136.
- (49) Seefeldt, L. C., Hoffman, B. M., and Dean, D. R. (2009) Mechanism of Mo-dependent nitrogenase. *Annu. Rev. Biochem.* *78*, 701–722.
- (50) Schindelin, H., Kisker, C., Schlessman, J. L., Howard, J. B., and Rees, D. C. (1997) Structure of ADP·AlF₄⁻-stabilized nitrogenase complex and its implications for signal transduction. *Nature* *387*, 370–376.
- (51) Lanzilotta, W. N., Christiansen, J., Dean, D. R., and Seefeldt, L. C. (1998) Evidence for coupled electron and proton transfer in the [8Fe-7S] cluster of nitrogenase. *Biochemistry* *37*, 11376–11384.
- (52) Christiansen, J., Tittsworth, R. C., Hales, B. J., and Cramer, S. P. (1995) Fe and Mo EXAFS of *Azotobacter vinelandii* nitrogenase in partially oxidized and singly reduced forms. *J. Am. Chem. Soc.* *117*, 10017–10024.

- (53) Tittsworth, R. C., and Hales, B. J. (1993) Detection of EPR signals assigned to the 1-equiv-oxidized P-clusters of the nitrogenase MoFe-protein from *Azotobacter vinelandii*. *J. Am. Chem. Soc.* *115*, 9763–9767.
- (54) Surerus, K. K., Hendrich, M. P., Christie, P. D., Rottgardt, D., Orme-Johnson, W. H., and Munck, E. (1992) Mössbauer and integer-spin EPR of the oxidized P-clusters of nitrogenase: P^{OX} is a non-Kramers system with a nearly degenerate ground doublet. *J. Am. Chem. Soc.* *114*, 8579–8590.
- (55) Zimmermann, R., Münck, E., Brill, W. J., Shah, V. K., Henzl, M. T., Rawlings, J., and Orme-Johnson, W. H. (1978) Nitrogenase X: Mössbauer and EPR studies on reversibly oxidized MoFe protein from *Azotobacter vinelandii* OP. Nature of the iron centers. *Biochim. Biophys. Acta* *537*, 185–207.
- (56) Pierik, A. J., Wassink, H., Haaker, H., and Hagen, W. R. (1993) Redox properties and EPR spectroscopy of the P clusters of *Azotobacter vinelandii* MoFe protein. *Eur. J. Biochem.* *212*, 51–61.
- (57) Seefeldt, L. C., Hoffman, B. M., and Dean, D. R. (2012) Electron transfer in nitrogenase catalysis. *Curr. Opin. Chem. Biol.* *16*, 19–25.
- (58) Huynh, B. H., Henzl, M. T., Christner, J. A., Zimmermann, R., Orme-Johnson, W. H., and Münck, E. (1980) Nitrogenase XII. Mössbauer studies of the MoFe protein from *Clostridium pasteurianum* W5. *Biochim. Biophys. Acta* *623*, 124–138.
- (59) Chan, J. M., Christiansen, J., Dean, D. R., and Seefeldt, L. C. (1999) Spectroscopic evidence for changes in the redox state of the nitrogenase P-Cluster during turnover. *Biochemistry* *38*, 5779–5785.

- (60) Pollock, R. C., Lee, H.-I., Cameron, L. M., DeRose, V. J., Hales, B. J., Orme-Johnson, W. H., and Hoffman, B. M. (1995) Investigation of CO bound to inhibited forms of nitrogenase MoFe protein by ^{13}C ENDOR. *J. Am. Chem. Soc.* *117*, 8686–8687.
- (61) Hoffman, B. M., Dean, D. R., and Seefeldt, L. C. (2009) Climbing nitrogenase: toward a mechanism of enzymatic nitrogen fixation. *Acc. Chem. Res.* *42*, 609–619.
- (62) Barney, B. M., Lee, H.-I., Dos Santos, P. C., Hoffman, B. M., Dean, D. R., and Seefeldt, L. C. (2006) Breaking the N_2 triple bond: insights into the nitrogenase mechanism. *Dalton Trans.* 2277–2284.
- (63) Thorneley, R. N. F., and Lowe, D. J. Kinetics and mechanism of the nitrogenase enzyme system, in *Molybdenum Enzymes*, pp 221–284. Wiley, New York.
- (64) Lowe, D. J., Fisher, K., and Thorneley, R. N. F. (1993) *Klebsiella pneumoniae* nitrogenase: pre-steady-state absorbance changes show that redox changes occur in the MoFe protein that depend on substrate and component protein ratio; a role for P-centres in reducing dinitrogen? *Biochem. J.* *292*, 93–98.
- (65) Igarashi, R. Y., Laryukhin, M., Dos Santos, P. C., Lee, H.-I., Dean, D. R., Seefeldt, L. C., and Hoffman, B. M. (2005) Trapping H^- bound to the nitrogenase FeMo-cofactor active site during H_2 evolution: characterization by ENDOR spectroscopy. *J. Am. Chem. Soc.* *127*, 6231–6241.
- (66) Lukoyanov, D., Yang, Z.-Y., Dean, D. R., Seefeldt, L. C., and Hoffman, B. M. (2010) Is Mo involved in hydride binding by the four-electron reduced (E_4) intermediate of the nitrogenase MoFe protein? *J. Am. Chem. Soc.* *132*, 2526–2527.
- (67) Benton, P. M. C., Laryukhin, M., Mayer, S. M., Hoffman, B. M., Dean, D. R., and Seefeldt, L. C. (2003) Localization of a substrate binding site on the FeMo-cofactor in

nitrogenase: trapping propargyl alcohol with an alpha-70-substituted MoFe protein.

Biochemistry 42, 9102–9109.

(68) Lee, H. I., Sørlie, M., Christiansen, J., Song, R. T., Dean, D. R., Hales, B. J., and Hoffman, B. M. (2000) Characterization of an intermediate in the reduction of acetylene by the nitrogenase α -Gln¹⁹⁵ MoFe protein by Q-band EPR and ¹³C, ¹H ENDOR. *J. Am. Chem. Soc.* 122, 5582–5587.

(69) Ryle, M. J., Lee, H. I., Seefeldt, L. C., and Hoffman, B. M. (2000) Nitrogenase reduction of carbon disulfide: freeze-quench EPR and ENDOR evidence for three sequential intermediates with cluster-bound carbon moieties. *Biochemistry* 39, 1114–1119.

(70) Barney, B. M., Lukoyanov, D., Igarashi, R. Y., Laryukhin, M., Yang, T.-C., Dean, D. R., Hoffman, B. M., and Seefeldt, L. C. (2009) Trapping an intermediate of dinitrogen (N₂) reduction on nitrogenase. *Biochemistry* 48, 9094–9102.

(71) Barney, B. M., Yang, T.-C., Igarashi, R. Y., Dos Santos, P. C., Laryukhin, M., Lee, H.-I., Hoffman, B. M., Dean, D. R., and Seefeldt, L. C. (2005) Intermediates trapped during nitrogenase reduction of N₂, CH₃-N=NH, and H₂N-NH₂. *J. Am. Chem. Soc.* 127, 14960–14961.

(72) Deng, H., and Hoffmann, R. (1993) How N₂ might be activated by the FeMo-cofactor in nitrogenase. *Angew. Chem.* 32, 1062–1065.

(73) Dance, I. (1996) Theoretical investigations of the mechanism of biological nitrogen fixation at the FeMo cluster site. *JBIC* 1, 581–586.

- (74) Barney, B. M., McClead, J., Lukoyanov, D., Laryukhin, M., Yang, T.-C., Dean, D. R., Hoffman, B. M., and Seefeldt, L. C. (2007) Diazene (HN=NH) is a substrate for nitrogenase: insights into the pathway of N₂ reduction. *Biochemistry* 46, 6784–6794.
- (75) Barney, B. M., Lukoyanov, D., Yang, T.-C., Dean, D. R., Hoffman, B. M., and Seefeldt, L. C. (2006) A methyldiazene (HN=N-CH₃)-derived species bound to the nitrogenase active-site FeMo cofactor: implications for mechanism. *Proc. Natl. Acad. Sci. U.S.A.* 103, 17113–17118.
- (76) Davis, L. C. (1980) Hydrazine as a substrate and inhibitor of *Azotobacter vinelandii* nitrogenase. *Arch. Biochem. Biophys.* 204, 270–276.
- (77) Thorneley, R. N. F., Eady, R. R., and Lowe, D. J. (1978) Biological nitrogen fixation by way of an enzyme-bound dinitrogen-hydride intermediate. *Nature* 272, 557–558.
- (78) Barney, B. M., Laryukhin, M., Igarashi, R. Y., Lee, H.-I., Dos Santos, P. C., Yang, T.-C., Hoffman, B. M., Dean, D. R., and Seefeldt, L. C. (2005) Trapping a hydrazine reduction intermediate on the nitrogenase active site. *Biochemistry* 44, 8030–8037.
- (79) Yates, M. G., and Lowe, D. J. (1976) Nitrogenase of *Azotobacter chroococcum*: a new electron paramagnetic-resonance signal associated with a transient species of the MoFe protein during catalysis. *FEBS Letters* 72, 127–130.
- (80) Davis, L. C., Henzl, M. T., Burris, R. H., and Orme-Johnson, W. H. (1979) Iron-sulfur clusters in the molybdenum-iron protein component of nitrogenase. Electron paramagnetic resonance of the carbon monoxide inhibited state. *Biochemistry* 18, 4860–4869.

- (81) Lowe, D. J., Eady, R. R., and Thorneley, N. F. (1978) Electron-paramagnetic-resonance studies on nitrogenase of *Klebsiella pneumoniae*. Evidence for acetylene- and ethylene-nitrogenase transient complexes. *Biochem J.* 173, 277–290.
- (82) Hoffman, B. M., Lukoyanov, D., Dean, D. R., and Seefeldt, L. C. (2013) Nitrogenase: a draft mechanism. *Acc. Chem. Res.* 46, 587–595.
- (83) Christiansen, J., Chan, J. M., Seefeldt, L. C., and Dean, D. R. (2000) The role of the MoFe protein α -125Phe and β -125Phe residues in *Azotobacter vinelandii* MoFe protein-Fe protein interaction. *J. Inorg. Biochem.* 80, 195–204.
- (84) Wolle, D., Kim, C., Dean, D., and Howard, J. B. (1992) Ionic interactions in the nitrogenase complex. Properties of Fe-protein containing substitutions for Arg-100. *J. Biol. Chem.* 267, 3667–3673.
- (85) Seefeldt, L. C. (1994) Docking of nitrogenase iron- and molybdenum-iron proteins for electron transfer and MgATP hydrolysis: the role of arginine 140 and lysine 143 of the *Azotobacter vinelandii* iron protein. *Protein Sci.* 3, 2073–2081.
- (86) Schmid, B., Einsle, O., Chiu, H.-J., Willing, A., Yoshida, M., Howard, J. B., and Rees, D. C. (2002) Biochemical and structural characterization of the cross-linked complex of nitrogenase: comparison to the ADP-AlF₄⁻-stabilized structure. *Biochemistry* 41, 15557–15565.
- (87) Thorneley, R. N., Lowe, D. J., Eady, R. R., and Miller, R. W. (1979) The coupling of electron transfer in nitrogenase to the hydrolysis of magnesium adenosine triphosphate. *Biochem. Soc. Trans.* 7, 633–636.
- (88) May, H. D., Dean, D. R., and Newton, W. E. (1991) Altered nitrogenase MoFe proteins from *Azotobacter vinelandii*. Analysis of MoFe proteins having amino acid

substitutions for the conserved cysteine residues within the β -subunit. *Biochem J.* 277, 457–464.

CHAPTER 2
CONFORMATIONAL GATING OF ELECTRON TRANSFER FROM Fe
PROTEIN TO MoFe PROTEIN*

ABSTRACT

The nitrogenase Fe protein contains a [4Fe-4S] cluster and delivers one electron at a time to the catalytic MoFe protein, during this electron delivery, the Fe protein in its [4Fe-4S]¹⁺ reduced state (Fe^{red}) binds two MgATP and forms a complex with the MoFe protein, with subsequent transfer of one electron to the MoFe protein in a reaction coupled to the hydrolysis of two ATP. Crystal structures with the nitrogenase complex in different nucleotide-bound states show major conformational changes which provide a structural underpinning to suggestions that inter-component electron transfer (ET) is ‘gated’ by conformational changes of the complex and/or of its component proteins. Although electron delivery is coupled to ATP hydrolysis, their connection is puzzling, for it appears that ET precedes both ATP hydrolysis and Pi release. We here test the gating hypothesis with studies of the intracomplex oxidation of Fe^{red} by MoFe protein in the presence of a variety of solutes. Conformational control of this process (gating) is revealed by the finding that it responds to changes in osmotic pressure (but not viscosity), with no fewer than 80 waters being bound during the reaction. The absence of a solvent kinetic isotope effect further implies that ATP hydrolysis does not occur during the ET step.

*Coauthored by Karamatullah Danyal, Diana Mayweather, Dennis Dean, Brian M. Hoffman and Lance C. Seefeldt (2011) *JACS* 135 (20), pp 6894-6895. Copyright 2010 American Chemical Society. Reprinted with Permission.

The Mo-dependent nitrogenase^{1,2} is comprised of two component proteins, denoted the Fe and MoFe proteins. The Fe protein contains a [4Fe-4S] cluster and delivers one electron at a time to the MoFe protein, which contains the multimetallic catalytic cluster [7Fe, Mo, 9S; X], designated FeMo-co, as well as the auxiliary [8Fe, 7S] P cluster, which may possibly mediate electron transfer from Fe protein to FeMo-co. During this electron delivery, the Fe protein in its [4Fe-4S]¹⁺ reduced state (Fe^{red}) binds two MgATP and forms a complex with the MoFe protein, with subsequent transfer of one electron to the MoFe protein in a reaction coupled to the hydrolysis of two ATP.

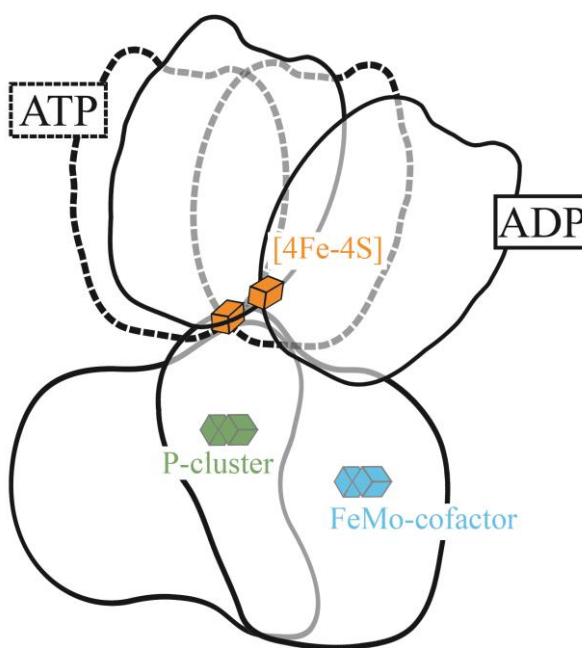


Figure 2-1: Representation of complexes between Fe protein (top) and MoFe protein (bottom) in ATP- like (dashed) and ADP-like bound forms; (adapted from Tezcan and coworkers³).

Crystal structures with the nitrogenase complex in different nucleotide-bound states show that major conformational changes occur upon ATP hydrolysis, **Figure 2-1**.^{3,4} This provides a structural underpinning to suggestions^{1,5,6} that inter-component electron transfer (ET) is “gated”⁷⁻⁹ by conformational changes of the complex and/or of its component proteins. Although electron delivery is coupled to ATP hydrolysis, their connection is puzzling, for it appears that ET precedes both ATP hydrolysis¹⁰ and Pi release.¹¹ Furthermore, none of the X-ray structures of the Fe protein-MoFe protein complex, [Fe: MoFe], reveals any perturbation of either of the two clusters within the MoFe protein that might produce conformational activation of electron transfer.⁴

To determine whether conformational changes control ET within the [Fe: MoFe] protein complex, we have measured oxidation of Fe^{red} by MoFe protein in the presence of solutes that increase the viscosity (η) and osmotic pressure of the solution. For a dynamical conformational transition in condensed media, an increase in viscosity alters the rate constant according to the formula, $k(\eta) \sim k^0/\eta$.¹² Changes in osmotic pressure instead modulate the energetics of reactions that change the number of bound waters.¹³ In such a case, the observed rate constant for ET, k_2 , varies exponentially with the molality (m) of added solute according to the equation,¹³ $k_2 \propto \exp[-(\Delta n/55.6)m]$ where Δn is the number of waters absorbed in the conformational transformation.

Figure 2-2 shows typical traces that monitor the oxidation of Fe^{red} by resting-state MoFe protein in solutions with varying concentrations of sucrose as viscogen/osmolyte. The ET reaction was initiated by the addition of MgATP to a solution of [Fe^{red}] and [MoFe] in the stopped flow. MgATP was added in sufficiently high concentrations to ensure that Fe^{red} binds two ATP and then binds to MoFe within the dead-time of the

instrument.¹⁴ As a result, the absorbance changes in these pre-steady-state experiments are wholly associated with Fe^{red} oxidation within the $[\text{Fe}^{\text{red}}(\text{MgATP})_2:\text{MoFe}]$ complex.^{15,16}

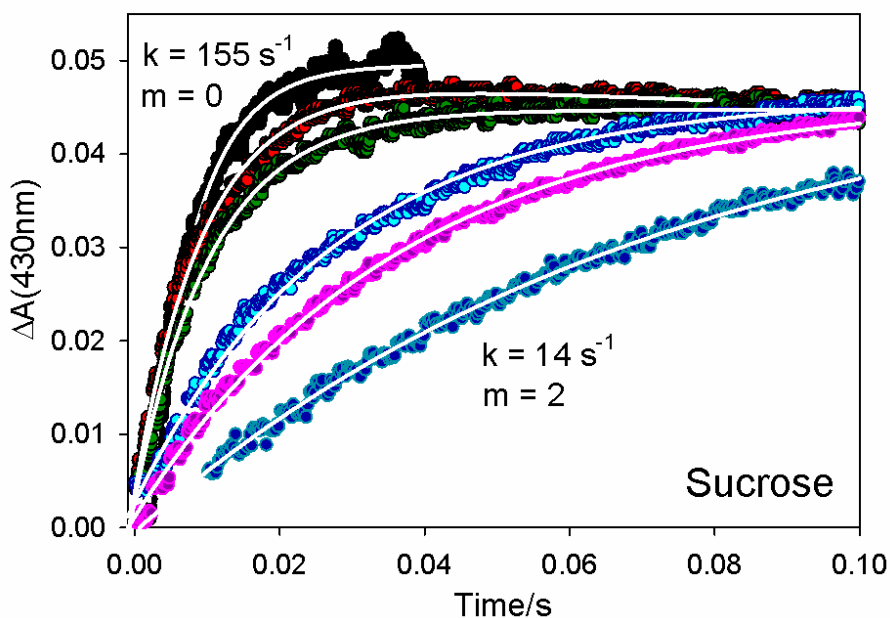


Figure 2-2: Stopped-flow oxidation of Fe^{red} within the $[\text{Fe}^{\text{red}}(\text{MgATP})_2:\text{MoFe}]$ complex. Sucrose concentrations vary from 0 to 2 *m*. Traces for $m = 0$ in H_2O (shown) and D_2O (not shown) overlay and give the same kinetic constants within error.

The increases in absorbance of the stopped-flow traces in **Figure 2-2** caused by the oxidation of Fe^{red} are well-described by an exponential rise; the rate constant for aqueous buffer, $k_2 = 158 \text{ s}^{-1}$, is in excellent agreement with previously reported measurements.^{1,17} Progressive additions of either sucrose (**Figure 2-2**), glucose and raffinose, PEGs 300, 600, or glycerol all cause progressively large decreases in the ET rate constant. This solute control of ET reveals that intra-complex oxidation of Fe^{red} by

resting-state MoFe protein is indeed ‘gated’ by a conformational transition that activates ET.

Figure 2-3 presents plots of $\log k_2$ vs the molality for each solute employed. Each plot is linear, revealing that osmotic pressure effects generate the changes in k_2 . This is confirmed by noting that, in all cases, the changes are larger than could be generated by viscosity effects alone. For example, with sucrose as solute, for $m = 2$ the increased viscosity could at most cause k to decrease by $1/0 \approx 1/5$, whereas the measured decrease is more than $1/10$; more dramatically, for glycerol as solute, with $m = 3.2$ the increased viscosity could at most cause a reduction of $\sim 1/2$, whereas k_2 decreases by $\sim 1/15$. In fact, it appears that viscosity plays *no* role in the solute-induced changes in ET. The plots of k_2 vs m for PEG300 and 600 completely overlay, although the viscosities differ by roughly a factor of two at any given molality, and thus the slopes of the plots should differ likewise if the ET rate constant varied inversely with viscosity.

When k_2 is controlled by osmotic pressure effects, the slope of the plot of $\log k$ vs m is proportional to $[-\Delta n]$ for the conformational conversion (see above).¹³ The negative slopes in **Fig 2-3** thus correspond to an *uptake* of waters, $\Delta n > 0$. Multiple osmolytes were employed because the value of Δn measured in osmotic pressure experiments in general differs among solutes because they can interact with the protein surface in different ways, displacing different numbers of bound waters and yielding different apparent values for Δn .¹³ The osmolyte whose slope is greatest interacts least and displaces the fewest waters, thereby giving the best value for Δn . In this study that osmolyte is sucrose,¹⁸ and its slope in **Figure 2-3** gives, $\Delta n \sim + 80$ as the best available

value lower bound for the number of waters that bind to newly exposed surfaces during the conformational transition.

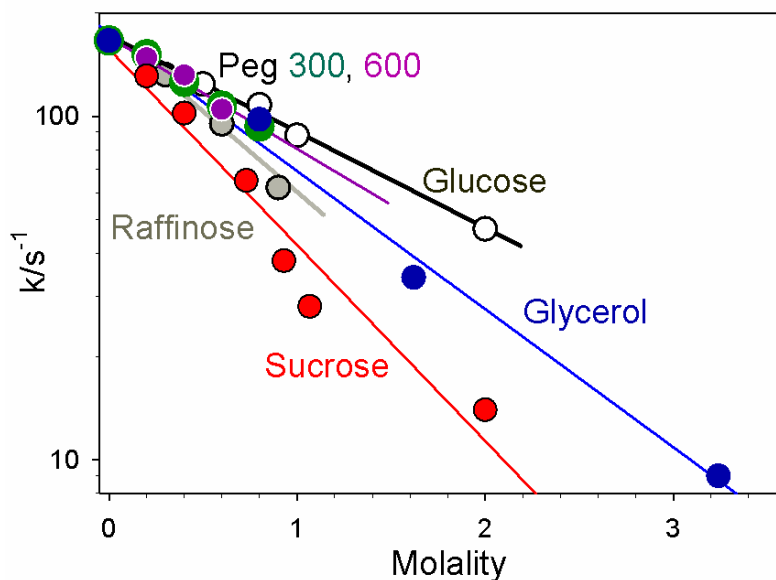


Figure 2-3: Log of the rate constants for oxidation of Fe^{red} within the $[\text{Fe}^{\text{red}}(\text{MgATP})_2:\text{MoFe}]$ complex as a function of osmolyte concentration.

Taking roughly one water to be bound per $\Delta A^0 \sim 10 \Delta^2$ of exposed surface, the binding of $\Delta n \sim 80$ waters would correspond to a conformational transition in which $\Delta A \sim 800 \Delta^2$ of surface becomes exposed. To calibrate this value, the ‘ADP’ structure of the $[\text{Fe}:\text{MoFe}]$ complex (**Figure 2-1**) exposes $\sim 2000 \Delta^2$ more protein surface than does the ‘ATP’ structure.^{3,4} Thus, the conformational change revealed by the present measurements can be plausibly attributed to the kind of large-scale motion of the Fe protein relative to MoFe protein shown in **Figure 2-1**, but likely one that is of somewhat lesser extent and thus exposes correspondingly less surface. However, one cannot rule out other types of structural changes.

Is this gated oxidation of Fe^{red} coupled to ATP hydrolysis? To test this we measured the solvent kinetic isotope effect, $sKIE = k_2(\text{H}_2\text{O})/k_2(\text{D}_2\text{O})$, for Fe^{red} oxidation. ATP hydrolysis is accompanied by the release of 0.5 protons/ATP,¹⁰ so if it were involved in the intra-complex oxidation of Fe^{red} , one would expect $sKIE \gg 1$. However, within error, we find that the oxidation of Fe^{red} has no kinetic isotope effect: $sKIE = 1$ (**Figure 2-1**). This indicates that ATP is not hydrolyzed during Fe^{red} oxidation,

How does conformational activation facilitate ET? One possibility is that it generates a transition state for Fe^{red} oxidation whose structure is optimized for direct ET from the $[\text{4Fe-4S}]^{1+}$ cluster of Fe^{red} to FeMo-co. If the transition state occurs along an (imagined) reaction coordinate whose beginning and end points are the ATP-like and ADP-bound structures, **Figure 2-1**, it is unlikely that the conformational changes would enhance ET by decreasing the donor-acceptor distance: this transition *increases* the distances from the $[\text{4Fe-4S}]$ cluster of the Fe protein to both the P cluster and FeMo-co.³ Among other possibilities, one may, imagine that the Δn waters being bound include ordered water in the interface of the active complex, and that those enhance ET.¹⁹

Alternatively, one would expect an absence of viscosity effects if the solute effects were indeed wholly energetic, and did not operate on a dynamical process. This could occur if the rate-limiting step were preceded by a rapid pre-equilibrium between the energetically favored structure of the ATP-bound form of the complex and a higher-energy structure activated for ET, **eq 1**:



The gating limit embodied in **eq 1**⁷ has been termed “conformational coupling.”⁹ If the activated structure binds Δn additional waters, then K^* , and thus the observed ET rate constant, $k_2 = kK^*$, would be independent of viscosity but vary exponentially with the osmolyte molality (m), in agreement with experiment (**Figure 2-3**).¹³

Experiments are under way to test the assignment of the gating motions to rearrangements such as those in **Figure 2-1**, the alternate mechanisms noted above, and the role of the P cluster. It seems likely to us that the nitrogenase complex employs a “compound” ET gate, with the gating motions revealed here being followed by as yet unknown conformational changes, at least some within the MoFe protein, which trigger events such as intra-MoFe ET, ATP hydrolysis,¹⁰ Pi release,¹¹ and dissociation of the complex.

REFERENCES

- (1) Burgess, B. K.; Lowe, D. J. *Chem. Rev. (Washington, D. C.)* **1996**, *96*, 2983-3011.
- (2) Seefeldt, L. C.; Hoffman, B. M.; Dean, D. R. *Annu. Rev. Biochem.* **2009**, *78*, 701-722.
- (3) Tezcan, F. A.; Kaiser, J. T.; Mustafi, D.; Walton, M. Y.; Howard, J. B.; Rees, D. C. *Science (Washington, DC, U. S.)* **2005**, *309*, 1377-1380.
- (4) Rees, D. C.; Tezcan, F. A.; Haynes, C. A.; Walton, M. Y.; Andrade, S.; Einsle, O.; Howard, J. B. *Phil. Trans. R. Soc. A* **2005**, *363*, 971-984.
- (5) Lanzilotta, W. N.; Parker, V. D.; Seefeldt, L. C. *Biochemistry* **1998**, *37*, 399-407.
- (6) Syrtsova, L. A.; Kotel'nikov, A. I.; Shkondina, N. I.; Lapshina, M. A. *Kinet. Catal.* **2004**, *45*, 31-39.
- (7) Hoffman, B. M.; Ratner, M. R. *J. Am. Chem. Soc.* **1987**, *109*, 6237-6243.

- (8) Patel, A. D.; Nocek, J. M.; Hoffman, B. M. *J. Phys. Chem.* **2008**, *112*, 11827-11837.
- (9) Davidson, V. L. *Acc. Chem. Res.* **2008**, *41*, 730-738.
- (10) Thorneley, R. N. F.; Ashby, G.; Howarth, J. V.; Millar, N. C.; Gutfreund, H. *Biochem. J.* **1989**, *264*, 657-661.
- (11) Lowe, D. J.; Ashby, G. A.; Brune, M.; Knights, H.; Webb, M. R.; Thorneley, R. N. F. In *Nitrogen Fixation: Fundamentals and Applications*; Tikhonovich, I. A., Ed.; Kluwer Academic Publishers: 1995; pp 103-108.
- (12) Steinfeld, J. I.; Francisco, J. S.; Hase, W. L. *Chemical Kinetics and Dynamics*; 2nd ed.; Prentice-Hall, Inc.: Upper Saddle River, New Jersey, 1999.
- (13) Parsegian, V. A.; Rand, R. P.; Rau, D. C. *Methods Enzymol.* **1995**, *259*, 43-94.
- (14) Oxidation of Fe^{red} to Fe^{ox} was followed at 430 nm with a Hi-Tech Instruments stopped-flow system placed inside an Ar-filled glove box. To compensate for absorbance changes from MgATP binding to Fe^{red}, a trace collected by mixing Fe^{red} with the MgATP solution was subtracted from each experimental trace. Fe and MoFe proteins were purified as described: Christiansen, J.; Goodwin, P. J.; Lanzilotta, W. N.; Seefeldt, L. C.; Dean, D. R. *Biochemistry* **1998**, *37*, 12611-12623.
- (15) Lowe, D. J.; Fisher, K.; Thorneley, R. N. F. *Biochem. J.* **1993**, *292*, 93-98.
- (16) Fisher, K.; Lowe, D. J.; Tavares, P.; Pereira, A. S.; Huynh, B. H.; Edmondson, D.; Newton, W. E. *J. Inorg. Biochem.* **2007**, *101*, 1649-1656.
- (17) Wilson, P. E.; Nyborg, A. C.; Watt, G. D. *Biophys. Chem.* **2001**, *91*, 281-304.
- (18) Indeed, it has been noted that sucrose behaves as an ideal solute for osmotic pressure studies, as it forms H-bonds with water with similar energetics to water-

water H-bonds and does not change the apparent density of water: Martinez-Julvez, M.; Medina, M.; Velazquez-Campoy, A. *Biophys. J.* **2009**, *96*, 4966-4975.

- (19) Lin, J.; Balabin, I. A.; Beratan, D. N. *Science (Washington, DC, U. S.)* **2005**, *310*, 1311-1313.

CHAPTER 3

**ELECTRON TRANSFER WITHIN NITROGENASE: EVIDENCE FOR A
DEFICIT SPENDING MECHANISM***

ABSTRACT

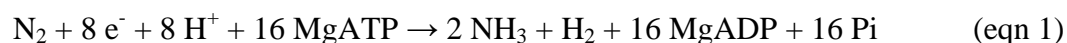
The reduction of substrates catalyzed by nitrogenase utilizes an electron transfer (ET) chain comprised of three metalloclusters distributed between the two component proteins, designated as the Fe protein and the MoFe protein. The flow of electrons through these three metalloclusters involves ET from the [4Fe-4S] cluster located within the Fe protein to an [8Fe-7S] cluster, called the P cluster, located within the MoFe protein and ET from the P cluster to the active site [7Fe-9S-X-Mo-homocitrate] cluster called FeMo-cofactor, also located within the MoFe protein. The order of these two electron transfer events, the relevant oxidation states of the P-cluster, and the role(s) of ATP, which is obligatory for ET, remain unknown. In the present work, the electron transfer process was examined by stopped-flow spectrophotometry using the wild-type MoFe protein and two variant MoFe proteins, one having the α -188^{Ser} residue substituted by cysteine and the other having the β -153^{Cys} residue deleted. The data support a "deficit-spending" model of electron transfer where the first event (rate constant 168 s^{-1}) is ET from the P cluster to FeMo-cofactor and the second, "backfill", event is fast ET (rate constant $>1700 \text{ s}^{-1}$) from the Fe protein [4Fe-4S] cluster to the oxidized P cluster. Changes in osmotic pressure reveal that the first electron transfer is conformationally gated, whereas the second is not. The data for the β -153^{Cys} deletion MoFe protein variant

*Coauthored by Karamatullah Danyal, Dennis Dean, Brian M. Hoffman and Lance C. Seefeldt (2011) *Biochemistry* 50 (43), pp 9255-9263. Copyright 2011 American Chemical Society. Reprinted with Permission.

provide an argument against an alternative two-step “hopping” ET model that reverses the two ET steps, with the Fe protein first transferring an electron to the P cluster, which in turn transfers an electron to FeMo-cofactor. The roles for ATP binding and hydrolysis in controlling the ET reactions were examined using $\beta\gamma$ -methylene-ATP as a pre-hydrolysis ATP analog and $\text{ADP} + \text{AlF}_4^-$ as a post-hydrolysis analog (a mimic of $\text{ADP} + \text{P}_i$).

INTRODUCTION

The reduction of N_2 to two ammonia molecules by nitrogenase requires eight electrons and eight protons, with two of the electrons and protons resulting in one H_2 formed for each N_2 reduced (eqn 1) (1).



For the Mo-dependent nitrogenase, electrons are delivered to substrates via an electron transfer (ET) chain comprised of three metal clusters that starts at the reduced $[\text{4Fe-4S}]^{1+}$ cluster in the Fe protein (designated as F^{1+} cluster) (2), then goes to the $[\text{8Fe-7S}]$ (P-cluster) in the MoFe protein, (3, 4) and ends on the $[\text{7Fe-9S-X-Mo-homocitrate}]$ cluster or FeMo-cofactor (M cluster) in the MoFe protein (5), where substrates bind and are reduced (**Figure 3-1**). Transfer of a single electron to the FeMo-cofactor is initiated when the Fe protein transiently associates with the MoFe protein, with each ET event coupled to the hydrolysis of two MgATP molecules (1). This ET event has recently been shown to be conformationally gated (6–8). The order of MgATP hydrolysis and ET and the nature of their coupling remain unknown, although there is evidence to suggest that MgATP hydrolysis follows ET (1, 6, 9, 10). After ET and hydrolysis of MgATP, the oxidized Fe protein dissociates from the MoFe protein, enabling the MoFe protein to bind

another reduced, MgATP-containing, Fe protein (11). This cycle must be repeated a sufficient number of times to support the reduction of the bound substrate.

At least three different models can be considered for the ATP-coupled delivery of an electron from the Fe protein to the catalytic site FeMo-cofactor. In "direct" ET, the Fe protein would reduce FeMo-cofactor directly, skipping the P cluster. The known distances and driving forces make this option theoretically possible (12, 13), but there are several lines of evidence against such a model, including evidence for changes in oxidation state of the P cluster during turnover (3, 4), and the location of the P cluster 'in-line' between the F and M clusters in X-ray structures of Fe protein-MoFe protein complexes (14–16). In a "sequential" or "hopping" model for ET, the rate-limiting step is the initial transfer of an electron from the reduced $[4\text{Fe-4S}]^{1+}$ cluster of the Fe protein (F^{1+}) to the resting state of the P cluster (P^{N}), generating a 'super-reduced' P-cluster (P^{S}). This initial inter-component ET step would then be followed by rapid intra-molecular ET from P^{S} to FeMo-cofactor (M^{N}), resulting in the resting P^{N} state and reduced FeMo-cofactor (M^{R}). This model is not attractive because it would require the reduction of the all ferrous P cluster (P^{N}) to a state (P^{S}) that has never been observed for the P cluster (17, 18). In fact, the reduction of an FeS cluster beyond the all ferrous state has never been observed for any protein (19–22).

A third model can be denoted "deficit-spending." In this model, the first ET event involves the transfer of an electron from the P^{N} -cluster to FeMo-cofactor ($\text{P}^{\text{N}} \rightarrow \text{M}^{\text{N}}$), resulting in the formation of a P-cluster state that has been oxidized by one electron relative to the resting P^{N} state (P^{1+}) and reduction of the M cluster by one

electron (M^R). The electron “deficit” in the P-cluster is then erased by “back-fill” ET from the Fe protein to the oxidized P cluster ($F^{1+} \rightarrow P^{1+}$). This model is the most attractive of the three, being consistent with the available information, although this model has yet to be experimentally tested.

In the present work, we have conducted stopped-flow kinetic measurements of ET from the reduced Fe protein to MoFe protein of nitrogenase that test both the deficit-spending and hopping models of ET and examine the roles of ATP binding/hydrolysis and protein conformational activation in ET. Key to these studies are two MoFe protein variants with different amino acid substitutions. In one, the β -153^{Cys} ligand to the P cluster was deleted, a change which tests aspects of the hopping model for ET. In the other, the β -188^{Ser} located in close proximity to the P cluster (**Figure 3-2**) was substituted by cysteine, giving a MoFe protein that contains a P cluster that exists extensively in an oxidized state (P^{1+}), (4). This feature was explained by a negative shift in E_m for the $P^{1+/N}$ couple (estimated to be -90 mV) that leaves P^{1+} as the majority state (~ 65%) even in the presence of the reductant dithionite, with the remaining 35 % in the P^N state. It was also suggested that E_m of the P cluster shifts because β -188^{Cys} forms a P-cluster ligand, thereby stabilizing the P^{1+} state. The availability of a catalytically competent MoFe protein whose P-cluster exhibits both P^N and P^{1+} states in the resting enzyme presented an opportunity to test the deficit-spending model by kinetic analysis of inter-component ET from Fe protein to the substituted MoFe protein through experiments both in aqueous buffer and in solutions of varying osmotic pressure. The roles for ATP binding and hydrolysis in controlling the electron transfer reactions were examined using β -methylene-ATP as a pre-hydrolysis ATP analog and $ADP + AlF_4^-$ as a post-hydrolysis

analog (a mimic of ADP + P_i).

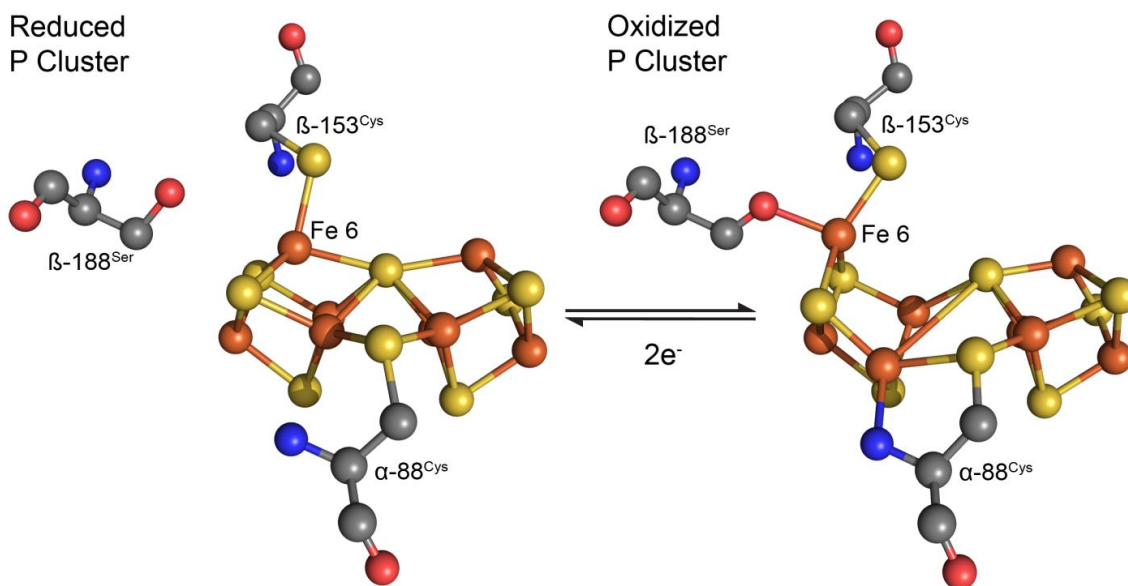


Figure 3-2: P-cluster in the oxidized and reduced states. Shown is the P-cluster in the reduced (P^N) state (left) and in the oxidized (P^{1+}) state (right) with the amino acids β -153^{Cys}, β -188^{Ser}, and α -88^{Cys} shown. Structures were generated from the PDB files 1M1N and 2MIN.

Materials and Methods

Materials and protein purification. All reagents were obtained from Sigma-Aldrich Chemicals (St. Louis, MO). *Azotobacter vinelandii* strains DJ995 (wild-type MoFe protein), DJ1190 (β -188^{Cys} MoFe protein), DJ1193 (β -188^{Cys} MoFe protein expressed in a $\Delta nifB$ background, resulting in a protein lacking FeMo-cofactor, called the apo- β -188^{Cys} MoFe protein), DJ1158 (β -153^{deletion} MoFe protein), and DJ1003 (wild-type MoFe protein expressed in a $\Delta nifB$ background, resulting in a protein lacking FeMo-

cofactor, called the apo-wild-type MoFe protein) were grown and nitrogenase MoFe proteins were expressed as described previously (23). All MoFe proteins contained a seven-histidine tag on the α -subunit. This allowed purification of each protein using the previously described metal affinity chromatography protocol (23). Based on SDS-PAGE analysis using Coomassie blue staining, all proteins were found to be greater than 95% homogeneous. The rates for proton reduction were determined using previously established protocols (24). The activity for wild-type MoFe was found to be ~2100 nmols H_2 /min/mg MoFe protein while the activity of β -188^{Cys} was found to be ~1200 nmols H_2 /min/mg MoFe protein, similar to previously reported values (4). Septum sealed vials, degassed and under an argon atmosphere, were used for all manipulation of proteins. Gastight syringes were used to transfer all gasses and liquids.

Stopped-flow spectrophotometry. Electron transfer (ET) from Fe protein to MoFe protein was monitored by the increase in absorbance at 430 nm. This increase in absorbance results from the oxidation of the Fe protein [4Fe-4S] from its reduced (1+) state to its oxidized (2+) state. The change in absorbance was monitored as a function of time after mixing in a Hi-Tech SF61 stopped-flow UV-visible spectrophotometer equipped with a data acquisition and curve fitting system (Salisbury, Wilts, U.K.). The sample handling unit was kept inside an N_2 -filled glovebox while the temperature of the reaction solutions was controlled using a circulating water bath kept outside the glovebox (25). All reactions were carried out at a temperature of 25°C, in a 100 mM HEPES buffer, pH 7.4, with 10 mM dithionite. The Fe protein and MoFe protein, when present, were contained in one drive syringe of the stopped-flow. The other drive syringe contained buffer with or without a nucleotide. The final concentrations of proteins and nucleotides

were chosen to provide two Fe proteins for each MoFe protein along with excess ATP as specified in the legends to the figures. The instrument dead-time following mixing was approximately 2 ms. Earlier work showed that the absorbance increase associated with the $F^{1+} \rightarrow F^{2+}$ oxidation can be followed by slower absorbance decreases related to re-reduction of F^{2+} (26). As we are concerned only with the F^{1+} oxidation step, the overall time-course of a stopped-flow trace was fit to the equation for a first-order sequential reaction corresponding to $F^{1+} \rightarrow F^{2+} \rightarrow F^{1+}$ reaction; we report only the observed rate constant, k_{obs} , for the $F^{1+} \rightarrow F^{2+}$ step, as the follow-up reaction involves multiple processes, including dissociation of the Fe-MoFe protein complex. The fits to this kinetic scheme were carried out in Sigmaplot (Systat Software Inc, San Jose, CA). Osmotic pressure effects on the ET rate were examined as described (6).

Results

ET from Fe protein to MoFe protein. Pre-steady state ET from the Fe protein to the resting-state MoFe protein is monitored through measurement of the increase in the absorbance at 430 nm that accompanies the oxidation of F^{1+} to F^{2+} (27, 28). Stopped-flow mixing of reduced Fe protein with wild-type resting-state MoFe protein in the presence of saturating MgATP yields stoichiometric oxidation of F^{1+} (**Figure 3-3**) in a process that is exponential, with a rate constant, $k_{\text{obs}} = 168 \text{ s}^{-1}$, that is consistent with earlier studies (26).

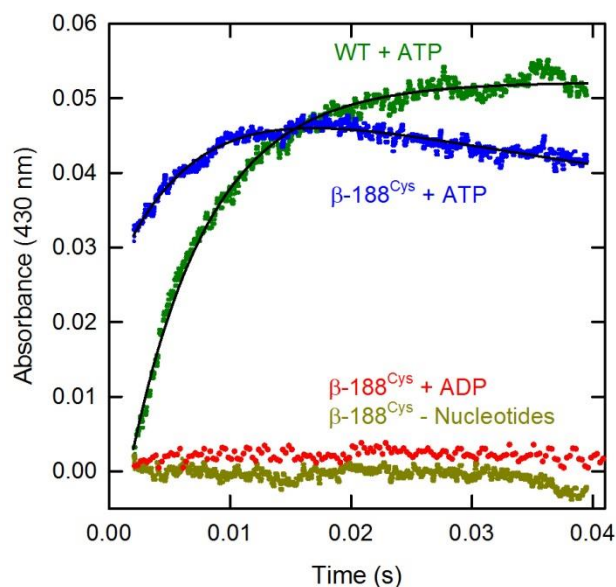


Figure 3-3: Electron transfer from the Fe protein to MoFe proteins monitored by stopped-flow spectroscopy. Shown is the absorbance at 430 nm plotted against the time after mixing Fe protein (75 μM) and MoFe proteins (20 μM) in one syringe against different solutions (without or with nucleotides at 18 mM). Shown is wild-type MoFe protein and Fe protein mixed with MgATP (WT+ ATP, green); $\beta\text{-188}^{\text{Cys}}$ MoFe protein and Fe protein mixed with MgATP ($\beta\text{-188}^{\text{Cys}} + \text{ATP}$, blue); $\beta\text{-188}^{\text{Cys}}$ MoFe protein and Fe protein mixed with MgADP ($\beta\text{-188}^{\text{Cys}} + \text{ADP}$, orange); and $\beta\text{-188}^{\text{Cys}}$ MoFe protein and Fe protein mixed with buffer without nucleotides ($\beta\text{-188}^{\text{Cys}} - \text{nucleotides}$, light green). The top two sets of data were fit to a single exponential (solid lines) for the wild-type MoFe protein data and to a single exponential with a decline for the $\beta\text{-188}^{\text{Cys}}$ MoFe protein data, with determined rate constants of 168 s^{-1} (WT+ATP) and 187 s^{-1} ($\beta\text{-188}^{\text{Cys}} + \text{ATP}$). The mixing dead-time is $\sim 2 \text{ ms}$. Other parameters and equations for fits are described in Materials and Methods.

When the β -188^{Cys} MoFe protein is mixed with reduced Fe protein plus MgATP, the absorbance change indicates that ET associated with oxidation of F¹⁺ also is stoichiometric (**Figure 3-3**). However, unlike reaction with the wild-type MoFe protein, the Fe protein oxidation by β -188^{Cys} MoFe protein shows an ET "burst", with ~ 65 % of the F¹⁺ oxidation occurring during the instrument dead-time (2 ms). The remaining 35% oxidation occurs with a resolved time-course that can be fit to an exponential with a rate constant $k_{\text{obs}} = 187 \text{ s}^{-1}$, essentially the same as observed for the wild-type MoFe protein (25). The β -188^{Cys} MoFe protein in dithionite solution was earlier shown to exist as an equilibrium mixture of 3 states of the P cluster (P¹⁺, P²⁺, and P^N), with the total contribution from the two oxidized forms, being ~ 65 % of the enzyme present with ~ 35 % existing as the resting oxidation state, P^N (4). The kinetically resolved phase of the stopped-flow trace, with rate constant equivalent to that for wild-type MoFe protein, is thus assigned to oxidation of F¹⁺ by β -188^{Cys} MoFe protein in the P^N/M^N state, with the "burst" ET phase being assigned to rapid oxidation of F¹⁺ by P¹⁺ of the β -188^{Cys} MoFe protein in the P¹⁺/M^N state. This assignment is confirmed below.

In a separate study, when the β -153^{Cys} of the MoFe protein was deleted, this MoFe protein variant showed stoichiometric oxidation of F¹⁺ with a rate constant essentially unchanged from that observed to the wild-type MoFe protein.

The roles of nucleotides in ET. We next consider the contributions of nucleotides to the ET events to the β -188^{Cys} MoFe protein. Both the binding and hydrolysis of ATP within the Fe protein is intimately linked to ET from the Fe protein to the wild-type MoFe protein during substrate reduction. MgADP and MgATP analogs do not support the ET reaction (29). As shown in **Figure 3-3**, MgADP also does not support

oxidation of the Fe protein by the β -188^{Cys} MoFe protein: neither the burst nor the resolved kinetic phases are observed. Thus, it can be concluded that MgATP binding, at a minimum, is required for both the burst-phase reduction of P^{1+} of the β -188^{Cys} MoFe protein in the P^{1+}/M^N state as well as the resolved ET to the P^N/M^N state.

To further differentiate the respective roles of ATP binding and hydrolysis in ET from the Fe protein to the β -188^{Cys} MoFe protein, ET reactions were monitored in the presence of ATP analogs. The complex between Fe protein and MoFe protein that contains the non-hydrolyzable analog $\beta\gamma$ -methylene-ATP was earlier shown to induce conformational changes in the Fe protein similar to those induced by MgATP, yet the analog is not hydrolyzed by nitrogenase (30–33). As previously reported (30), $\beta\gamma$ -methylene-ATP does not support ET from the Fe protein to the wild-type MoFe (**Figure 3-4**). Likewise, this analog does not support the resolved phase of Fe protein oxidation by the β -188^{Cys} MoFe protein. However, this ATP analog does support the burst ET from the Fe protein to P^{1+} . Thus, the conformational changes in the Fe protein and/or in the Fe protein-MoFe protein complex induced by binding of $\beta\gamma$ -methylene-ATP are sufficient to enable the rapid $F^{1+} \rightarrow P^{1+}$ ET, but not the ET from F^{1+} to the MoFe protein in the P^N/M^N state.

It has been proposed for several ATP-hydrolyzing enzymes (34, 35), including nitrogenase, that the state following ATP hydrolysis, but before Pi release, [MoFe-Fe(2MgADP + 2 Pi)], is simulated when MgADP + AlF_4^- is bound (15). In the wild-type nitrogenase, this analog induces a tight complex between the Fe protein and the MoFe protein (15, 36). This complex does not exhibit the normal Fe protein oxidation, only very slow ET from Fe protein to MoFe protein. In agreement with this, we observe no

ET over the normal observation times (0.5 s) for a complex that includes wild-type MoFe protein, reduced Fe protein, and this nucleotide analog (**Figure 3-5, panel B**). Likewise, the resolved phase of Fe protein oxidation is suppressed in the β -188^{Cys} MoFe protein-Fe[MgADP + AlF₄⁻] protein complex; however, the complex shows that the burst oxidation of the Fe protein during the mixing time is preserved (**Figure 3-5, panel A**). Thus, both the non-hydrolyzable ATP analog, $\beta\gamma$ -methylene-ATP, and the analog for ADP + Pi, MgADP + AlF₄⁻, promote the rapid $F^{1+} \rightarrow P^{1+}$ ET reaction, whereas neither analog supports the resolved ET from the Fe protein to either wild-type or β -188^{Cys} MoFe protein that contains P^N.

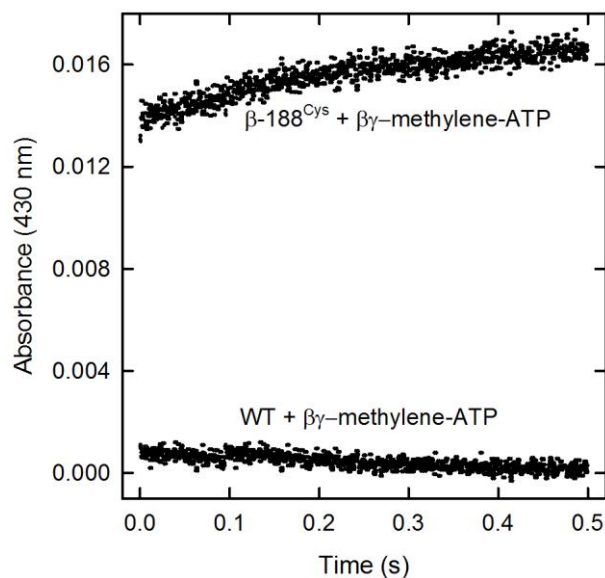


Figure 3-4: Electron transfer from Fe protein to MoFe proteins with the nucleotide analog $\beta\gamma$ -methylene ATP. Shown is the absorbance at 430 nm plotted against the time after mixing Fe protein (75 μ M) and MoFe proteins (20 μ M) in one syringe with the nucleotide analog $\beta\gamma$ -methylene-ATP (18 mM). Shown are β -188^{Cys} MoFe protein and Fe protein mixed against $\beta\gamma$ -methylene-ATP (β -188^{Cys} + $\beta\gamma$ -methylene-ATP); and wild-type MoFe protein and Fe protein mixed against $\beta\gamma$ -methylene-ATP (WT + $\beta\gamma$ -methylene-ATP).

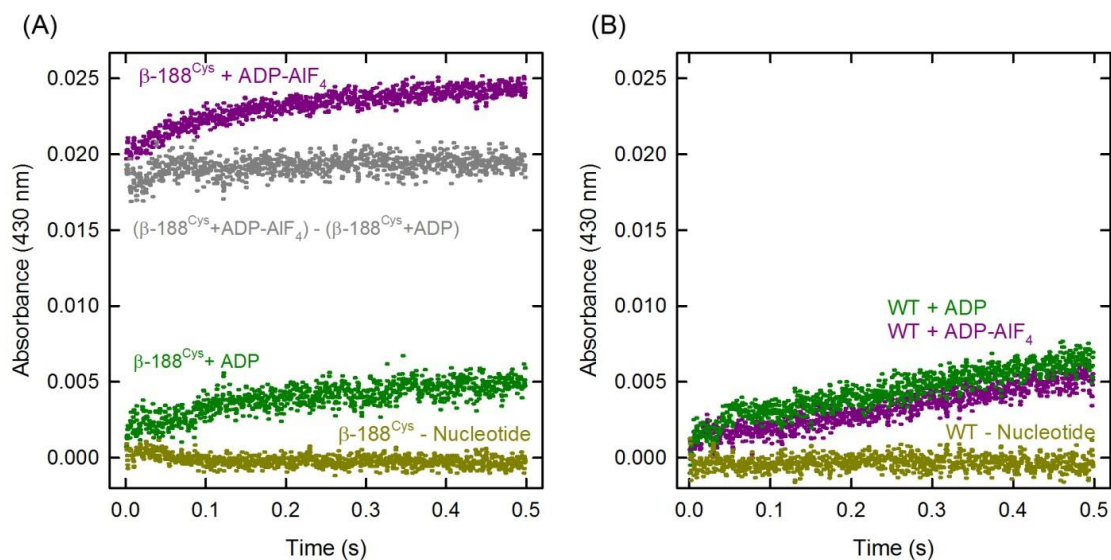


Figure 3-5: Electron transfer from Fe protein to MoFe proteins with the nucleotide analog MgADP-AIF₄⁻. Shown is the absorbance at 430 nm plotted against the time after mixing MoFe protein (20 μM) and Fe protein (75 μM) with buffer (without or with nucleotide, 10 mM) in the stopped-flow. Shown in **panel A** is $\beta\text{-188}^{\text{Cys}}$ MoFe protein and Fe protein mixed with MgADP-AIF₄⁻ ($\beta\text{-188}^{\text{Cys}} + \text{MgADP-AIF}_4^-$, purple); with MgADP ($\beta\text{-188}^{\text{Cys}} + \text{MgADP}$, green); without nucleotide ($\beta\text{-188}^{\text{Cys}} - \text{nucleotide}$, light green). Also shown is the difference spectrum ($(\beta\text{-188}^{\text{Cys}} + \text{ADP-AIF}_4^-) - (\beta\text{-188}^{\text{Cys}} + \text{ADP})$, grey). Shown in **panel B** is wild-type MoFe protein and Fe protein mixed with MgADP (WT + ADP, green); with ADP-AIF₄⁻ (WT + ADP-AIF₄⁻, purple); and without nucleotide (WT - nucleotide, light green).

The role of FeMo-cofactor in the ET. Electrons transferred into the MoFe protein ultimately end up on FeMo-cofactor. If the ET burst observed when $\beta\text{-188}^{\text{Cys}}$ MoFe protein and Fe protein are mixed with MgATP indeed reflects ET from the Fe protein [4Fe-4S] cluster to P¹⁺, then the FeMo-cofactor should not be involved in this ET event and its absence should have no influence on the observed ET burst. To test this, we purified variants of both wild-type and $\beta\text{-188}^{\text{Cys}}$ MoFe proteins that do not contain FeMo-cofactor (called apo-wild-type and apo- $\beta\text{-188}^{\text{Cys}}$ MoFe proteins) (4, 23). When apo-wild-type MoFe protein is used, no ET is observed (**Figure 3-6**). When the apo- $\beta\text{-188}^{\text{Cys}}$ MoFe protein and Fe protein were mixed against MgATP, the stopped-flow trace exhibited an

ET burst that was indistinguishable from that seen for the FeMo-cofactor containing β -188^{Cys} MoFe protein (**Figure 3-6**), while the slower, resolved phase was absent. These observations confirm that the kinetically resolved ET represents $P^N \rightarrow M^N$ ET, whereas the burst observed for the β -188^{Cys} is $F^{1+} \rightarrow P^{1+}$ ET.

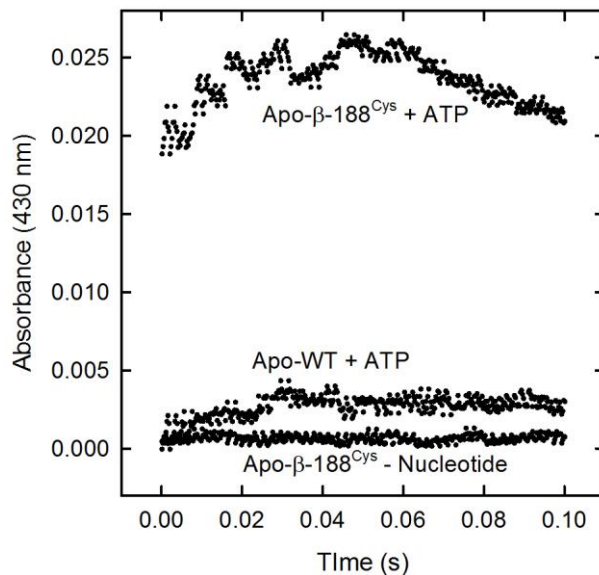


Figure 3-6: Electron transfer from Fe protein to apo-MoFe proteins. Shown is the absorbance at 430 nm plotted against the time after mixing Fe protein (75 μ M) and MoFe protein (42 μ M) with buffer (without or with nucleotides, 10 μ M) in the stopped-flow. Shown are apo- β -188^{Cys} MoFe and Fe protein mixed with MgATP (Apo- β -188^{Cys} + ATP); apo-wild-type MoFe protein and Fe protein mixed with MgATP (Apo-WT + ATP); and apo- β -188^{Cys} MoFe and Fe protein mixed with buffer lacking nucleotides (apo- β -188^{Cys} - nucleotides). See the legend to Figure 3-6 for other details.

Conformationally gated ET. Recently, it was shown that the rate of ET from the Fe protein to the wild-type MoFe protein is sensitive to osmotic pressure, indicating that the rate-limiting step in the ET reaction is gated by large protein conformational changes (6). Changes in osmotic pressure modulate the energetics of reactions that involve conformational changes in which the number of bound waters is changed. The rate constant (k_m) for such a process varies exponentially with the molality (m) of added

solute according to the equation, $k_m \propto \exp[-(\Delta n/55.6)m]$, where Δn is the number of waters absorbed in the transformation (6).

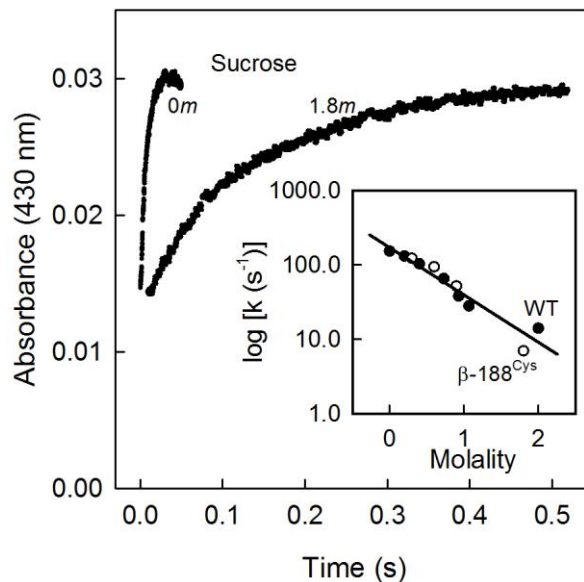


Figure 3-7: Osmotic pressure effects on electron transfer reactions from Fe protein to MoFe protein. Stopped-flow traces for ET from the Fe protein to the β -188^{Cys} MoFe protein in the presence of 0, 0.6, 0.9 and 1.8 m sucrose (traces for 0 and 1.8 m sucrose are shown). The observed slow phases of the traces were fit to an exponential function to determine the rate constant (k_{obs}). (Inset) The log of the rate constants (k_{obs}) are plotted against the osmotic pressure of sucrose (m) for the β -188^{Cys} (open circle) and wild-type (WT, closed circle) MoFe proteins and the points are collectively fit to a straight line.

Repeating this experiment with β -188^{Cys} MoFe protein shows that the relative proportions of the burst and resolved ET phases are independent of the presence of sucrose as osmolyte up to a sucrose concentration of ~ 2 m (**Figure 3-7**). This indicates that the presence of the osmolyte does not alter the reduction potential of P cluster, which would alter the relative proportions of P^{1+} and P^N forms and thus the relative contributions of the two kinetic phases. Unlike the burst phase, the resolved phase of the ET is dependent on osmotic pressure. The inset to **Figure 3-7** shows that rate constants ($k_{obs}(m)$) for ET from Fe protein to either the wild-type MoFe protein or the resolved

phase ET to the β -188^{Cys} MoFe protein have essentially identical responses to sucrose addition, with the rate constants depending exponentially on the molality (m) of added sucrose with a slope corresponding to $\Delta n \sim + 80$ waters. Taking roughly one water to be bound per $\sim 10 \text{ \AA}^2$ of exposed surface, $\Delta n \sim 80$ waters would correspond to a conformational transition in which $\sim 800 \text{ \AA}^2$ of surface becomes exposed (6).

The present results thus indicate that ET to the MoFe state that contains P^N and M^N is conformationally gated in both wild-type MoFe and β -188^{Cys} MoFe protein, and that the amino acid substitution of β -188^{Ser} by a cysteine does not alter the conformational gate. In contrast, the presence of sucrose osmolyte up to 2 m does not affect the burst ET to the point where it becomes visible after the dead-time of the instrument. These results suggest that whereas the resolved oxidation of F^{1+} by the MoFe protein in the P^N/M^N state is conformationally gated, the rapid $F^{+1} \rightarrow P^{1+}$ ET event is not.

Discussion

While a deficit-spending scheme for nitrogenase ET events is the most reasonable of the three proposed, this model has proven difficult to test experimentally. For example, until now it has not been possible to measure the contributions of the individual inter- and intra-molecular ET events postulated by this model (k_{FP} and k_{PM} , respectively, **Figure 3-1**, panel B) to the observed ET rate constant (k_{obs}). We discuss how the experiments described in this report support a deficit-spending model of ET in nitrogenase and further argue against a hopping ET scheme, and provide insights into the roles of nucleotides in ET. We conclude by presenting a model for the sequence of events for the entire nitrogenase ET cycle that integrates the present results with earlier findings.

ET by a deficit-spending mechanism. In the present work, the deficit spending model was addressed by using the β - ^{188}Cys -substituted MoFe protein, which has P^{1+} in the resting state (4). This situation offered the opportunity to directly monitor the $\text{F}^{1+} \rightarrow \text{P}^{1+}$ ET event (backfill) without the need for a prior $\text{P}^{\text{N}} \rightarrow \text{M}^{\text{N}}$ ET step. For this substituted protein, the rapid intermolecular ET event from the Fe protein to the MoFe protein could be assigned to the $\text{F}^{1+} \rightarrow \text{P}^{1+}$ ET event, which was found to be faster than the dead-time of the stopped-flow instrument with a rate constant that can be estimated $k_{FP} > 1700 \text{ s}^{-1}$. This rate constant is far greater than $k_{obs} = 168 \text{ s}^{-1}$ observed for ET from the Fe protein to MoFe protein in the $\text{P}^{\text{N}}/\text{M}^{\text{N}}$ state, indicating that intramolecular $\text{P}^{\text{N}} \rightarrow \text{M}^{\text{N}}$ ET is the rate-limiting step.

In the ET traces for β - ^{188}Cys -substituted MoFe protein, the initial ET burst assigned to $\text{F}^{1+} \rightarrow \text{P}^{1+}$ is followed by a slower resolved ET phase. This slower phase is assigned to ET from the Fe protein to the β - ^{188}Cys MoFe protein in the $\text{P}^{\text{N}}/\text{M}^{\text{N}}$ state., and its rate constant is the same as that observed for ET from the Fe protein to the wild-type MoFe protein in the $\text{P}^{\text{N}}/\text{M}^{\text{N}}$ state. Thus, measurement of electron transfer using the β - ^{188}Cys -substituted MoFe protein reveals both the $\text{F}^{1+} \rightarrow \text{P}^{1+}$ ET event observed as a burst and the $\text{P}^{\text{N}} \rightarrow \text{M}^{\text{N}}$ ET event observed as a slower, resolved phase.

These observations are in full accord with expectations based on the deficit-spending model. In this model, the $\text{P}^{\text{N}} \rightarrow \text{M}^{\text{N}}$ ET event is the rate-limiting step in ET from the Fe protein to the MoFe protein, and the observed ET rate constant for the oxidation of F^{1+} by the MoFe protein in the $\text{P}^{\text{N}}/\text{M}^{\text{N}}$ state is assigned to this event: $k_{obs} = k_{PM}$. The subsequent ‘backfill’ ET (k_{FP}) reaction, $\text{F}^{1+} \rightarrow \text{P}^{1+}$, does not contribute to the observed ET because it is at least 10-times faster. This sequence of ET events, with the

corresponding large differences in rate constants, provides an explanation for the fact that only very low levels of a P^{1+} or P^{2+} state have been observed by electron paramagnetic resonance (EPR) spectroscopy when the nitrogenase complex is freeze-trapped during steady-state turnover (1, 37, 38). Although the P^{1+} state is EPR active, it cannot build up to any appreciable concentration in the deficit-spending mechanism because the rate of reduction of P^{1+} by the Fe protein ($F^{1+} \rightarrow P^{1+}$) is much faster than the rate of oxidation of P^N by M cluster ($P^N \rightarrow M^N$), resulting in mostly the P^N state (which is EPR silent) under steady-state turnover.

Gated ET. The rate constant for ET from the Fe protein to the MoFe protein (k_{obs}) is sensitive to osmotic pressure, which has been assigned to protein conformational changes that gate the intermolecular ET event (6). This conformational change was calculated to involve exposure of a substantial ($>800 \text{ \AA}^2$) protein surface area (6). The present study shows no modulation of the rapid backfill ET ($F^{1+} \rightarrow P^{1+}$) by changes in osmotic pressure, suggesting that this ET step is not gated by protein conformational changes; in any case, this step is so rapid that it cannot be involved in determining the observed rate of ET. Thus, it can be concluded that the protein conformational gate for ET applies specifically to the $P^N \rightarrow M^N$ intramolecular ET step.

What conformational processes could be coupled to the $P^N \rightarrow M^N$ ET reaction? Examination of X-ray structures of various complexes of the Fe protein with the MoFe protein (with or without nucleotides bound) reveal large changes in the Fe protein-MoFe protein interface, involving changes in exposed protein surface area, but do not reveal any significant changes within the MoFe protein that could explain how the Fe protein with two bound 2ATP might activate the $P^N \rightarrow M^N$ ET (14). An attractive “compound

gate” model can be developed, however, from examination of the X-ray structure of an oxidized MoFe protein (P^{1+} , M^N) (39). From this structure, the P^{2+} cluster is stabilized by the coordination of the side-chain of β -188^{Ser} to an Fe atom of the P cluster (39). We suggest that conformational activation of resting-state MoFe protein by an as-yet unidentified change in the Fe protein-MoFe protein interface could cause the β -188^{Ser} side-chain to transiently coordinate to an Fe atom of P^N , thereby creating an activated state of the P cluster (designated P^{N*}) with a lowering of the potential to the point that $P^{N*} \rightarrow M^N$ ET becomes favorable. For the β -188^{Cys} MoFe protein, the assumption is that a cysteine at this position shifts the equilibrium in favor of the state with the cysteinate bound to the Fe of the P cluster, and that the redox equilibrium between P^N and P^{1+} in the presence of dithionite also involves a ligation equilibrium, with ~ 65% of the P cluster in the form of P^{1+} with bound cysteine, and ~35% in the form of P^N with cysteine not bound as in the wild-type MoFe protein. This picture would account for the observation that the resolved ET phase for the β -188^{Cys} MoFe protein behaves the same as that for the wild-type MoFe protein. Lowe and Thorneley (26) further treat ET as occurring only as part of the transfer of an ‘H-atom’, namely an electron and a proton.

Two recent reports describing ET to the MoFe protein in the absence of the Fe protein also support an activation step that could facilitate the intramolecular $P^{N*} \rightarrow M^N$ ET step. It has been found that attaching a Ru-ligand complex onto the surface of the MoFe protein near the P cluster can be used to photoinduce ET from the Ru-ligand complex into the MoFe protein, allowing acetylene reduction (40). In the absence of the Fe protein, the rates of acetylene reduction were very low (0.2% of the rate observed with Fe protein and ATP), consistent with the need for some activation of the $P \rightarrow M$ ET

process to promote full substrate reduction rates. In a separate study, it was found that a low potential Eu(II)-ligand complex could be used to drive electrons into the MoFe protein in the absence of the Fe protein in support of reduction of hydrazine ($\text{H}_2\text{N-NH}_2$) to two ammonia (41). In this system, substrate reduction was observed only when an amino acid residue located between the P cluster and M cluster was substituted by another amino acid, suggesting that the conformational switch normally activated by Fe protein binding involves changes in residues located between the P cluster and FeMo-cofactor and that the key conformational changes can be partially mimicked by an amino acid substitution (41).

Further evidence against a hopping model. The strongest argument against a hopping or sequential ET model for nitrogenase is the improbability that the P cluster can be reduced beyond the all ferrous P^{N} state, as would occur following an initial ET event: $\text{F}^{1+} \rightarrow \text{P}^{\text{N}}$. Super-reduction of all-ferrous P^{N} would require the formation of an Fe(I) with tetrahedral coordination by sulfur, an unknown Fe state. However, our results show that this step would have to be gated, and one might imagine that the activation process might involve a transient loss of a cysteinate ligand from one of the Fe atoms. This would create an activated $\text{P}^{\text{N}\dagger}$ cluster state that has a three-coordinate Fe(II) and a more positive reduction potential. Such a state might accept an electron from F^{1+} , and then re-binding of the cysteinate could create a strongly reducing P^{S} state that undergoes prompt follow-up $\text{P}^{\text{S}} \rightarrow \text{M}^{\text{N}}$ ET.

To test this possibility, we examined ET from F^{1+} to a MoFe protein where one of the cysteine ligands to the P cluster was removed ($\beta\text{-153}^{\text{Cys}}\Delta$). It was found that the rate

of oxidation of F^{1+} to this MoFe protein variant is unchanged from the rate to the wild-type MoFe protein, providing further evidence against the hopping ET model.

Role for nucleotides. MgATP binding and hydrolysis are both essential to intermolecular ET from the Fe protein to the MoFe protein (42). In the absence of ATP hydrolysis, the Fe protein does not transfer an electron to the resting-state MoFe protein (P^N , M^N). The role of ATP hydrolysis in this ET process cannot be filled by the non-hydrolyzable ATP analog $\beta\gamma$ - CH_2 -ATP or the ADP+Pi analog, ADP-AlF₄. However, results reported here reveal that ATP hydrolysis is not necessary for the backfill ET ($F^{1+} \rightarrow P^{1+}$). Rather, the burst ET to the β -188^{Cys} MoFe protein is supported by both $\beta\gamma$ - CH_2 -ATP and ADP-AlF₄. Thus, the backfill electron transfer event ($F^{1+} \rightarrow P^{1+}$) is not conformationally gated and requires nucleotide binding but not hydrolysis.

In contrast to this finding, neither of the ATP analogs supported the slower, resolved phase ET assigned to the $P^N \rightarrow M^N$ ET reaction, pointing to this ET step as requiring an ATP-bound state that has not yet been achieved. Both MgATP and MgADP binding to the Fe protein have been shown to equally lower the midpoint reduction potential of the $[4Fe-4S]^{2+/1+}$ couple (33), yet MgADP does not support either the $P^N \rightarrow M^N$ or the $F^{1+} \rightarrow P^{1+}$ ET events, revealing that it is not simply an issue of driving force for the ET. Thus, the studies presented here pinpoint (i) the conformational gate and (ii) the specific need for ATP binding/hydrolysis to the $P^N \rightarrow M^N$ ET step.

Summary sequence of events. The findings presented here, taken with earlier findings, can be used to propose an overall model for the events associated with ET from the Fe protein to the MoFe protein (**Figure 3-8**). In this model, the ET process is initiated by the association of the Fe protein (2MgATP) with the resting state of the

MoFe protein (**Figure 3-8**, step 1). Although the binding of 2 MgATP to the Fe protein causes a major structural change and lowers its reduction potential by -120 mV (43), the osmotic pressure dependence of the oxidation of F^{1+} indicates that the complex initially formed between Fe protein-2MgATP and MoFe protein is not competent for ET (6). Instead, ET is initiated by a conformational activation (**Figure 3-8**, step 2), presumably involving motion at the Fe protein-MoFe protein interface, with exposure of as many as ~80 water molecules (6). In this model, the interface motion is coupled to a conformational change (second gate) (**Figure 3-8**, step 3) within the MoFe protein that shifts the P cluster to an activated state (P^{N*}) that transiently favors intramolecular ET from the P^{N*} state to the M^N cluster (**Figure 3-8**, step 4) (6). The final step in this sequence involves the rapid 'backfill' ET to the oxidized P cluster ($F^{1+} \rightarrow P^{1+}$), resulting in an oxidized Fe protein and a reduced MoFe protein that has its metal clusters in the P^N and M^R states (**Figure 3-8**, step 5).

The specific contributions for MgATP binding and hydrolysis to the individual steps remains to be resolved, but our studies show that the backfill ET process requires nucleotide binding but not hydrolysis, while the activated $P^{N*} \rightarrow M^N$ ET initial step is not facilitated by any of the ATP analogs examined, requiring ATP itself. Studies of a wide range of ATP utilizing enzymes, in particular transport proteins, have led to the general

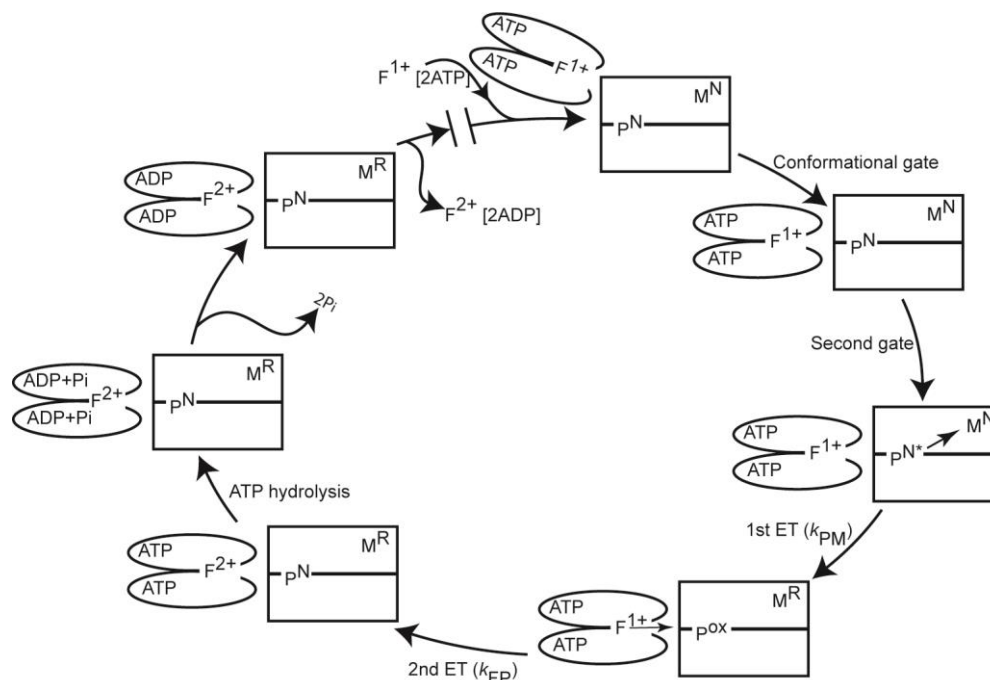


Figure 3-8: Models for nitrogenase mechanism. Shown is one catalytic cycle for a functional half of nitrogenase composed of an $\alpha\beta$ -unit of the MoFe protein (rectangles) and a homodimeric Fe protein (ovals) with the associated metal clusters: F = [4Fe-4S] in the 1+ or 2+ oxidation states, P = P cluster in the N or ox oxidation states, and M = FeMo-cofactor in the N or R oxidation states. The cycle starts at the top with reduced Fe protein +2 MgATP associating with the $\alpha\beta$ -unit of the MoFe protein (1). The remaining steps are numbered (clockwise): (2) the conformational gate, (3) the second gate, (4) the first ET (k_{PM}), (5) the backfill ET (k_{FP}), (6) ATP hydrolysis, (7) release of 2 Pi, (1) and replacement of oxidized Fe protein + 2MgADP with reduced Fe protein + 2MgATP.

view that energy transduction in these proteins occurs during the binding of MgATP, which induces a conformational state activated for the particular function of the ATPase ('taut' state). ATP hydrolysis occurs after the functional/catalytic step, initiating

relaxation from the taut state to a relaxed state with ADP bound, which in turn leads to a resetting of the system for another round of catalysis (34, 35).

While the order of ET and MgATP hydrolysis in nitrogenase has not been well established by previous work, the consensus model is that MgATP hydrolysis follows the ET events (1, 44, 45), in agreement with the current views of ATPase function in other proteins. MgATP binding to the Fe protein is known to induce protein conformational changes that increase the affinity of the Fe protein for binding to the MoFe protein, but given that further activation is needed to induce ET, it would appear that conversion to some as yet uncharacterized ATP binding state (perhaps a true transition state) is required to activate the $P^N \rightarrow M^N$ ET. In this model, the MgATP hydrolysis reaction is placed late in the reaction, after all ET events, although as just noted, this order has not been clearly resolved (**Figure 3-8**, step 6). The present results reveal that the backfill ET from $F^{+1} \rightarrow P^{1+}$ requires an ATP-bound state, but does not require ATP hydrolysis. It thus seems reasonable to suggest that nitrogenase functions similarly to other ATPases, and that ATP hydrolysis during nitrogenase ET is a late event that relaxes the Fe protein for dissociation from the MoFe protein. The rate limiting step for the overall reduction of substrates has been shown to be dissociation of the oxidized Fe protein with two bound 2MgADP from the MoFe protein (**Figure 3-8**, step 7), with a rate constant of $\sim 6 \text{ s}^{-1}$ (26).

References

1. Burgess, B. K., and Lowe, D. J. (1996) Mechanism of molybdenum nitrogenase, *Chem. Rev.* 96, 2983-3012.

2. Georgiadis, M. M., Komiya, H., Chakrabarti, P., Woo, D., Kornuc, J. J., and Rees, D. C. (1992) Crystallographic structure of the nitrogenase iron protein from *Azotobacter vinelandii*. *Science* 257, 1653-1659.
3. Lowe, D., Fisher, K., Pau, R., and Thorneley, R. (1993) Kinetics and mechanism of nitrogenase - a role for P centers in dinitrogen reduction. *Curr. Plant Sci. Biotech. Agricul.* 17, 95-100.
4. Chan, J. M., Christiansen, J., Dean, D. R., and Seefeldt, L. C. (1999) Spectroscopic evidence for changes in the redox state of the nitrogenase P-cluster during turnover. *Biochemistry* 38, 5779-5785.
5. Chan, M. K., Kim, J., and Rees, D. C. (1993) The nitrogenase FeMo-cofactor and P-cluster pair: 2.2 Å resolution structures. *Science* 260, 792-794.
6. Danyal, K., Mayweather, D., Dean, D. R., Seefeldt, L. C., and Hoffman, B. M. (2010) Conformational gating of electron transfer from the nitrogenase Fe protein to MoFe protein. *J. Am. Chem. Soc.* 132, 6894-6895.
7. Davidson, V. L. (2008) Protein control of true, gated, and coupled electron transfer reactions. *Acc. Chem. Res* 41, 730-738.
8. Hoffman, B. M., and Ratner, M. A. (1987) Gated electron transfer: when are observed rates controlled by conformational interconversion? *J. Am. Chem. Soc.* 109, 6237-6243.
9. Mensink, R. E., and Haaker, H. (1992) Temperature effects on the MgATP-induced electron transfer between the nitrogenase proteins from *Azotobacter vinelandii*, *Eur. J. Biochem.* 208, 295-299.

10. Thorneley, R. N., Ashby, G., Howarth, J. V., Millar, N. C., and Gutfreund, H. (1989) A transient-kinetic study of the nitrogenase of *Klebsiella pneumoniae* by stopped-flow calorimetry. Comparison with the myosin ATPase, *Biochem. J.* 264, 657-661.
11. Hageman, R. V., and Burris, R. H. (1978) Nitrogenase and nitrogenase reductase associate and dissociate with each catalytic cycle, *Proc. Natl. Acad. Sci. U.S.A.* 75, 2699-2702.
12. Edwards, P. P., Gray, H. B., Lodge, M. T. J., and Williams, R. J. P. (2008) Electron transfer and electronic conduction through an intervening medium, *Angew. Chem. Int. Ed. Engl* 47, 6758-6765.
13. Gray, H. B., and Winkler, J. R. (2010) Electron flow through metalloproteins, *Biochim. Biophys. Acta* 1797, 1563-1572.
14. Tezcan, F. A., Kaiser, J. T., Mustafi, D., Walton, M. Y., Howard, J. B., and Rees, D. C. (2005) Nitrogenase complexes: multiple docking sites for a nucleotide switch protein, *Science* 309, 1377-1380.
15. Schindelin, H., Kisker, C., Schlessman, J. L., Howard, J. B., and Rees, D. C. (1997) Structure of ADP x $\text{AlF}_4^{(-)}$ -stabilized nitrogenase complex and its implications for signal transduction, *Nature* 387, 370-376.
16. Chiu, H., Peters, J. W., Lanzilotta, W. N., Ryle, M. J., Seefeldt, L. C., Howard, J. B., and Rees, D. C. (2001) MgATP-Bound and nucleotide-free structures of a nitrogenase protein complex between the Leu 127 Delta-Fe-protein and the MoFe-protein, *Biochemistry* 40, 641-650.

17. Yoo, S. J., Angove, H. C., Papaefthymiou, V., Burgess, B. K., and Münck, E. (2000) Mössbauer study of the MoFe protein of nitrogenase from *Azotobacter vinelandii* using selective ^{57}Fe enrichment of the M-centers, *J. Am. Chem. Soc* 122, 4926-4936.
18. Lindahl, P. A., Papaefthymiou, V., Orme-Johnson, W. H., and Münck, E. (1988) Mössbauer studies of solid thionin-oxidized MoFe protein of nitrogenase, *J. Biol. Chem* 263, 19412-19418.
19. Mouesca, J.-M., Noodleman, L., and Case, D. A. (1994) Analysis of the ^{57}Fe hyperfine coupling constants and spin states in nitrogenase P-clusters, *Inorg. Chem.* 33, 4819-4830.
20. Surerus, K. K., Hendrich, M. P., Christie, P. D., Rottgardt, D., Orme-Johnson, W. H., and Münck, E. (1992) Mössbauer and integer-spin EPR of the oxidized P-clusters of nitrogenase: POX is a non-Kramers system with a nearly degenerate ground doublet, *J. Am. Chem. Soc* 114, 8579-8590.
21. Angove, H. C., Yoo, S. J., Münck, E., and Burgess, B. K. (1998) An all-ferrous state of the Fe protein of nitrogenase. Interaction with nucleotides and electron transfer to the MoFe protein, *J. Biol. Chem* 273, 26330-26337.
22. Chakrabarti, M., Deng, L., Holm, R. H., Münck, E., and Bominaar, E. L. (2010) The modular nature of all-ferrous edge-bridged double cubanes, *Inorg Chem* 49, 1647-1650.
23. Christiansen, J., Goodwin, P. J., Lanzilotta, W. N., Seefeldt, L. C., and Dean, D. R. (1998) Catalytic and biophysical properties of a nitrogenase Apo-MoFe protein

- produced by a *nifB*-deletion mutant of *Azotobacter vinelandii*, *Biochemistry* 37, 12611-12623.
24. Barney, B. M., Igarashi, R. Y., Dos Santos, P. C., Dean, D. R., and Seefeldt, L. C. (2004) Substrate interaction at an iron-sulfur face of the FeMo-cofactor during nitrogenase catalysis, *J. Biol. Chem* 279, 53621-53624.
 25. Lanzilotta, W. N., Fisher, K., and Seefeldt, L. C. (1996) Evidence for electron transfer from the nitrogenase iron protein to the molybdenum-iron protein without MgATP hydrolysis: characterization of a tight protein-protein complex, *Biochemistry* 35, 7188-7196.
 26. Thorneley, R., and Lowe, D. (1985) Kinetics and mechanism of the nitrogenase enzyme, in *Molybdenum Enzymes*, pp 221-284. Wiley-Interscience Publications, New York.
 27. Thorneley, R. N. (1975) Nitrogenase of *Klebsiella pneumoniae*. A stopped-flow study of magnesium-adenosine triphosphate-induced electron transfer between the component proteins, *Biochem. J* 145, 391-396.
 28. Thorneley, R. N., and Lowe, D. J. (1984) The mechanism of *Klebsiella pneumoniae* nitrogenase action. Pre-steady-state kinetics of an enzyme-bound intermediate in N₂ reduction and of NH₃ formation, *Biochem. J* 224, 887-894.
 29. Thorneley, R. N., Lowe, D. J., Eday, R. R., and Miller, R. W. (1979) The coupling of electron transfer in nitrogenase to the hydrolysis of magnesium adenosine triphosphate, *Biochem. Soc. Trans* 7, 633-636.

30. Weston, M. F., Kotake, S., and Davis, L. C. (1983) Interaction of nitrogenase with nucleotide analogs of ATP and ADP and the effect of metal ions on ADP inhibition, *Arch. Biochem. Biophys* 225, 809-817.
31. Lanzilotta, W. N., Holz, R. C., and Seefeldt, L. C. (1995) Proton NMR investigation of the $[4\text{Fe--4S}]^{1+}$ cluster environment of nitrogenase iron protein from *Azotobacter vinelandii*: defining nucleotide-induced conformational changes, *Biochemistry* 34, 15646-15653.
32. Meyer, J., Gaillard, J., and Moulis, J. M. (1988) Hydrogen-1 nuclear magnetic resonance of the nitrogenase iron protein (Cp2) from *Clostridium pasteurianum*, *Biochemistry* 27, 6150-6156.
33. Zumft, W. G., Palmer, G., and Mortenson, L. E. (1973) Electron paramagnetic resonance studies on nitrogenase. II. Interaction of adenosine 5'-triphosphate with azoferredoxin, *Biochim. Biophys. Acta* 292, 413-421.
34. Locher, K. P. (2009) Structure and mechanism of ATP-binding cassette transporters, *Phil. Trans. Royal Soc. B* 364, 239-245.
35. Linton, K., and Higgins, C. (2007) Structure and function of ABC transporters: the ATP switch provides flexible control, *Plugers Archiv. Eur. J. Phys.* 453, 555-567.
36. Duyvis, M. G., Wassink, H., and Haaker, H. (1996) Formation and characterization of a transition state complex of *Azotobacter vinelandii* nitrogenase, *FEBS Lett* 380, 233-236.
37. Lowe, D. J., Fisher, K., and Thorneley, R. N. (1993) *Klebsiella pneumoniae* nitrogenase: pre-steady-state absorbance changes show that redox changes occur in

- the MoFe protein that depend on substrate and component protein ratio; a role for P-centres in reducing dinitrogen?, *Biochem. J.* 292, 93-98.
38. Cameron, L. M., and Hales, B. J. (1998) Investigation of CO binding and release from Mo-nitrogenase during catalytic turnover, *Biochemistry* 37, 9449-9456.
 39. Peters, J. W., Stowell, M. H., Soltis, S. M., Finnegan, M. G., Johnson, M. K., and Rees, D. C. (1997) Redox-dependent structural changes in the nitrogenase P-cluster, *Biochemistry* 36, 1181-1187.
 40. Roth, L. E., Nguyen, J. C., and Tezcan, F. A. (2010) ATP- and iron-protein-independent activation of nitrogenase catalysis by light, *J. Am. Chem. Soc.* 132, 13672-13674.
 41. Danyal, K., Inglet, B. S., Vincent, K. A., Barney, B. M., Hoffman, B. M., Armstrong, F. A., Dean, D. R., and Seefeldt, L. C. (2010) Uncoupling nitrogenase: catalytic reduction of hydrazine to ammonia by a MoFe protein in the absence of Fe protein-ATP, *J. Am. Chem. Soc.* 132, 13197-13199.
 42. Howard, J. B., and Rees, D. C. (1994) Nitrogenase: a nucleotide-dependent molecular switch, *Annu. Rev. Biochem.* 63, 235-264.
 43. Lanzilotta, W. N., and Seefeldt, L. C. (1997) Changes in the midpoint potentials of the nitrogenase metal centers as a result of iron protein-molybdenum-iron protein complex formation, *Biochemistry* 36, 12976-12983.
 44. Mensink, R. E., Wassink, H., and Haaker, H. (1992) A reinvestigation of the pre-steady-state ATPase activity of the nitrogenase from *Azotobacter vinelandii*. *Eur. J. Biochem.* 208, 289-294.

45. Lowe, D., Ashby, G., Brune, M., Knights, H., Webb, M., and Thorneley, R. (1995)
ATP hydrolysis and energy transduction by nitrogenase, in *Nitrogen Fixation:
Fundamentals and Applications*, pp 103-108. Kluwer Academic Publishers, St.
Petersburg, Russia.

CHAPTER 4
TEMPERATURE INVARIANCE OF THE NITROGENASE ELECTRON
TRANSFER MECHANISM*

ABSTRACT

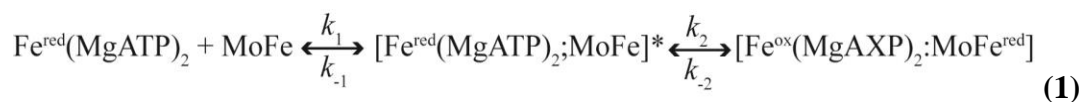
Earlier studies on electron transfer (ET) from the nitrogenase Fe protein to the MoFe protein concluded that the mechanism for ET changed during cooling from 25°C to 5°C, based on the observation that the rate constant for Fe protein to MoFe protein ET decreases strongly, with a non-linear Arrhenius plot. They further indicated that the ET was reversible, with complete ET at ambient but with an equilibrium constant near unity at 5°C. These studies were carried out with buffers having a strong temperature coefficient. We have examined the temperature variation in the kinetics of oxidation of the Fe protein by the MoFe protein at constant pH = 7.4 fixed by the buffer MOPS, which has a very small temperature coefficient. Using MOPS, we also observe temperature dependent ET rate constants, with non-linear Arrhenius plots. But, we find that ET is gated across the temperature range by a conformational change that involves the binding of numerous water molecules, consistent with an unchanging ET mechanism. Furthermore, there is no *sKIE* throughout the temperature range studied, again consistent with an unchanging mechanism. In addition, the non-linear Arrhenius plots are explained by the change in heat capacity caused by the binding of waters in an invariant gating ET

*Coauthored by Diana Mayweather, Karamatullah Danyal, Dennis Dean, Lance C. Seefeldt, and Brian M. Hoffman (2012) *Biochemistry* 51 (42), pp 8391-8398. Copyright 2012 American Chemical Society. Reprinted with Permission.

mechanism. Together, these observations contradict the idea of a change in ET mechanism with cooling. Finally, the extent of ET at constant pH does not change significantly with temperature, in contrast to the previously proposed change in ET equilibrium.

INTRODUCTION

Nitrogenase catalyzes the multi-electron reduction of dinitrogen (N_2) to two ammonia (NH_3), a reaction that is the major contributor to N_2 fixation in the biosphere.⁽¹⁾ The enzyme comprises two component proteins, called the Fe protein and the MoFe protein, which associate and dissociate each time an electron is delivered from the Fe protein to the MoFe protein, which contains the catalytically active FeMo-cofactor, [7Fe, Mo, 9S; C; homocitrate].⁽²⁻⁴⁾ This process of electron transfer (ET) from Fe to MoFe protein can be summarized by the deceptively simple kinetic scheme of **Eq 1**: the reduced Fe protein with two bound ATP [$Fe^{red}(MgATP)_2$] rapidly forms an activated complex with the MoFe protein, where the rate constant for binding is k_1 and that for dissociation is k_{-1} ,



ET from the Fe protein to the MoFe protein then creates a one-electron reduced MoFe protein denoted $MoFe^{red}$. This forward ET is characterized by a single ET rate constant k_2 ; the possibility of reverse ET is incorporated by inclusion of rate constant k_{-2} .

A key challenge in defining the mechanism of nitrogenase is to understand the steps in the kinetic scheme of **eq 1** at a detailed molecular level. The process begins when the ATP-bound Fe protein with a reduced [4Fe-4S] cluster docks to the MoFe protein, **Figure 4-1**. The subsequent intracomplex ET from the Fe protein to the MoFe protein was shown to be gated in a study that employed variations in viscosities/osmotic pressures.⁽⁵⁾ The variation of the ET rate constant with osmotic pressure showed that ~80 waters bind to the protein surfaces during the reaction. This binding induces conformational changes to the MoFe protein that initiate ‘gated’ electron transfer (ET)^(6, 7) within the MoFe protein, from the P cluster [8Fe-7S] to FeMo-cofactor.⁽⁵⁾ This process in turn creates an electron ‘deficit’ on the P cluster, which is back-filled by rapid electron transfer from the Fe protein to the oxidized P cluster.

X-ray crystal structures of MoFe protein:Fe protein complexes have been solved in various states of nucleotide binding.^(8, 9) From these structures, it is clear that the Fe protein exhibits major conformational differences in different nucleotide-bound states, and that it binds at different sites on the surface of the MoFe protein in the different states, suggesting that motion between sites is involved in the gating and inspiring the scheme implied in **Figure 4-1**. However, these structures do not show any differences within the MoFe protein, thus leaving open the nature of the motions within the MoFe protein that contribute to the gated ET.^(10, 11, 12)

This ET process, which has been termed “deficit spending”,⁽¹³⁾ is linked to the hydrolysis of two ATP molecules bound to the Fe protein. Although ATP hydrolysis may well follow the ET reaction, in analogy to other NTPases,⁽¹⁴⁾ the order of electron transfer

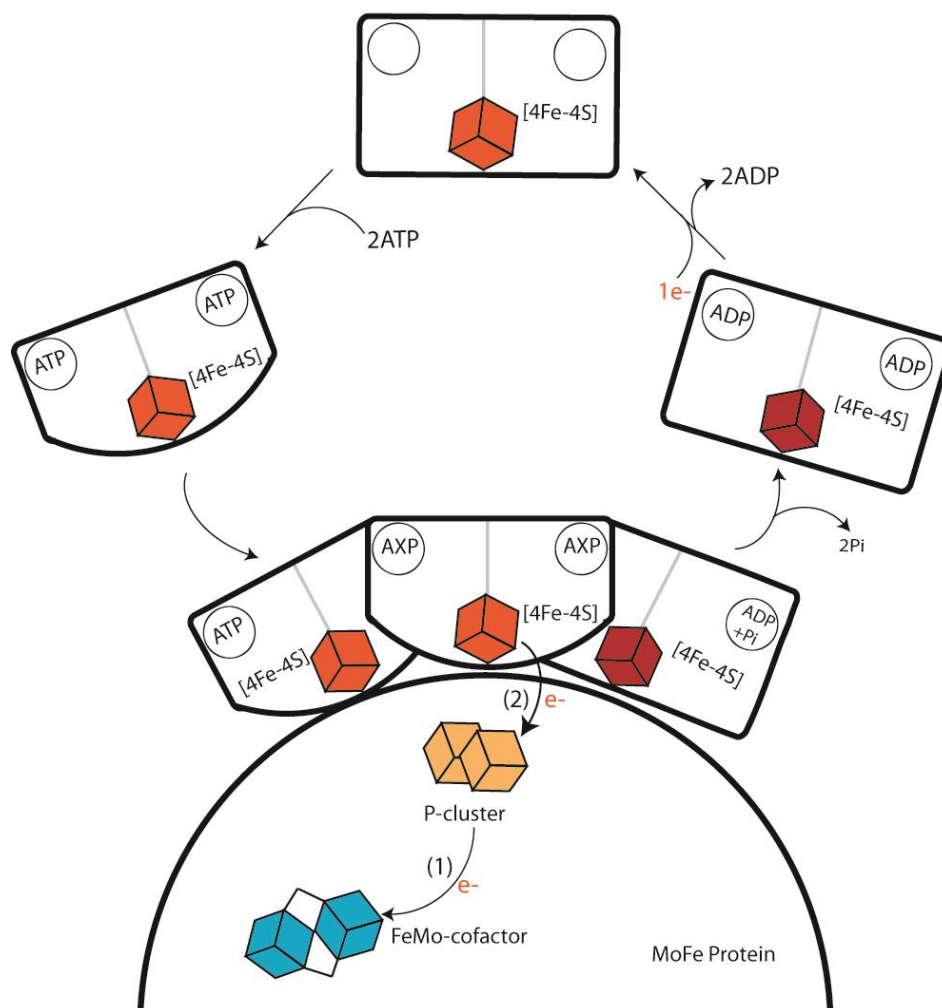


Fig 4-1. Events proposed as occurring at the interface of the MoFe protein and the Fe protein as the latter delivers an electron to the former. Here MoFe protein is represented by the semi-circle. The Fe protein (coming in from the left) binds two ATPs. The binding of ATP to the Fe protein causes conformational changes in the Fe protein which bring the [4Fe-4S] cluster closer to the surface of the protein. Conformational changes subsequent to binding ‘gate’ the conversion to an ET-active state. As the order of ET and ADP hydrolysis is uncertain, in this state the nucleotide is written ‘AXP’. The final step is the departure of the Fe protein (right).

and ATP hydrolysis has not been clearly established,^(2, 15, 16) and so in **Fig 4-1** the state of the nucleotide in the ET-active conformation is not specified ($X = T$ or D). The absence of a solvent kinetic isotope effect ($sKIE$)⁽⁵⁾ at ambient temperature implied that ATP hydrolysis, which should be slowed by the presence of D versus H , is not involved in the rate-limiting step of ET.

Equation 1 is written as though the ET step is reversible. Although ET is quantitative at ambient temperature, previous studies found that the absorbance change associated with the oxidation of Fe^{red} by MoFe protein (ΔA) decreases as the temperature is lowered.^(2, 16) This was interpreted as indicating that ET is an equilibrium process, with an equilibrium constant at ambient temperature that is large, $K_2 = k_2/k_{-2} \gg 1$, corresponding to quantitative ET, but that decreases to $K_2 \sim 1$ at $5^\circ C$. If ET is indeed reversible, then either it precedes ATP hydrolysis, or the hydrolysis also must be reversible.

A number of studies investigated the temperature dependence of ET as a means of exploring mechanism.^(2, 16, 17) They suggested that the actual mechanism of ET from the Fe protein to the MoFe protein changes upon cooling. Thus, a non-linear Arrhenius plot of the observed ET rate constant versus inverse temperature was interpreted as having a 'break' at $\sim 14-16^\circ C$, and used as the basis for a suggestion that one mechanism operates at higher temperatures, another at lower, each with a characteristic activation enthalpy. The proposal of a change in mechanism was supported by stopped-flow (SF) isothermal calorimetry (ITC) measurements, which were interpreted as showing that in the low-temperature regime the hydrolysis of ATP precedes the electron transfer event, whereas at ambient temperature the ET event occurs prior to ATP hydrolysis.⁽¹⁶⁾

Here, we have re-examined the temperature variations at constant pH in the extent and rate constants for oxidation of the Fe protein by the MoFe protein within the pre-formed complex, and have tested for the persistence of gating at low temperature and for the appearance of an *sKIE* on ET. Our findings show that the ET mechanism does not change during cooling at constant pH.

MATERIALS AND METHODS

All reagents for these experiments were purchased from Sigma-Aldrich Chemicals (St. Louis, MO). Wild type MoFe protein was expressed in *Azotobacter vinelandii* strain DJ995, while wild type Fe protein was obtained from strain DJ884 grown as described previously.⁽¹⁸⁾ MoFe protein purification was performed using previously described metal affinity chromatography method due to the seven-histidine tag on the α -subunit of the protein while Fe protein was purified, with some modifications, using ion exchange and size exclusion as previously described.^(18, 19) Both proteins utilized in these experiments were found to be of greater than 95% purity based on SDS-PAGE analysis using Coomassie blue staining. Septum sealed degassed vials, under an argon atmosphere were used to determine the activity of the proteins. The wild type Fe protein activity was found to be ~1750 nmols while the wild type MoFe protein activity was found to be ~2100 nmols. Both activities were similar to previously reported values for the activity of these proteins.⁽²⁰⁾ All liquids were transferred using gastight syringes.

The increase in absorbance at 430 nm was monitored to follow the ET event from the Fe protein to the MoFe protein. This increase in absorbance occurs due to the Fe protein's oxidation by one electron from its reduced (1^+) state to the (2^+) state; there is no

significant accompanying change in absorbance of the MoFe protein. The change of absorbance as a function of time after the mixing of the two proteins was observed using a Hi-Tech SF61 stopped flow (SF) UV-visible spectrophotometer equipped with data acquisition software (Salisbury, Wits, U.K.). The SF unit of the spectrophotometer was housed inside a nitrogen filled glovebox. The temperature during the experiments was controlled by a circulating water bath housed outside the glove box.⁽²¹⁾ All reactions, except for the change in temperature experiments, were carried out at 25°C. Differing buffer systems, HEPES and MOPS, pH 7.4 were used with 10mM dithionite. Due to the change in pH with temperature in the HEPES buffer, MOPS was utilized for the temperature dependency experiments to keep the pH constant.⁽²²⁾ During the SF experiments Fe and MoFe protein were contained in one drive syringe of the unit while the other syringe contained MgCl₂ and ATP. Both syringes contained buffer (HEPES/MOPS 100mM pH 7.4) and 10mM dithionite. The dead time of the Hi-Tech SF61 SF system is 2 ms.

In the present experiments, the formation of the [Fe^{red}(MgATP*)₂; MoFe] complex is essentially quantitative and complete within the deadtime of the experiment. Thus, the SF trace monitors the intra-complex oxidation, Fe^{red} → Fe^{ox}, by MoFe protein, the second step in **Eq 1**. In the SF experiment, the absorbance of the mixed solutions prior to Fe^{red} → Fe^{ox} oxidation is obtained with a non-reactive ‘push’ in which ATP is omitted, then the instrument output is ‘nulled’ by subtraction of this absorbance. As a result, the SF traces represent the time-variation of the absorbance-difference caused by reaction, relative to that of the initial mixed, unreacted solution.

Previous studies typically obtained the rate constant for the oxidation of Fe^{red} , denoted here k_{obs} , by fitting the initial portion of the SF traces with an exponential rise-to-maximum.^(25, 16, 17) However, as can be seen in the data presented below (**Figure 4-2**) and in **SI**, the SF traces for the oxidation of Fe^{red} by MoFe protein in general have a more complex shape, which indicates that the oxidation of Fe^{red} is followed by a slower reaction to a state with a smaller absorbance-difference. Haaker and coworkers attribute this follow-up reaction to hydrolysis of ATP. Alternatively, we suggest this may represent a partial re-reduction of the resulting Fe^{ox} back to Fe^{red} that occurs as part of a complex set of reactions that involves dissociation of Fe^{ox} , re-reduction to Fe^{red} , and re-binding to MoFe.⁽²³⁾

In this report we are interested only in the rate constant and absorbance-difference associated with the initial intra-complex oxidation, $\text{Fe}^{\text{red}} \rightarrow \text{Fe}^{\text{ox}}$, by MoFe protein. As shown in **SI**, neither of these parameters is accurately derived with a rise-to-maximum fit if the followup phase of the SF trace is appreciable, so we have employed the simplest possible kinetic model to treat the observed traces. We find that the overall traces can be well-modeled by a kinetic scheme that includes two sequential first-order reactions, **Eq 2**,



the first representing the initial oxidation of Fe^{red} by MoFe protein, the second a followup reaction to an unspecified state, denoted **C**. This model leads to an equation for the resolved time-course of the absorbance difference, $\Delta A(\tau)$, given by **Eq 3**:

$$\Delta A(\tau) = \Delta A_o + \Delta A_r \left[\left(\frac{k_{obs}}{k_{obs} - k_{Dr}} \right) * \left(e^{-k_{Dr} * \tau} - e^{-k_{obs} * \tau} \right) \right] + \Delta A_{Dr} \left\{ 1 - \left[\left(\frac{-k_{Dr}}{k_{obs} - k_{Dr}} \right) * e^{-k_{obs} * \tau} + \left(\frac{k_{obs}}{k_{obs} - k_{Dr}} \right) * e^{-k_{Dr} * \tau} \right] \right\} \quad (3)$$

where $\tau = t - t_{DT}$, with t_{DT} being the time at which mixing artifacts have subsided (dead-time). In this equation, k_{obs} is the rate constant for the oxidation of Fe^{red} by MoFe protein, and k_{Dr} is the rate constant for the follow-up process. This equation takes into account possible reaction during the dead-time leading to an absorbance-difference, ΔA_o . As a result of such a phenomenon, the total absorbance-difference associated with the first-step intracomplex oxidation of Fe^{red} (**Eq 2**), denoted here ΔA , equals the absorbance change associated with the initial oxidation step in the resolved phase of **Eq 3**, ΔA_r , plus the absorbance change from the portion of the oxidation reaction that occurs during the dead-time, ΔA_o : $\Delta A = \Delta A_o + \Delta A_r$. As incorporated into **Eq 3**, State **C** is characterized by a net absorbance-difference, ΔA_{Dr} , relative to the initial state. In the Results section we discuss only the parameters associated with the initial oxidation of Fe^{red} by MoFe protein: k_{obs} and ΔA ; for completeness only, values for the parameters associated with the unspecified followup process, k_{Dr} and ΔA_{Dr} , are given in **SI**.

As discussed in detail in the **SI**, the fits to **Eq 3** give as much as a two-fold smaller rate constant, k_{obs} , than a rise-to-maximum fit. However, we note that such trends as changes with temperature or osmotic pressure, which are the focus of this work, are comparably represented by the two approaches (**Figure 4-S1**).

RESULTS AND ANALYSIS

Influence of temperature and solvent isotope on ET

Figure 4-2 shows the SF traces at different temperatures for the oxidation of Fe^{red} by the MoFe protein in H_2O (**top**) and D_2O (**bottom**) solutions with MOPS as the buffer. As this buffer has a negligible temperature coefficient of pKa vs T,⁽²²⁾ these measurements thus are carried out with essentially invariant $\text{pH} = \text{pD} = 7.4$ over the temperature range, 25 - 5°C. As discussed in **Materials and Methods**, at temperatures above 5°C the absorbance changes associated with the initial oxidation of Fe^{red} by MoFe do not show a simple rise-to-maximum; the initial absorbance increase is followed by a decrease in absorbance associated with re-reduction of Fe^{red} or the change in absorbance of Fe^{ox} due to hydrolysis of ATP. To obtain the rate constants for the initial Fe^{red} oxidation, the traces were fit to a sequential model in which the oxidation of Fe^{red} is followed by a slower re-reduction process, as described in **Materials & Methods**. In discussing these results, we consider only the rate constants and absorbance changes associated with the initial Fe^{red} oxidation.

To test for the congruence of the current results to those reported earlier, the traces of **Figure 4-2** were truncated and fit to a rise-to-maximum. As mentioned in **Materials and Methods** and shown in **SI**, such fits typically give larger values for k_{obs} , in keeping with those reported earlier,^(2, 16, 17) but the trends with temperature are completely equivalent, **Figure 4-S1**. Thus, trends reported in this study can be appropriately compared to those in earlier reports. However, we believe that the magnitudes of k_{obs} based on fits to **Eq 3** which are notably lower than earlier values, are more appropriate.

The temperature responses of the rate constants and absorbance changes associated with the initial Fe^{red} oxidation for D_2O and H_2O solutions (MOPS pH = pD = 7.4), denoted k_{obs} and ΔA , are plotted, respectively, in **Figure 4-3** and **Figure 4-4**. The observed ET rate constants decrease strongly with temperature (**Figure 4-3**), and the k_{obs} values for H_2O and D_2O solutions with MOPS are the same within experimental error. The finding that $k_{\text{obs}}(\text{H}_2\text{O}) = k_{\text{obs}}(\text{D}_2\text{O})$ at ambient temperature confirms our earlier report that there is no *sKIE* at 25°C; the equivalence of the rate constants at all temperature shows that an *sKIE* does not emerge upon cooling.

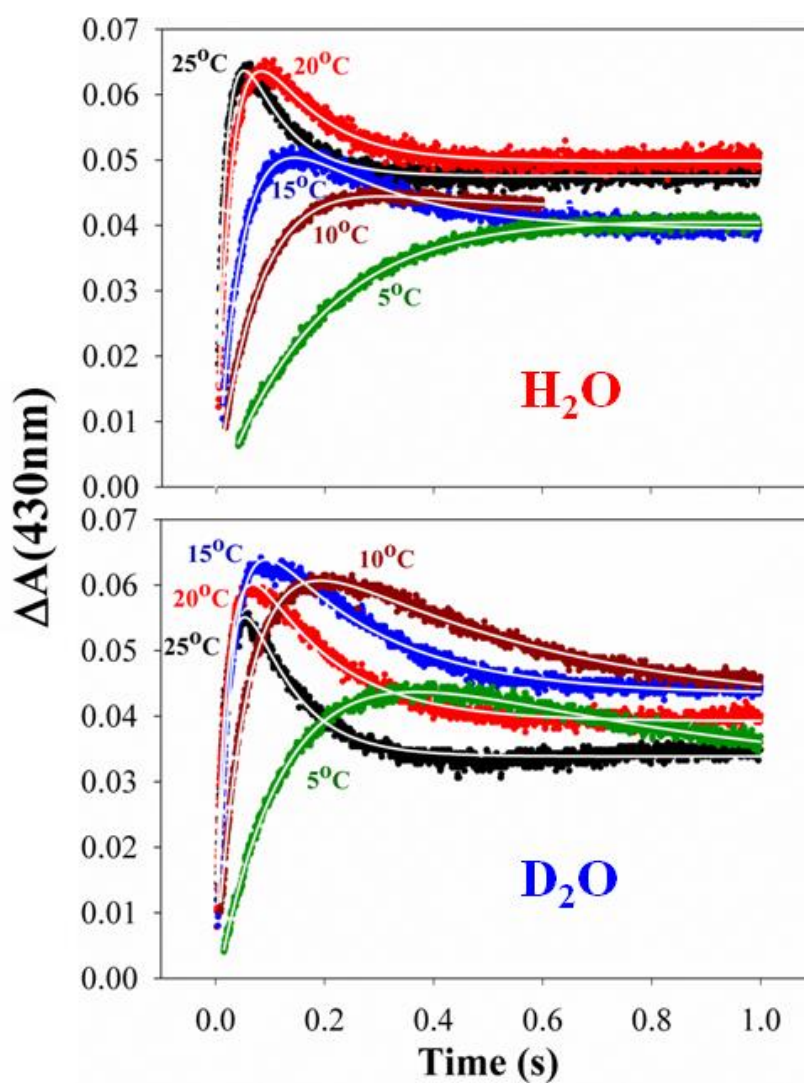


Figure 4-2. Temperature-response stopped-flow traces for oxidation of Fe^{red} within $[\text{Fe}^{\text{red}}(\text{MgATP})_2;\text{MoFe}]$ complex in H_2O and D_2O buffers. Top: H_2O , Bottom: D_2O . Plots are labeled with the temperature ($^{\circ}\text{C}$) from 25°C to 5°C in the respective color of the traces. White lines through each trace are fits as described in **Materials and Methods.**

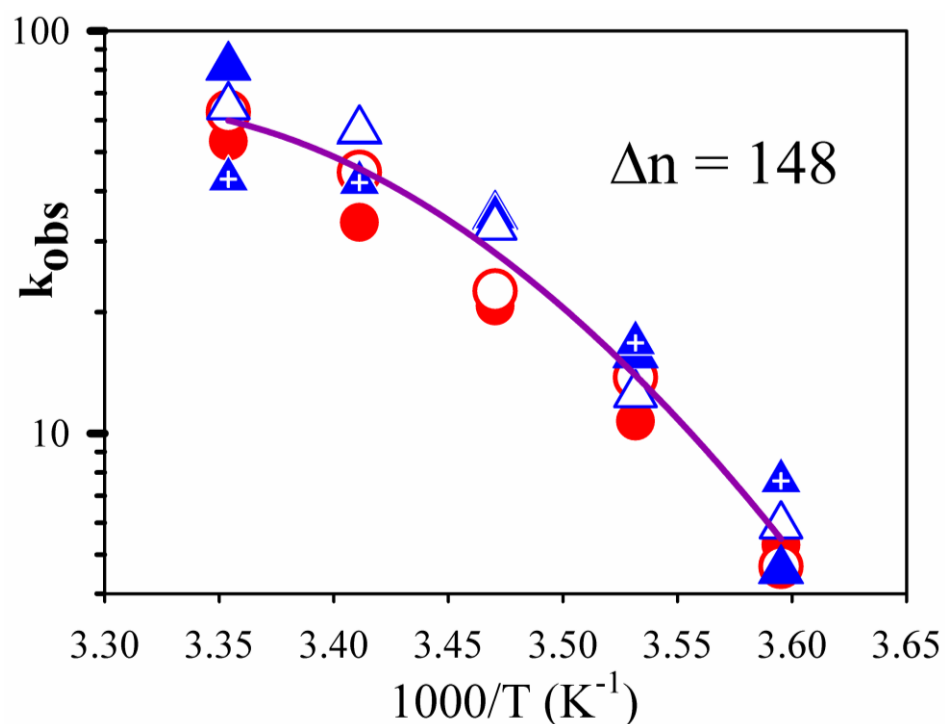


Figure 4-3. Semi-logarithmic plot of the observed rate constants, k_{obs} for D_2O (blue symbols) and H_2O (red symbols). Individual experiments are visualized by open, closed, or crossed points. Purple solid line is a fit to all data sets, assuming that there is no difference in k_{obs} for H_2O and D_2O buffers.

Temperature dependent ET equilibrium?

Thorneley et al. reported that the absorbance change (ΔA) associated with $\text{Fe}^{\text{red}} \rightarrow \text{MoFe ET}$ in H_2O buffer diminishes with decreasing temperature,⁽²⁾ a finding corroborated by Mensink and Haaker.⁽¹⁶⁾ The absorbance decrease was interpreted in terms of a temperature dependence of an ET equilibrium between the two proteins, as represented by the second step of **Eq 1**. It was proposed that ET was essentially quantitative at 25°C, $k_2 \gg k_{-2}$ (**Eq 1**), but by 5°C only ~50% of the complexes showed ET ($k_2 \approx k_{-2}$).

There are multiple reasons for concern about these conclusions. First, the experiments were carried out with solutions that used TES/NaOH buffer, and as a result were not performed at constant pH as the temperature was lowered. TES buffers have a large temperature coefficient,⁽²²⁾ causing an increase in pH from 7.4 to ~ 7.7 as the temperature is lowered from 25°C to 5°C. Second, the kinetic traces were fit to a simple rise-to-maximum function, which does not necessarily give a good representation of the maximum absorbance change when the reaction involves more than one stage (**Eq 1**). In particular, as has been reported, the kinetic traces often show a rise-to-maximum, slight fall, then slow rise.⁽²⁾

We thus analyzed the temperature dependence of the absorbance changes associated with the ET kinetics measurements discussed above. **Figure 4-4** shows that these absorbance changes fluctuate appreciably from one experiment to the next, even though the kinetic constants do not (**Figure 4-3**). However, within the error of our measurements the absorbance changes with MOPS as buffer are the same for H_2O and D_2O solutions, and are invariant with temperature; the same is true for the absorbance changes obtained from rise-to-maximum fits (Fig. **S2**). We tested whether the implied

constancy in the extent of ET is modified by a change with cooling of the difference between the extinction coefficients of oxidized and reduced Fe protein, $\Delta\varepsilon = \varepsilon(\text{Fe}^{\text{ox}}) - \varepsilon(\text{Fe}^{\text{red}})$. As shown in **Figure 4-S3** within error, this difference is temperature invariant down to 5°C. We thus interpret the results of **Figure 4-4** as showing that the quantitative ET in MOPS buffer at pH 7.4 is essentially unchanged during cooling at constant pH from 25°C to 5°C. In the description of nitrogenase ET given by **Eq 1**, the observed ET rate constant is related to the microscopic rate constants by, $k_{\text{obs}} = k_2 + k_{-2}$. However, when ET is quantitative, the ET rate constants obey the inequality, $k_2 \gg k_{-2}$, and thus we may assign $k_{\text{obs}} = k_2$ throughout the temperature range examined.

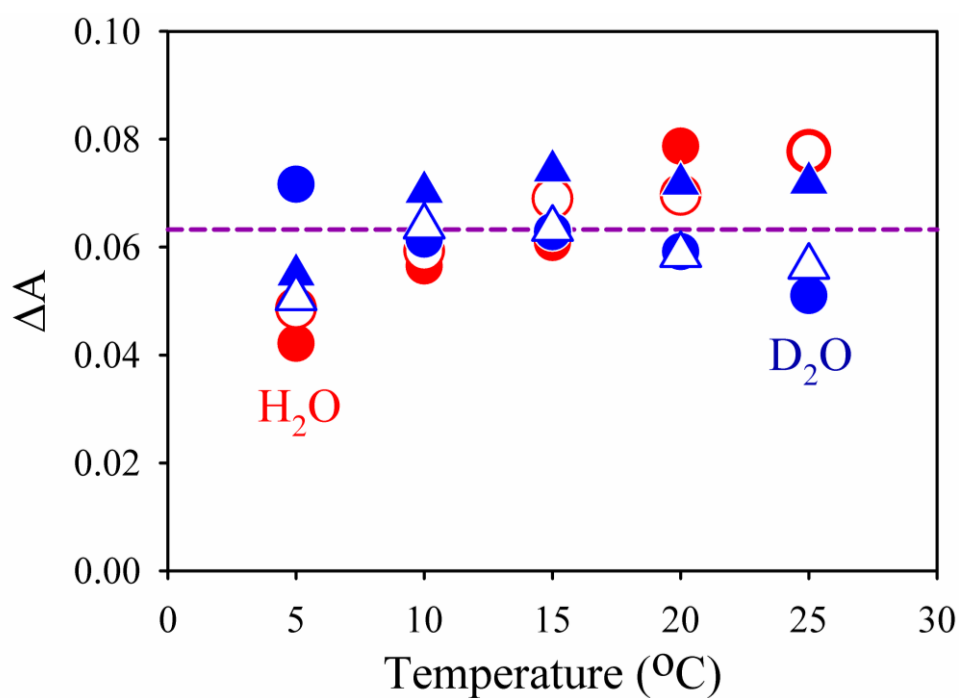


Figure 4-4: Temperature dependence of absorbance changes ΔA , (Eq 3) obtained from intracomplex oxidation of $\text{Fe}^{\text{red}}(\text{ATP})_2$ by MoFe as a function of temperature.

Purple dashed line is the average of all values.

To test whether the previously reported temperature response of ΔA associated with $\text{Fe}^{\text{red}} \rightarrow \text{MoFe ET}$ in H_2O buffer could be attributed to a change in pH upon cooling, the temperature dependence of ET was reexamined using samples prepared with HEPES/ H_2O buffer (**Figure 4-S4**). HEPES has a temperature coefficient similar to that of TES, used by Haaker and coworkers; with HEPES as buffer the pH increases from 7.4 to ~ 7.8 as the temperature is lowered from 25°C to 5°C . As shown in **Figure 4-S5**, the absorbance change associated with $\text{Fe}^{\text{red}} \rightarrow \text{MoFe protein ET}$ for H_2O solutions of HEPES buffer indeed drops by roughly 50% from 25 to 5°C , whereas the absorbance change does not decrease for the D_2O solutions of HEPES buffer (**Figure 4-S4**), and if anything increases slightly with decreasing temperature. The differing behavior for the H_2O and D_2O solutions with HEPES presumably reflect an equilibrium isotope effect on the pH dependence of the extent of ET. This inference is supported by measurements over a range of pH values in HEPES buffer, all carried out at 5°C (**Figure 4-S6 and 4-S7**). These show that k_{obs} does not change significantly with pH for either buffer; there is a substantial variation in ΔA with pH for the H_2O buffers, but negligible change for the D_2O buffers.

Gating at Low Temperature?

To reveal if conformational gating of ET from the Fe protein to the MoFe protein persists at temperatures below the apparent break temperature ($T_b \sim 14^\circ\text{C}$ - 16°C) as concluded in earlier studies, we examined the influence of osmolytes on k_{obs} for ET at

6°C. Sucrose, glycerol, and glucose were studied as osmolytes because they generated the strongest, intermediate, and weakest effects seen at ambient temperatures.⁽⁵⁾ As illustrated for sucrose as solute in **Figure 4-5, inset**, progressive additions of each osmolyte cause progressive decreases in k_{obs} at 6°C, thus indicating that ET is under conformational control at this low temperature as well as at ambient temperatures. Given the observed control of ET by osmotic pressure effects at 6°C as well as at 25°C, we conclude that the gating mechanism that controls ET persists throughout the temperature range.

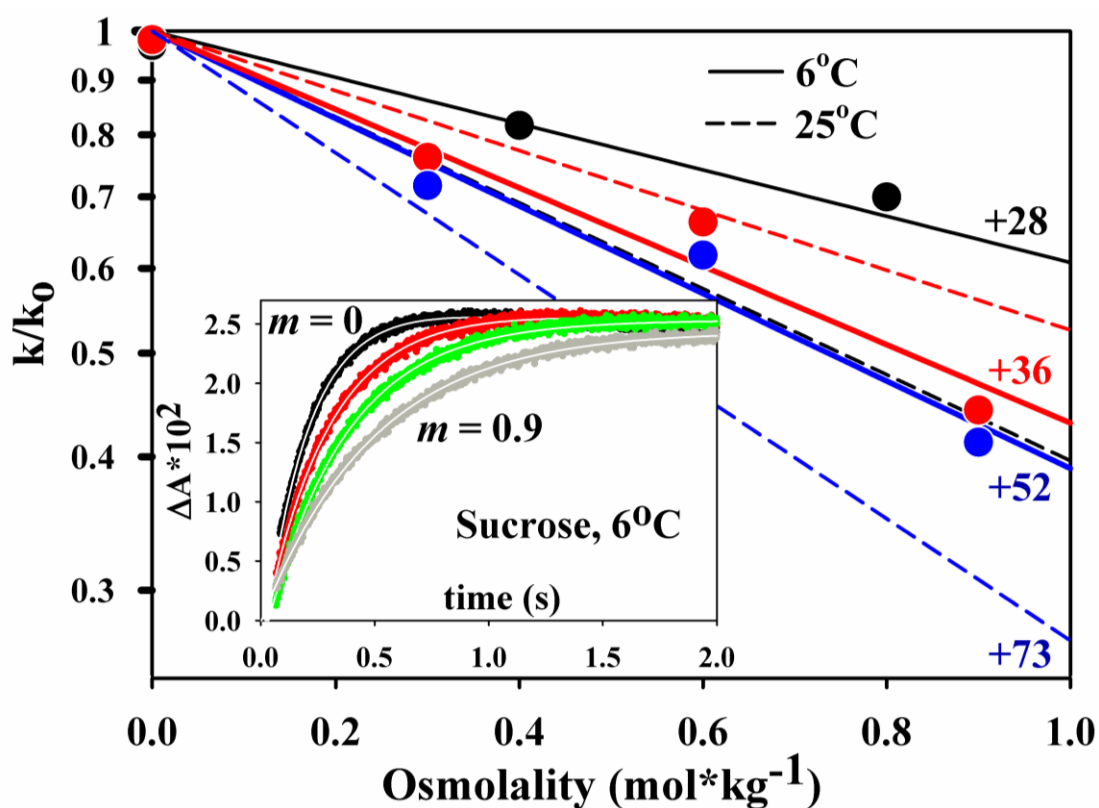


Figure 4-5. Plot of the solute-dependent osmotic effect on nitrogenase. Black = glycerol, red = glucose, blue = sucrose. Points and solid lines represent results at 6°C; dashed lines represent the previously published results at 25°C; glycerol alone could be examined to higher m and the additional points are shown in **Figure 4-S1**. **Inset:**

Stopped-flow oxidation of Fe^{red} within $[\text{Fe}^{\text{red}}(\text{MgATP})^2:\text{MoFe}]$ complex with increasing amounts of sucrose.

Changes in osmotic pressure modulate the energetics of reactions that change the number of bound waters. The rate constant for such a process varies exponentially with the molality of added solute (m) according to the equation,⁽²⁴⁾ $k(m) \propto \exp[-(\Delta n/55.6)m]$, where Δn is the number of waters absorbed in the transformation. Logarithmic plots of k_{obs} at 6°C vs molality for each solute employed are linear, as they are at ambient, **Figure 4-5**, revealing that the osmotic pressure effects that control ET at ambient persist at reduced temperatures. This linearity persists to higher osmolalities, as shown in **Figure 4-S8**. The slopes of these lines, which differ for the different osmolytes, reflect the numbers of waters absorbed during ET: $\text{slope} = -(\Delta n/55.6)$. At 25°C, $\Delta n = 50-80$ for the three osmolytes; at 5°C, $\Delta n = 30-50$. The decreased values of Δn at 6°C suggest that the osmolytes interact more strongly with the surface as the temperature is decreased.

The absence of an H_2O vs. D_2O solvent kinetic isotope effect (*sKIE*) for ET between the Fe protein and the MoFe protein at 6°C indicates that ATP hydrolysis is not rate limiting at low temperatures, just as it is not rate limiting at 25°C. In combination with the unchanging osmotic pressure effects over the temperature range, the results indicate that the order of the ATP hydrolysis event is unaffected by the change in temperature, and are consistent with there being no change in the mechanism with changing temperature. This conclusion is contrary to the earlier ITC findings that ATP hydrolysis precedes electron transfer at lower temperatures.

Does the temperature variation of k_{obs} imply a change of mechanism?

The Arrhenius plots of $\ln(k_{\text{obs}})$ vs $1/T$ presented in **Figure 4-3** for solutions carried out with both H_2O and D_2O MOPS solutions are non-linear, consistent with earlier findings for experiments carried out with H_2O buffer solutions.^(2, 17) The earlier work interpreted this nonlinearity to indicate a change in ET mechanism as the temperature is lowered from ambient. Those temperature variations were analyzed in terms of an apparent “break” at $T_b \sim 14^\circ\text{C}$ - 16°C that separates two linear segments in the plots of $\ln(k_{\text{obs}})$ vs $1/T$. Each segment was fit to its own slope, $(-\Delta H^\ddagger/R)$; each temperature range was assigned a different mechanism with a characteristic enthalpy of activation, ΔH^\ddagger , that is constant over the range. However, a real ‘break’ in slope is not possible for a finite system.⁽²⁵⁾ Instead, our finding that waters become bound to the protein-protein complex during the ET process *requires* that the Arrhenius plot be curved, even though the mechanism does not change. The binding of Δn waters during the ET reaction causes a change in the heat capacity, ΔC_p , which one can approximate as, $\Delta C_p \sim \Delta n[C_{\text{pm}}(\text{ice}) - C_{\text{pm}}(\text{liquid})] \sim \Delta n[-37\text{J/K}\cdot\text{mol}]$. This heat capacity difference in turn makes the enthalpy change, associated with the ET event temperature dependent, which induces curvature into the Arrhenius plot.

Taking the ET reaction as being governed by a conformational gating process that involves water binding,⁽⁵⁾ we now show that the temperature variation of the ET rate constant $k_{\text{obs}} = k_2$ can be described with a single set of thermodynamic parameters over the entire range of temperatures examined. Taking as a reference temperature that of the apparent “break”, T_b , one can write the enthalpy change for the ET reaction at any

temperature within this range as the sum of a temperature-independent enthalpy change, $\Delta H(T_b)$, plus the temperature-dependent contribution associated with water binding, ⁽²⁶⁾

$$\Delta H(T) = \Delta H(T_b) + \Delta C_p (T - T_b) \quad (4)$$

A Gibbs-Helmholtz equation for k_{obs} then leads to a temperature dependence, **Eq 5**. ⁽²⁶⁾

$$\ln \frac{k_{obs}(T)}{k_{obs}(T_b)} = -\frac{\Delta H(T_b)}{R} \left(\frac{1}{T} - \frac{1}{T_b} \right) + \frac{\Delta C_p}{R} \left[\ln \left(\frac{T}{T_b} \right) + \frac{T_b}{T} - 1 \right] \quad (5)$$

As shown in **Figure 4-3**, the combined temperature responses of k_{obs} in H₂O and D₂O buffers are indeed well described by the continuous function, **Eq 5**, with a single set of enthalpic parameters, $\Delta H(T_b)$ and ΔC_p , and thus by a single mechanism.

The resulting constant contribution to the enthalpy change, $\Delta H(T_b) = 130 \text{ kJ} \cdot \text{mol}^{-1}$, of **Eq 5**, is roughly the average of the values that would be obtained from a partition of the experimental data into two linear segments, with separate fits for each segment. The value, $\Delta C_p = -5.5 \text{ kJ} \cdot \text{mol}^{-1} \cdot \text{K}^{-1}$, corresponds to the uptake of $\Delta n \sim +150$ waters. Although Δn is considerably larger than Δn as determined in the osmotic pressure measurements, given that the latter suggest that Δn may change with T and the simplified form of **Eq 4**, we take the osmotic pressure measurements and temperature dependence of the ET rate constants as being satisfactorily self-consistent.

DISCUSSION

In this report, we have examined the temperature variation in the kinetics of oxidation of the Fe protein by the MoFe protein and tested for osmotic pressure effects and *sKIE*. The reported findings can be summarized as follows. (i) As the temperature is

lowered from 25 to 5°C at a constant pH fixed by MOPS buffer, the observed rate constant for $\text{Fe}^{\text{red}} \rightarrow \text{MoFe}$ protein ET decreases strongly, but with a non-linear Arrhenius plot, consistent with previous reports that employed buffers with high temperature coefficients. (ii) ET remains gated at the lowest temperature by a conformational change that involves the binding of numerous water molecules, and cooling does not introduce a solvent kinetic isotope effect (*sKIE*). (iii) These observations contradict the earlier proposals of a change in ET mechanism with cooling. (iv) In support of this mechanistic invariance, it is shown that the nonlinear Arrhenius plot for the ET rate constant arises from the change in heat capacity associated with the binding of waters, and does not indicate a change in mechanism. (v) Finally, it is shown that the Fe protein to MoFe protein extent of ET at constant pH does not change substantially with temperature, in contrast to the changing ET equilibrium inferred previously from experiments where cooling is accompanied by an increase in pH. Overall, these findings address multiple issues associated with inter-component oxidation of Fe^{red} by MoFe and overturn some long-held views about this process.

Our earlier study of intracomplex ET at ambient temperature employed the addition of viscogen/osmolyte solutes to reveal that the process is gated and responds to osmotic pressure effects, not changes in viscosity.⁽⁵⁾ The changes in k_{obs} with osmolality were interpreted as reflecting the binding of $\Delta n = \sim 50\text{-}80$ waters during ET, and it was inferred that this is associated with motions at the Fe-MoFe protein interface. We here show that osmotically controlled gating persists to 5°C. The osmolality dependence of k_{obs} at 5°C indicates that somewhat fewer waters bind upon cooling, $\Delta n = +30\text{-}50$, a result

that may be attributed to an increased interaction of osmolytes with protein surfaces at the lower temperatures.

The finding that ET remains gated down to the lowest temperature examined, along with the finding that ET is independent of solvent isotopic composition over the entire temperature range, suggests that the ET mechanism does not change upon cooling. Moreover, the observed osmotic pressure dependence provides the foundation for the explanation of the non-linear Arrhenius plots of k_{obs} in terms of a single, *unchanging* mechanism. The proposed analysis in terms of two linear segments that intersect at a ‘break’ temperature of 15°C that separates two temperature regions in which different mechanisms operated,^(16, 17) is thermodynamically untenable, while the finding that waters become bound during ET *requires* that the Arrhenius plot be nonlinear even *without* a change in mechanism. When waters bind during the reaction, the enthalpy of activation, ΔH^\ddagger , becomes temperature dependent because the heat capacity is different for free and bound waters (**Eq 4**). Application of the Gibbs-Helmholtz equation to the ET rate constant then necessarily yields a non-linear Arrhenius plot, **Eq 4**. As shown in **Figure 4-3**, the temperature response of k_{obs} can be well described by a fit to **Eq 5**, with a plausible value for the number of waters bound during ET. This eliminates the basis of the earlier suggestions for a change in mechanism.

This report further gives an alternative explanation to earlier reports that the extent of ET decreases from ~ 100% at ambient temperature to ~ 50% as the temperature decreases to ~ 5°C. The present experiments carried out with MOPS, a buffer whose pKa changes negligibly with temperature, indicate that at constant pH the extent of ET does *not* change within error upon cooling from 25 to 5 °C, and that this invariance is

independent of solvent isotope (H/D). Thus, our measurements indicate that the extent of ET at constant pH is not temperature dependent.

We do corroborate the finding that the extent of ET *does* change upon cooling of solutions prepared with buffers with a large temperature coefficient (HEPES buffer in our experiments, TES buffer in previous work). The pH changes by roughly 0.5 units upon cooling these buffer solutions to 5°C, and thus the changes in behavior upon cooling can be assigned not to the temperature variation of ET but to a pH dependence of the extent of ET at 5°C, which has been observed explicitly (**SI**). A determination of the origin of this dependence is beyond the scope of this report.

Conclusions: The “deficit spending” mechanism for $\text{Fe}^{\text{red}} \rightarrow \text{MoFe}$ protein ET mechanism that operates at ambient temperature does not change upon cooling to 5°C at constant pH. This mechanism likely is associated in some part with motions at the interface between the two proteins of the type schematized in **Figure 4-1**. The change in heat capacity caused by binding of waters during the ET process leads to a non-linear Arrhenius plot of the rate constant for ET versus inverse temperature, invalidating earlier interpretations of this non-linearity in terms of a change in ET mechanism. The extent of ET observed at ambient temperature does not change during cooling at constant pH, but likely varies with pH at constant, low temperature, where it also depends on solvent isotope. The origin of this last effect, suggestive of an equilibrium solvent isotope effect, remains to be determined.

REFERENCES

- (1) Smil, V. (2001) *Enriching the Earth: Fritz Haber, Carl Bosch, and the Transformation of World Food Production*, MIT Press, Cambridge, MA.
- (2) Thorneley, R. N. F., Ashby, G., Howarth, J. V., Millar, N. C., and Gutfreund, H. (1989) A transient-kinetic study of the nitrogenase of *Klebsiella pneumoniae* by stopped-flow calorimetry. Comparison with the myosin ATPase. *Biochem. J.* 264, 657-661.
- (3) Burgess, B. K., and Lowe, D. J. (1996) Mechanism of molybdenum nitrogenase. *Chem. Rev.* 96, 2983-3011.
- (4) Wilson, P. E., Nyborg, A. C., and Watt, G. D. (2001) Duplication and extension of the Thorneley and Lowe kinetic model for *Klebsiella pneumoniae* nitrogenase catalysis using a MATHEMATICA software platform. *Biophys. Chem.* 91, 281-304.
- (5) Danyal, K., Mayweather, D., Dean, D. R., Seefeldt, L. C., and Hoffman, B. M. (2010) Conformational gating of electron transfer from the nitrogenase Fe protein to MoFe protein. *J. Am. Chem. Soc.* 132, 6894–6895.
- (6) Hoffman, B. M., and Ratner, M. R. (1987) Gated electron transfer: when are observed rates controlled by conformational interconversion? *J. Am. Chem. Soc.* 109, 6237-6243.
- (7) Hoffman, B. M., Ratner, M. A., and Wallin, S. A. (1990) Energetics and dynamics of gated reactions: control of observed rates by conformational interconversion, in *Advances in Chemistry Series* (Johnson, M. K., King, R. B.,

- Kurtz, D. M., Jr., Kutsal, C., Norton, M. L., and Scott, R. A., Eds.), pp 125-146, American Chemical Society, Washington, DC.
- (8) Tezcan, F. A., Kaiser, J. T., Mustafi, D., Walton, M. Y., Howard, J. B., and Rees, D. C. (2005) Nitrogenase complexes: multiple docking sites for a nucleotide switch protein. *Science (Washington, DC, U. S.)* 309, 1377-1380.
- (9) Rees, D. C., Tezcan, F. A., Haynes, C. A., Walton, M. Y., Andrade, S., Einsle, O., and Howard, J. B. (2005) Structural basis of biological nitrogen fixation. *Phil. Trans. R. Soc. A* 363, 971-984.
- (10) Although binding of water at an interface can enhance ET (refs 11 and 12), and thus may contribute to gating, we surmise it is the unknown motions within the MoFe protein that are most important here.
- (11) de la Lande, A., Babcock, N. S., Rezac, J., Sanders, B. C., and Salahub, D. R. (2010) Surface residues dynamically organize water bridges to enhance electron transfer between proteins. *Proc. Natl. Acad. Sci. U. S. A.* 107, 11799-11804.
- (12) Keinan, S., Nocek, J. M., Hoffman, B. M., and Beratan, D. N. (2012) Interfacial hydration, dynamics and electron transfer: multi- scale ET modeling of the transient [Myoglobin, Cytochrome b5] complex. *Phys. Chem. Chem. Phys., in press*
- (13) Danyal, K., Dean, D. R., Hoffman, B. M., and Seefeldt, L. C. (2011) Electron transfer within nitrogenase: evidence for a deficit-spending mechanism. *Biochemistry* 50, 9255-9263.

- (14) Altenberg, G. A. (2004) Structure of multidrug-resistance proteins of the ATP-binding cassette (ABC) superfamily. *Curr. Med. Chem.: Anti-Cancer Agents* 4, 53-62.
- (15) Lowe, D. J., Ashby, G. A., Brune, M., Knights, H., Webb, M. R., and Thorneley, R. N. F. (1995) ATP hydrolysis and energy transduction by nitrogenase, in *Nitrogen Fixation: Fundamentals and Applications* (Tikhonovich, I. A., Provorov, N.A., Romanov, V.I., Newton, W.E. EDs.), pp 103-108, Kluwer Academic Publishers. Dordrecht, Netherlands.
- (16) Mensink, R. E., and Haaker, H. (1992) Temperature effects on the magnesium-ATP-induced electron transfer between the nitrogenase proteins from *Azotobacter vinelandii*. *Eur. J. Biochem.* 208, 295-299.
- (17) Lanzilotta, W. N., Parker, V. D., and Seefeldt, L. C. (1998) Electron transfer in nitrogenase analyzed by marcus theory: evidence for gating by MgATP. *Biochemistry* 37, 399-407.
- (18) Christiansen, J., Goodwin, P. J., Lanzilotta, W. N., Seefeldt, L. C., and Dean, D. R. (1998) Catalytic and biophysical properties of a nitrogenase apo-MoFe protein produced by a *nifB*-deletion mutant of *Azotobacter vinelandii*. *Biochemistry* 37, 12611-12623.
- (19) Burgess, B. K., Jacobs, D. B., and Stiefel, E. I. (1980) Large-scale purification of high activity *Azotobacter vinelandii* nitrogenase. *Biochim. Biophys. Acta* 614, 196-209.
- (20) Seefeldt, L. C., Morgan, T. V., Dean, D. R., and Mortenson, L. E. (1992) Mapping the site(s) of MgATP and MgADP interaction with the nitrogenase of

Azotobacter vinelandii. Lysine 15 of the iron protein plays a major role in MgATP interaction. *J. Biol. Chem.* 267, 6680-6688.

- (21) Lanzilotta, W. N., Fisher, K., and Seefeldt, L. C. (1996) Evidence for electron transfer from the nitrogenase iron protein to the molybdenum-iron protein without MgATP hydrolysis: characterization of a tight protein-protein complex. *Biochemistry* 35, 7188-7196.
- (22) Good, N. E., Winget, G. D., Winter, W., Connolly, T. N., Izawa, S., and Singh, R. M. M. (1966) Hydrogen ion buffers for biological research. *Biochemistry* 5, 467-477.
- (23) Thorneley, R. N. F., and Lowe, D. J. (1985) Kinetics and mechanism of the nitrogenase enzyme system, in *Molybdenum Enzymes* (Spiro, T. G., Ed.), pp 89-116, Wiley-Interscience, New York.
- (24) Parsegian, V. A., Rand, R. P., and Rau, D. C. (1995) Macromolecules and water: probing with osmotic stress. *Methods Enzymol.* 259, 43-94.
- (25) An abrupt "break" in a plot such as that of Fig 4 would imply the existence of a 2nd order phase change, and could not actually occur in a molecular system.
- (26) If the ET rate constant corresponds to that for the conformational gate, then its temperature response is characterized by the activation enthalpy. If ET involves a conformational preequilibrium, then the temperature variation would be described by the sum of the enthalpy change for the gating equilibrium and the ET activation enthalpy. In either case, in a precise application of transition-state theory the ratio, $[k_{\text{obs}}(T)/k_{\text{obs}}(T_b)]$ would be replaced by $[T_b(k_{\text{obs}}(T)/T(k_{\text{obs}}(T))]$,

but over the narrow range of temperatures examined, the parameters derived from such a fit differ insignificantly from that to the more intuitive **Eq 5**.

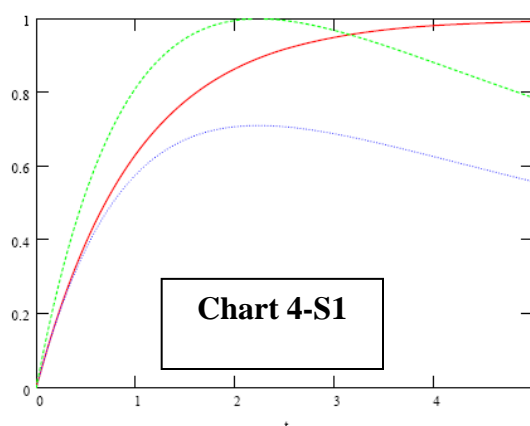
APPENDIX

Supporting Information

TEMPERATURE INVARIANCE OF THE NITROGENASE ELECTRON TRANSFER MECHANISM

Chart S1 and Fits to Eq 2

Prompted by comments from a reviewer, we incorporate **Chart 4-S1** from a Mathcad spreadsheet that demonstrates why fitting many of the traces to **Eq 2** is essential, by explicitly comparing a plot of an exponential rise-to-maximum to plots of **Eq 2**. This graph demonstrates that it is not appropriate to fit the multiphasic traces of **Figure 4-2** to a rise-to-maximum.



The **red** trace in the Chart corresponds to a simple exponential rise-to-maximum (set $\Delta A_r = 1$) for Fe^{red} oxidation, rate constant k_{obs} (consider $k_{\text{obs}} = 1$, or view the x-axis as being $x = k_{\text{obs}} * t$).

The **blue** trace is a plot of **Eq 2** for the same $k_{\text{obs}} = 1$ and $\Delta A_r = 1$, but with a slow followup reaction having $k_{\text{Dr}} = k_{\text{obs}}/5$ to a product with $\Delta A_{\text{Dr}} = 1/10$. The shape of this trace is qualitatively like many in our paper.

The **green** trace normalizes the **blue** trace for comparison to the simple exponential rise.

Firstly, one sees that the absorbance maximum of the **blue** trace is suppressed; a fit of this trace to a rise-to-maximum would underestimate ΔA_r .

Secondly, comparison of the *red* (exponential rise) and *green* (normalized **Eq 2**) traces shows that the apparent rise rate in the *green* trace for **Eq 2** is greater than the k_{obs} rise. Thus fitting an experimental trace to a rise-to-maximum would give a rate constant larger than k_{obs} , as well as an absorbance change too small.

Thus, to get the proper absorbance change and rate constant for oxidation of Fe^{red} from multiphasic SF traces like those of **Figure 4-2** one should use **Eq 2**.

However, as we explicitly state in Materials and Methods, the trends in the resulting parameters obtained by earlier workers as a consequence of changing temperature/osmotic pressure (including ourselves; see below), are correctly represented.

We further comment on the absorbance change during the deadtime, incorporated in **eq 2** as ΔA_0 . Given the relative timescales for the first and second step of the two-step reaction, this absorbance change can indeed be assigned to intracomplex oxidation of Fe^{red} . However, the state formed will convert slowly to **C**, and thus this term, in principle, has a time dependence (rate constant, k_{Dr}) as well. However, we have explored the consequences of including this phenomenon in the fits, and find that this added complexity causes negligible change in the parameters of importance, k_{obs} and ΔA . Therefore we have chosen not to incorporate what amounts to a pseudo-sophistication.

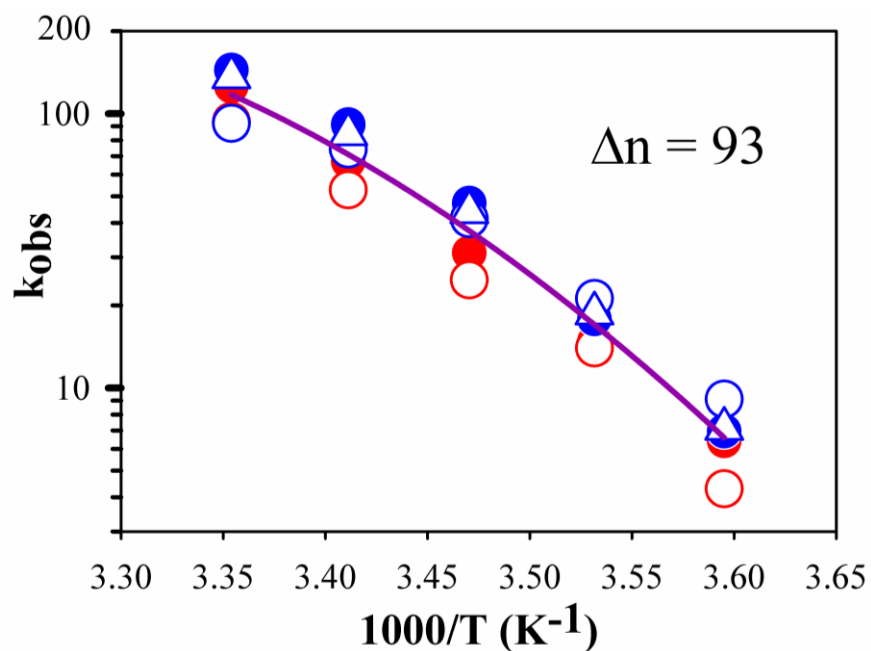


Figure 4-S2: Semi-logarithmic plot of the observed rate constants, k_{obs} , vs inverse temperature for D₂O and H₂O when traces are truncated to 0.5s and fit to a rise-to-maximum. Purple solid line is a fit to all data sets, assuming that k_{obs} is the same for H₂O and D₂O buffers.

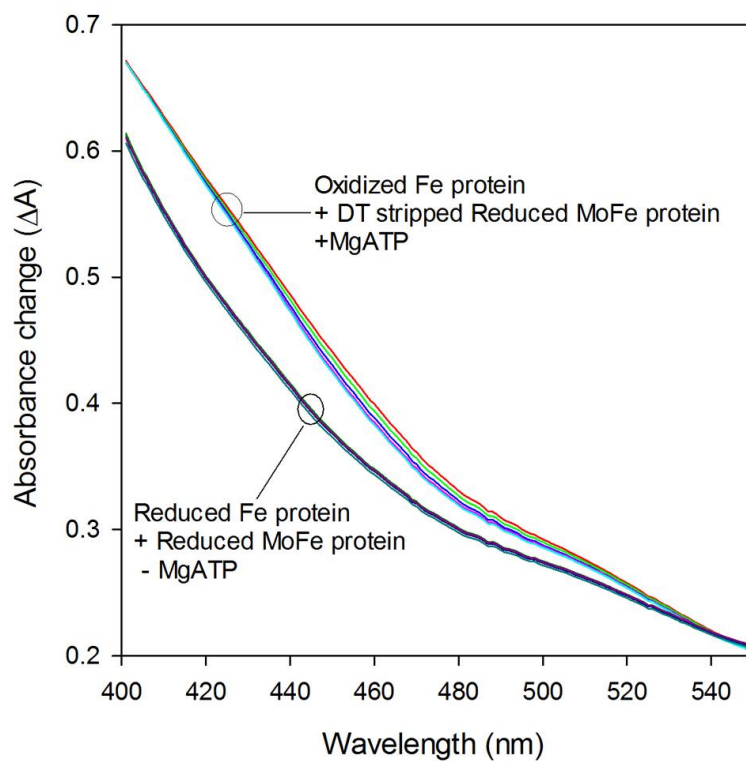


Figure 4-S3. Temperature profile of the optical change in the Fe protein in the presence of the MoFe protein. Colors represent different temperatures equally spaced within the range, 25°C-5°C, and overlay within error.

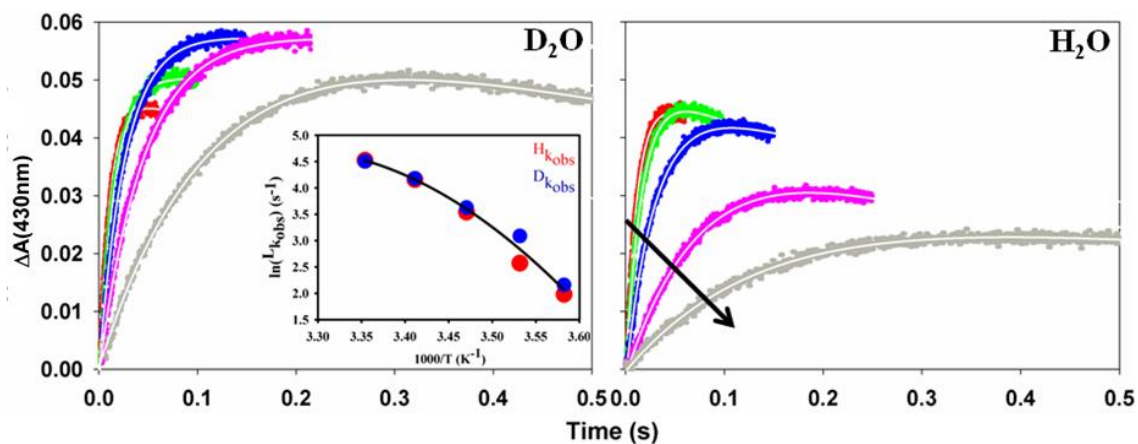


Figure 4-S4. Temperature-response stopped-flow traces for oxidation of Fe^{red} within $[\text{Fe}^{\text{red}}(\text{MgATP})_2;\text{MoFe}]$ complex in HEPES buffer for H_2O and D_2O . Arrow in H_2O plot points in the direction of decreasing temperature, from 25°C to 5°C . D_2O plot has corresponding color scheme with temperature. **Inset:** Logarithmic plot of the observed rate constants, $^Lk_{\text{obs}}$ for $L = \text{D}$ (D_2O) and $L = \text{H}$ (H_2O). Black solid line is a fit to both data sets, assuming that there is no difference in $^Lk_{\text{obs}}$ for $L = \text{H}, \text{D}$, and $\Delta n = +136$.

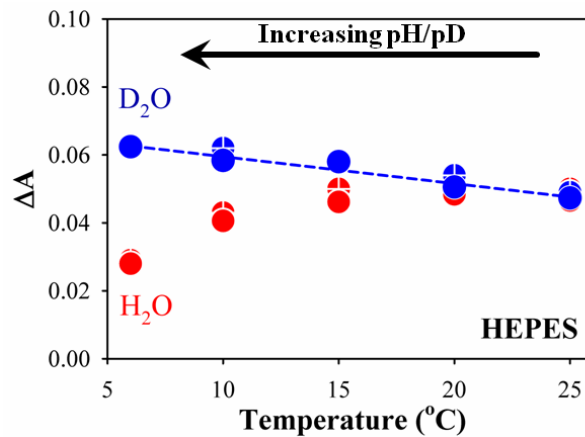


Figure 4-S5: Temperature dependence of absorbance changes ΔA , (Eq 2) obtained from intracomplex oxidation of $\text{Fe}^{\text{red}}(\text{ATP})_2$ by MoFe as a function of temperature in HEPES buffer. Blue circles: D_2O , red circles: H_2O . Blue dashed line is a linear fit to D_2O data. Black arrow indicates the direction of increasing pH/pD with temperature in HEPES buffer.

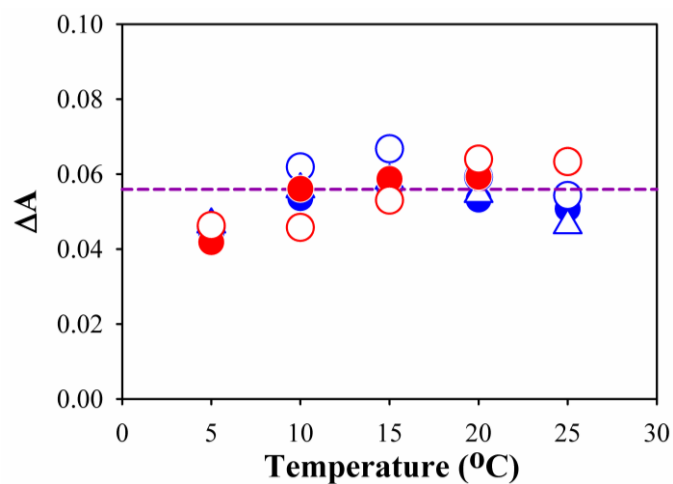


Figure 4-S6: Temperature dependence of absorbance changes ΔA , (**Eq 2**) obtained from intracomplex oxidation of $\text{Fe}^{\text{red}}(\text{ATP})_2$ by MoFe as a function of temperature for traces that have been truncated to 0.5s and fit to a rise-to-maximum. Purple dashed line is the average of all values.

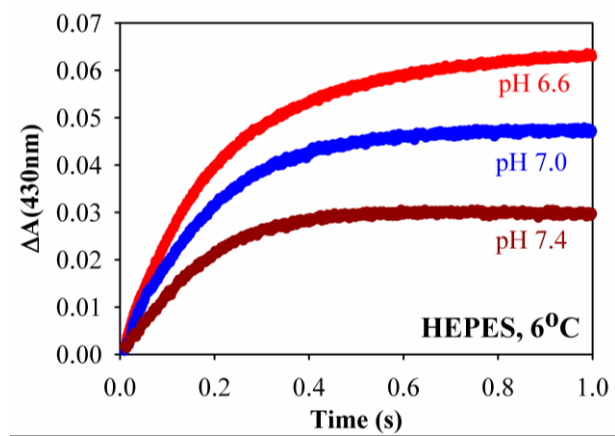


Fig 4-S7: pH dependence of ET kinetic traces for reaction carried out in HEPES at 5°C. pH 6.6 (red) pH 7.0 (blue) and pH 7.4 (Dark red) are shown.

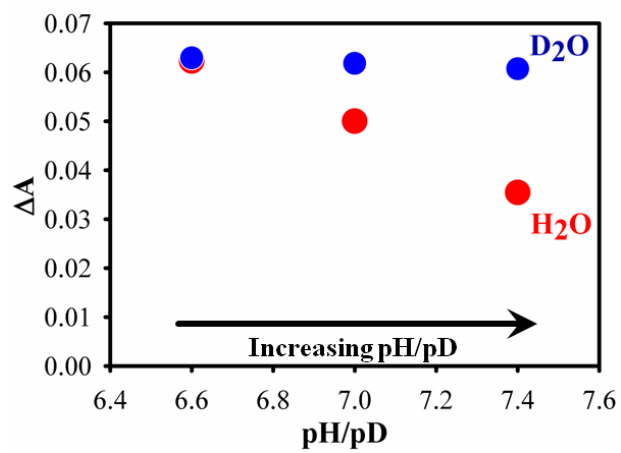


Fig 4-S8: pH/pD dependence of absorbance changes ΔA , in HEPES buffer at 5°C. Black arrow indicates the direction of increasing pH/pD.

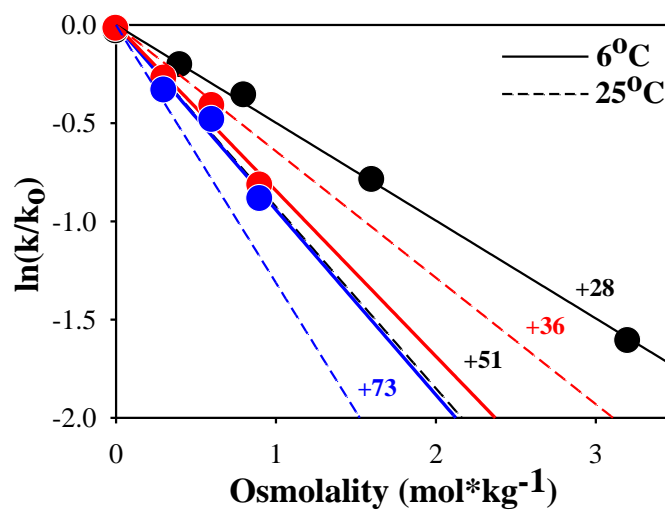


Figure 4-S9. Plot of the solute-dependent osmotic effect on Nitrogenase. **Black** = glycerol, **red** = glucose, **blue** = sucrose. Points and solid lines represent results at 6°C; dashed lines represent the previously published results at 25°C.

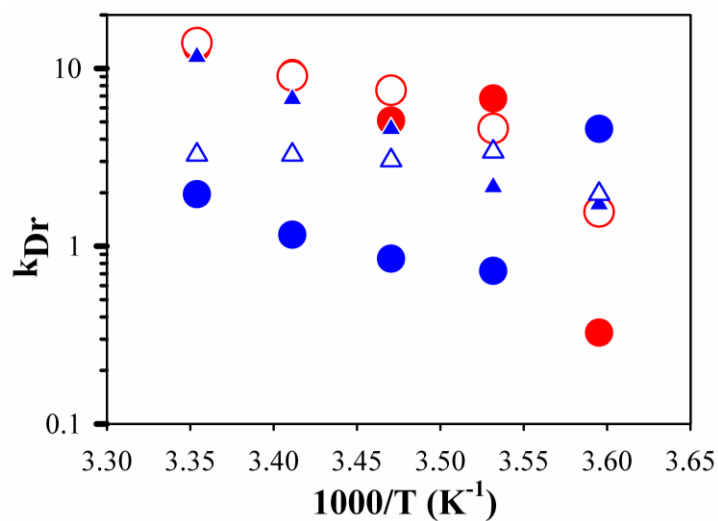


Figure 4-S10: Semi-logarithmic plot of the rate constant vs inverse temperature for the re-reduction of Fe^{ox} to Fe^{red}, k_{Dr} **Eq 2**, for D₂O and H₂O buffers. Blue circles and triangles represent D₂O, while red circles represent H₂O. Open and closed circles and triangles represent separate experiments.

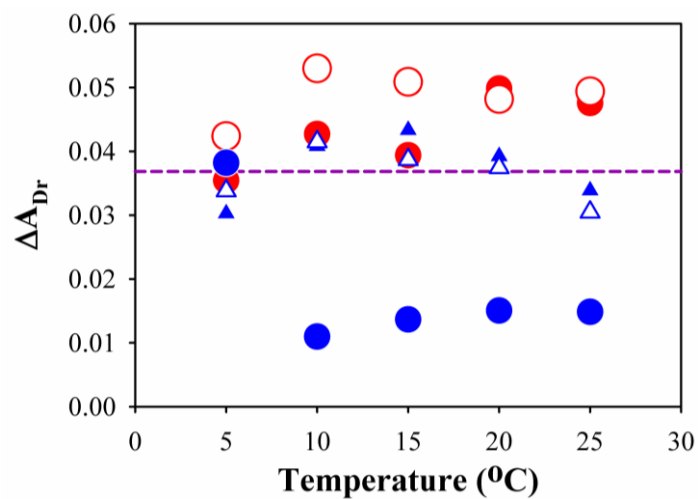


Figure 4-S11: Temperature dependence of absorbance changes ΔA_{Dr} , (Eq 2) associated with the re-reduction of Fe^{ox} to Fe^{red} as a function of temperature. Purple dashed line is the average of all values.

CHAPTER 5

**ELECTRON TRANSFER PRECEDES ATP HYDROLYSIS DURING
NITROGENASE CATALYSIS***

ABSTRACT

The biological reduction of N_2 to NH_3 catalyzed by Mo-dependent nitrogenase requires at least eight rounds of a complex cycle of events associated with ATP-driven electron transfer (ET) from the Fe protein to the catalytic MoFe protein, with each ET coupled to the hydrolysis of two ATP molecules. While steps within this cycle have been studied for decades, the nature of the coupling between ATP hydrolysis and ET, in particular the order of ET and ATP hydrolysis, has been elusive. Here, we have measured first-order rate constants for each key step in the reaction sequence, including direct measurement of the ATP hydrolysis rate constant: $k_{ATP} = 70 \text{ s}^{-1}$, 25°C . Comparison of the rate constants establishes the reaction sequence involves four sequential steps: (i) conformationally gated ET ($k_{ET} = 140 \text{ s}^{-1}$, 25°C), (ii) ATP hydrolysis ($k_{ATP} = 70 \text{ s}^{-1}$, 25°C), (iii) Pi release ($k_{Pi} = 16 \text{ s}^{-1}$, 25°C), and (iv) Fe protein dissociation from the MoFe protein ($k_{diss} = 6 \text{ s}^{-1}$, 25°C). These findings allow the completion of a comprehensive thermodynamic model for the cycle undergone by the Fe protein, revealing that it is not the energy of ATP hydrolysis, but rather the energy of ATP binding and protein-protein formation that drives ET.

*Coauthored by Simon Duval, Karamatullah Danyal, Sudipta Shaw, Anna K Lytle, Dennis Dean, Brian M. Hoffman, Edwin Antony and Lance C. Seefeldt (2013) manuscript submitted to PNAS on 06/12/2013.

INTRODUCTION

Biological nitrogen fixation catalyzed by the Mo-dependent nitrogenase has a limiting reaction stoichiometry shown in **eq 1** (1, 2):



The ATP-driven reduction of one N_2 with evolution of one H_2 requires a minimum of 8e^- and the hydrolysis of 16 ATP molecules in a complex cascade of events in which electron transfer (ET) from the nitrogenase Fe protein to the catalytic MoFe protein is coupled to the hydrolysis of two ATP molecules (1, 3, 4). The Fe protein is a homodimer with a single [4Fe-4S] cluster and two nucleotide binding sites, one in each subunit (5). The MoFe protein is an $\alpha_2\beta_2$ tetramer, with each $\alpha\beta$ pair functioning as a catalytic unit that binds an Fe protein (6). Each $\alpha\beta$ unit contains an [8Fe-7S] cluster (abbreviated P-cluster) and a [7Fe-9S-Mo-C-R-homocitrate] cluster (abbreviated FeMo-cofactor or M-cluster) (6–10). In each ET event, the Fe protein, in the reduced (1+) state with two bound ATP, first associates with the MoFe protein (**Figure 5-1**). In a recent model, termed “deficit-spending,” it is proposed that this association triggers a two-step ET event (11, 12). The first ET step occurs inside the MoFe protein, involving ET from the P cluster resting state (P^{N}) to the resting FeMo-cofactor (M^{N}) cluster, resulting in an oxidized P cluster (P^{1+}) and a reduced FeMo-cofactor (M^{R}) (12). This ET event is conformationally gated (11) with an apparent first order rate constant (k_{ET}) between 100–140 s^{-1} (11, 12). In the second ET step, an electron is transferred from the Fe protein [4Fe-4S] cluster to the oxidized P^{1+} cluster, resulting in the return of the P cluster to the resting oxidation state (P^{N}) and an oxidized $[\text{4Fe-4S}]^{2+}$ cluster in the Fe protein (12). This second step is fast, having a rate constant greater than 1700 s^{-1} (12).

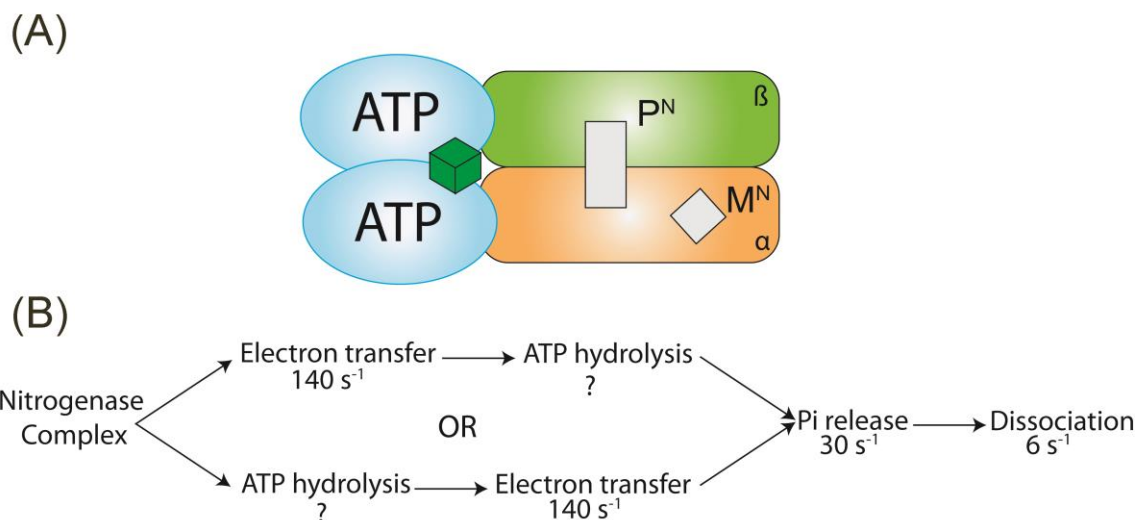


Figure 5-1: Order of events in nitrogenase complex. (A) The Fe protein subunits are shown as two blue ovals (left) with an ATP bound in each subunit and the [4Fe-4S] cluster (green cubane). The MoFe protein α subunit (orange) and beta subunit (green) are shown on the right, with the P^N cluster shown as a gray box and the FeMo-cofactor (M^N) shown as a gray diamond. (B) From left to right, order of events in the nitrogenase electron transfer is shown with rate constants (s^{-1}) displayed where known.

Transfer of one electron from the Fe protein to an $\alpha\beta$ -unit of MoFe protein is known to be coupled to the hydrolysis of the two ATP molecules bound to the Fe protein, yielding two ADP and two Pi (2). Following the hydrolysis reaction, the two Pi are released from the protein complex with a first order rate constant (k_{Pi}) of $22 s^{-1}$ at $23^\circ C$ (13). The last event in the cycle is the release of the oxidized Fe protein with two ADP bound, $[Fe^{ox}(ADP)_2]$ from the MoFe protein with a rate constant (k_{diss}) of $\sim 6 s^{-1}$, the rate-limiting step in catalysis at high electron flux (14). After dissociation from the MoFe

protein, the $[\text{Fe}^{\text{ox}}(\text{ADP})_2]$ protein is prepared for a second round of electron delivery by one-electron reduction to $[\text{Fe}^{\text{red}}(\text{ADP})_2]$ and replacement of the two MgADP by MgATP. This cycle is repeated until enough electrons are transferred to the MoFe protein to achieve substrate reduction (15).

Although the energetic coupling between ET and ATP hydrolysis is firmly established (1, 3, 4, 16), the nature of this coupling has remained unresolved: does ATP hydrolysis itself provide the principal energy input for the conformational change(s) that drive ET from Fe protein to the MoFe protein, or, does the bound ATP induce the formation of a reactive, “activated” conformation of the complex, with ET being driven by the free energy of ATP-activated protein-protein binding. These alternatives are characterized by different orders of ET and ATP hydrolysis, but the order has never been established. Some studies have indicated that ATP hydrolysis occurs after ET (13, 17, 18), while other studies have suggested just the opposite; namely that ATP hydrolysis occurs before ET (15, 16, 19, 20). One of the reasons for this lack of clarity in the order of these key events is the absence of direct measurement of ATP hydrolysis rates by nitrogenase within a single catalytic cycle. The rate constant for Pi release during one cycle has been measured, thereby establishing a lower limit on the rate constant for ATP hydrolysis (13). However, the rate constant for ATP hydrolysis could be much faster than Pi release, and could be faster than the rate constant for ET.

Here, we have directly measured the rate constant for ATP hydrolysis for a single nitrogenase turnover cycle, as well as measuring the rate constants for each of the other key steps under the same conditions, thereby allowing an unequivocal assignment of the

order of events in a single electron-transfer cycle. Establishing the order of events allows a full thermodynamic Fe protein cycle to be constructed.

RESULTS

ATP hydrolysis and Pi release. The hydrolysis of the 2 ATP bound in the Fe protein to 2 ADP + 2 Pi is initiated during the transient association of the Fe protein with the MoFe protein; ATP hydrolysis is not catalyzed by the Fe protein alone (1). Pre-steady state rates of ATP hydrolysis during a single Fe-MoFe protein association event have never been reported, although steady-state rates have been reported in several earlier studies, with typical rates ranging from 3600-4500 nmols.min⁻¹.(mg MoFe protein)⁻¹ (21). These prior steady-state measurements relied on quantification of released ADP or Pi over multiple turnovers, and thus provide little insight into the rate of ATP hydrolysis during the first turnover (21).

Establishing a pre-steady state rate for ATP hydrolysis is challenging, requiring quantification of ATP consumed and ADP formed on a millisecond time scale. To make this measurement, we employed a rapid chemical-quench approach to stop ATP hydrolysis at selected times after initiating the reaction, with an instrument dead-time of 4 ms and time resolution of 1 ms. The ATP and ADP in each quenched solution were quantified by utilizing ³²P-ATP (labeled on the α -phosphate) as a tracer. For each sample, ATP was separated from ADP by thin-layer chromatography, with quantification of each nucleotide accomplished by counting of the ³²P. Using this approach, it was possible to establish the precise concentration of ADP formed as a function of time after

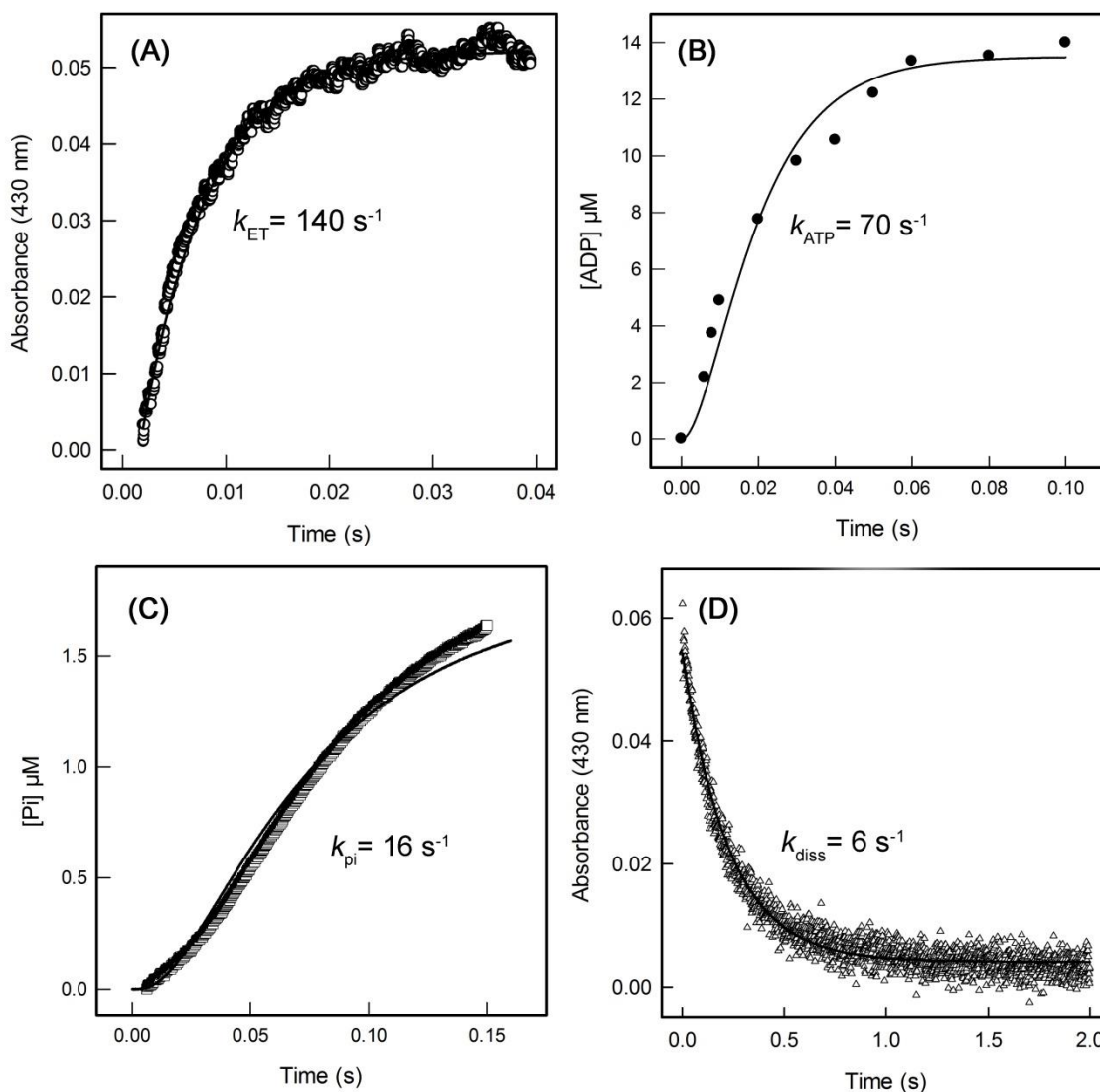


Figure 5-2: Kinetics of key nitrogenase catalytic steps. (A) Electron transfer is monitored as the change in absorbance at 430 nm as a function of time (open circles). The data were fit to the sequential kinetic model (eqn 2) (line), with a calculated k_{ET} of 140 s^{-1} . (B) ATP hydrolysis is monitored as the formation of $\alpha\text{-}^{32}\text{P}\text{-ADP}$ as a function of time (closed circles). The data were fit to eqn 2 (line), with a calculated k_{ATP} of 70 s^{-1} . (C) Phosphate (Pi) release is monitored by the increase in fluorescence from Pi binding to MDCC-labeled phosphate binding protein as a function of time (open square). The data were fit to eqn 2 (line), with a calculated k_{Pi} of 16 s^{-1} . (D) Dissociation of Fe from the MoFe protein is monitored by the decrease in absorbance at 430 nm as a function of time (open triangle). The data were fit to a single exponential equation (solid line) with a first order rate constant (k_{diss}) of 6 s^{-1} . All four experiments were carried out under the same experimental conditions at $25 \text{ }^\circ\text{C}$.

initiating the reaction by rapid-mixing (**Figure 5-2B**). Over the time range examined (up to 200 ms), the quantity of ADP formed was observed to rise rapidly to a plateau. These data were initially fit to an exponential rise to maximum to get an estimated rate constant, that was found to be noticeably less than k_{ET} , and then the ATP hydrolysis data were fit to the kinetic model described in Materials and Methods (eq 2), yielding a rate constant for ATP hydrolysis, $k_{ATP} = 70 \pm 7 \text{ s}^{-1}$ at 25°C.

The rate constant for ATP hydrolysis determined here can be compared to the rate constant for Pi release. In earlier studies, pre-steady state Pi release was found to have a rate constant (k_{Pi}) of $\sim 22 \text{ s}^{-1}$, roughly three-fold less than k_{ATP} (13). The conditions used in the earlier studies were different from the conditions used in the ATP hydrolysis studies reported here, so the Pi release experiment was conducted under the same conditions used for the measurement of ATP hydrolysis. Pi release was detected by binding of the free Pi to a phosphate-binding protein labeled with a fluorescent reporter (MDCC-PBP) that shows a 7-fold increase in fluorescence upon Pi binding, thereby allowing real-time monitoring of Pi release using a stopped-flow fluorometer (**Figure 5-2C**) (22). The concentration of Pi released as a function of time was fit to the kinetic model described in Materials and Methods (**eq 2**), yielding a rate constant, $k_{Pi} = 16 \pm 1 \text{ s}^{-1}$, which is consistent with earlier reports. **Figure 5-2C** shows that the kinetic model fits the Pi release data up to almost 150 ms quite satisfactorily, but it was also recognized that at later times the Pi release was more complex due to the achievement of a steady state. As indicated by the result, $k_{Pi} < k_{ATP}$, and as visualized when the progress curves for ATP hydrolysis and Pi release are plotted together on a logarithmic time plot (**Figure 5-3**), Pi

is not released promptly upon ATP hydrolysis, but rather occurs as a subsequent kinetic step with a detectable delay after ATP hydrolysis.

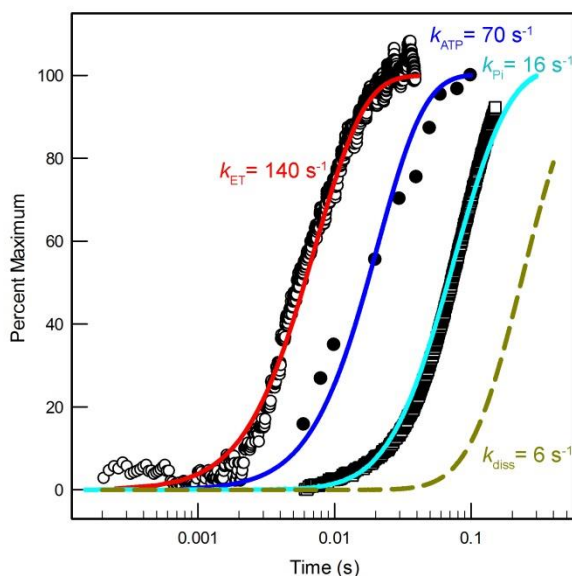


Figure 5-3: Time course for key steps in the nitrogenase cycle. The data for ET (\circ), ATP hydrolysis (\bullet), and Pi release (\square) are plotted as a function of the logarithm of time. Each data set was fit to the model in eqn 2 (solid lines), with the calculated rate constants noted. The protein-protein dissociation is represented by a simulation (dashed green line) generated using the kinetic model (**eqn 2**), with rate constants fixed at $k_{ET} = 140 \text{ s}^{-1}$, $k_{ATP} = 70 \text{ s}^{-1}$, and $k_{Pi} = 16 \text{ s}^{-1}$.

ATP hydrolysis compared to electron transfer. The rate constant for ET from the Fe protein to the MoFe protein (k_{ET}) has been reported to be between 100-150 s^{-1} (23), depending on reaction conditions and the proteins used. This rate constant was re-examined in the present study under identical conditions to the Pi release and ATP hydrolysis measurements. ET is monitored by the absorbance increase that accompanies

oxidation of the Fe protein [4Fe-4S] cluster after initiation of the reaction (**Figure 5-2A**). Fit of these data to the kinetic model (eq 2) yields an apparent first order rate constant of $k_{\text{ET}} = 140 \pm 10 \text{ s}^{-1}$. This rate constant reflects the oxidation of the Fe protein as an electron is delivered to the MoFe protein, a process recently shown to be gated by protein conformational changes (11). In the deficit-spending model of ET, the observed ET is the last ET event, following conformational gating and ET from the P cluster to FeMo-cofactor (12). Thus, the observed first order rate constant of 140 s^{-1} reflects both protein conformational changes and all ET events.

The rate constant for ATP hydrolysis of $k_{\text{ATP}} = 70 \text{ s}^{-1}$ is half that of the measured ET rate constant, clearly placing ATP hydrolysis as a distinct kinetic step that *follows* ET. The order of events is visualized by comparing ET, ATP hydrolysis, and Pi release data on a logarithmic time plot (**Figure 5-3**): ET occurs first, followed by ATP hydrolysis, followed by Pi release.

Protein-protein dissociation. Earlier studies have shown that Fe protein dissociation from the MoFe protein is the last event in the cycle, with a first order rate constant (k_{diss}) ranging from 5 to 10 s^{-1} (14). We directly determined this dissociation rate constant, as described in Materials and Methods, under the same conditions as the other measurements (**Figure 5-2D**), finding a first order rate constant of $k_{\text{diss}} = 6 \pm 2 \text{ s}^{-1}$ from a fit to an exponential of the absorbance change associated with $\text{Fe}(\text{ADP})_2$ reduction subsequent to mixing of $[\text{Fe}^{\text{ox}}(\text{ADP})_2;\text{MoFe}]$ upon mixing. This value is consistent with protein-protein dissociation being a discrete kinetic step and the last event during the catalytic cycle. The dissociation event is simulated with the kinetic model (**eq 2**), by fixing the ET, ATP hydrolysis, Pi release, and dissociation rate constants. The simulation (presented as a rise to maximum) clearly places the dissociation as the last event in the series, in a kinetic step distinct from Pi release (**Figure 5-3**).

DISCUSSION

Model for Events in the Nitrogenase Cycle. The measurement of the pre-steady state rate constant for ATP hydrolysis reported here defines the order of the key events involved in electron transfer within the Fe protein-MoFe protein complex. As is evident in the kinetic progress curves shown in **Figure 5-3**, the order of events is established as: (i) ET, (ii) ATP hydrolysis, (iii) Pi release, followed by (iv) dissociation of the Fe protein from the MoFe protein.

The findings of the current study can be combined with earlier findings to construct a model of the key events that occur during one round of Fe protein-MoFe protein association (**Figure 5-4**). The process begins with the formation of a complex between $\text{Fe}^{\text{red}}(\text{ATP})_2$ and an $\alpha\beta$ catalytic unit of the MoFe protein (**Figure 5-4**, upper left). This association is known to be fast, with a second order rate constant (k_{assoc}) of $5 \times 10^7 \text{ M}^{-1} \text{ s}^{-1}$ (24). At the concentration of Fe protein used in the present study, the association event is much faster than subsequent events, so all the measurements described here correspond to first-order, intra-complex steps.

Recent studies on the effects of osmotic pressure on the rate of ET have established that following protein-protein association, large scale ($\sim 800 \text{ \AA}^2$ changes in buried surface) conformational changes within the complex gate subsequent ET events (11). It has been suggested that these conformational changes result in activation of the P cluster to a state (P^*) that transfers an electron to FeMo-cofactor, forming the oxidized P cluster (P^{1+}). In this model, subsequent ET from $\text{Fe}^{\text{red}}(\text{ATP})_2$ to the oxidized P cluster is fast and not gated by protein conformational changes, and generates the final product of intra-complex ET, $\text{Fe}^{\text{ox}}(\text{ATP})_2$ bound to MoFe protein containing a resting P cluster and

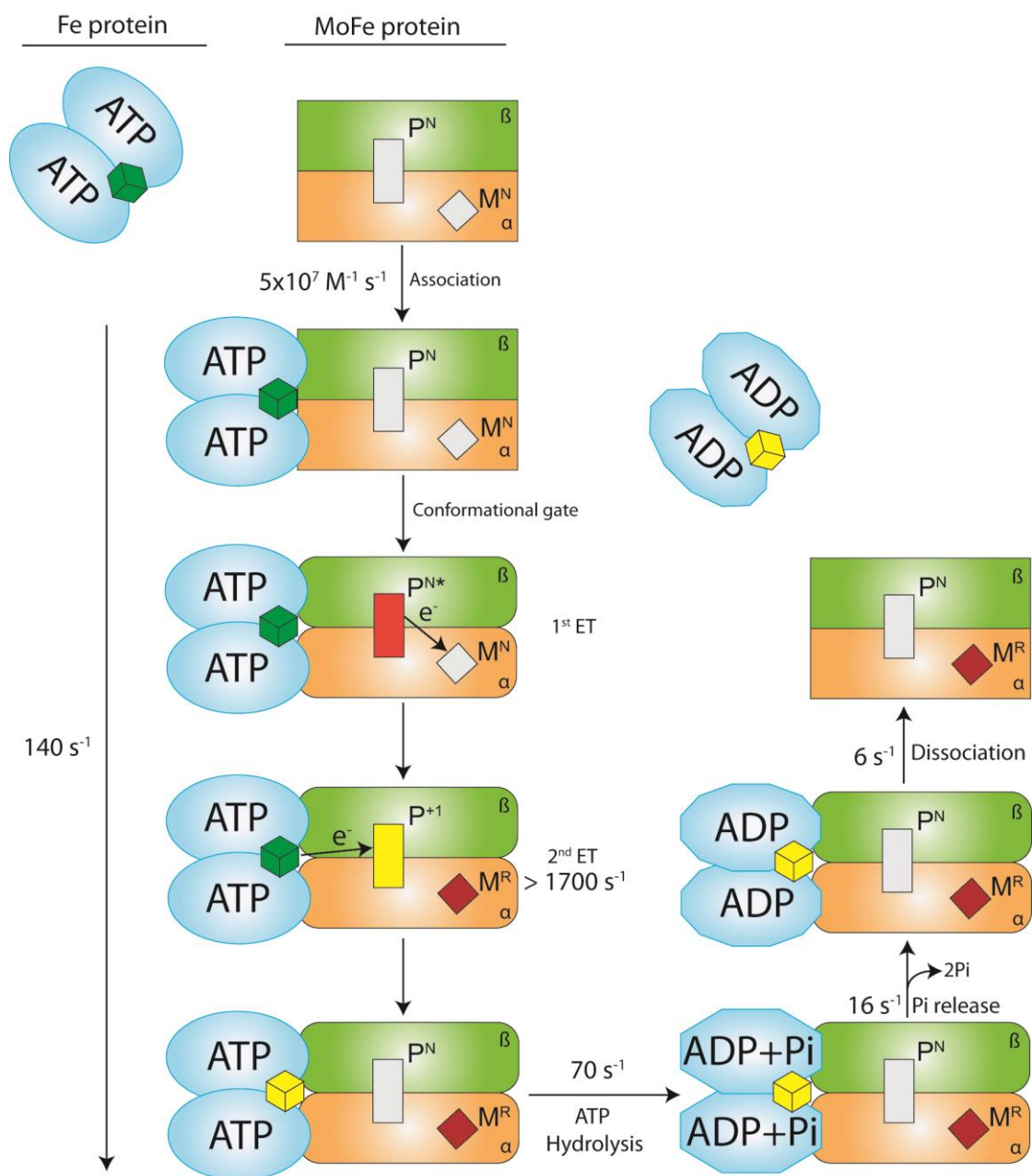


Figure 5-4: Model of nitrogenase order of events. Shown are the Fe protein (blue ovals) with the [4Fe-4S] cluster in the +1 (green cube) or +2 (yellow cube) oxidation state. The MoFe protein (α subunit orange and β subunit green) with the P cluster (rectangle, grey P^N, red activated P^{N*} and yellow P⁺¹ states) and the M cluster (diamond, grey M^N and maroon M^R state). The reaction sequence starts at the top left with the association of the Fe protein with the MoFe protein and ends at top right with the dissociation of the oxidized Fe protein from the reduced MoFe protein. First order rate constant ($k, \text{ s}^{-1}$) values for 25°C are shown. Conformational changes in the Fe protein and MoFe protein are denoted by changes in shape of the ovals or rectangles.

one-electron reduced FeMo-cofactor (M^R). The overall rate constant for the multiple steps in the ET process is 140 s^{-1} (12).

As established here, hydrolysis of the two ATP molecules to ADP and Pi occurs as a distinct kinetic step that follows this ET process. Data shown in **Figure 5-3** further establishes that Pi is not released from the protein-protein complex immediately upon ATP hydrolysis, but Pi is released in a distinct, subsequent step. It seems reasonable to conclude that upon ATP hydrolysis, the complex undergoes conformational changes, although the extent of such changes has not been established. Likewise, it seems reasonable that the release of Pi is accompanied by additional protein conformational changes, but again such changes have not been measured directly.

The final step in the ET process is the release of the $\text{Fe}^{\text{ox}}(\text{ADP})_2$ from the one-electron reduced MoFe protein (**Figure 5-4**) in a process that is not synchronous with Pi release, but follows as a discrete step with a rate constant of 6 s^{-1} , as has been established in earlier studies (1, 13, 14). The MoFe protein that contains a one electron reduced FeMo-cofactor is then free to be reduced additional times by repeating the process presented in **Figure 5-4**, beginning with the binding of a second $\text{Fe}^{\text{red}}(\text{ATP})_2$ (15). The released $\text{Fe}^{\text{ox}}(\text{ADP})_2$ is ready to be returned to the $\text{Fe}^{\text{red}}(\text{ADP})_2$ state by reduction of its $[\text{4Fe-4S}]^{2+}$ cluster reduced back to the +1 oxidation state, and replacement of ADP by ATP.

The Fe-protein Cycle. By revealing that intra-complex $\text{Fe}^{\text{red}}(\text{ATP})_2 \rightarrow \text{MoFe}$ protein ET is followed by ATP hydrolysis (**Figure 5-4**), this work also completes the overall 'Fe-protein cycle' first formulated by Lowe and Thorneley (LT) to summarize the steps undergone by the Fe protein as it delivers an electron to the MoFe protein (1, 17).

Figure 5-5 presents the key Fe-protein reactions formulated as a thermodynamic cycle. The cycle begins with free $\text{Fe}^{\text{ox}}(\text{ADP})_2$ (upper right), the final form of Fe protein at the end of a previous ET cycle, and ends with a return to this state upon completion of the cycle. **Figure 5-5** is further annotated to emphasize the function of the Fe protein as a ‘nucleotide switch’ (25, 26) that uses ATP binding/hydrolysis to ‘transport’ an electron from an electron source/reductant to the MoFe protein. Viewed in this way, **Figure 5-5** introduces a correspondence of the thermodynamic cycle for ATP-dependent ‘electron transport’ by the Fe protein with the thermodynamic cycle for ATP-dependent substrate export by ABC transporters (27–30).

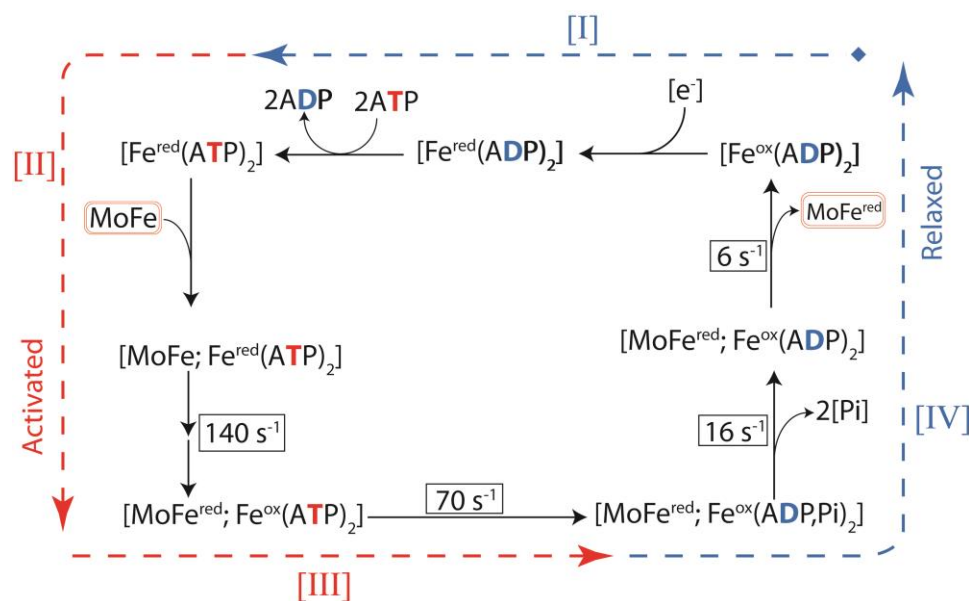


Figure 5-5: Thermodynamic Fe-protein cycle. Drawn with a focus on Fe protein electron transport to MoFe protein, it can be viewed as starting at upper right. MoFe^{red} represents reduced MoFe protein. Dashed arrows and notation that surround the cycle refer to analogy with ABC exporter thermodynamic cycle (see text).

The Fe-protein cycle of **Figure 5-5** (top, right to left) begins with the reduction of $\text{Fe}^{\text{ox}}(\text{ADP})_2$ to $\text{Fe}^{\text{red}}(\text{ADP})_2$, which triggers rapid replacement of the two ADP by two ATP (1, 17). The structure of the Fe protein undergoes major changes upon ATP binding, leading to numerous changes in its properties, but historically interest has focused on an ~ -120 mV change in the reduction potential of the [4Fe-4S] cluster of nucleotide-free Fe protein upon ATP binding, and the possibility that this change in potential is central to initiating the transfer of an electron to MoFe protein. Although the more negative midpoint potential would favor ET (1), for present purposes it is important to note (**Figure 5-5**) that the second step in the thermodynamic Fe protein-cycle is not ATP binding to free Fe protein, but replacement of bound ADP by ATP. Namely, the free Fe^{red} does not appear in the thermodynamic cycle regardless of the mechanistic details of the nucleotide interchange. In fact, the reduction potentials of $\text{Fe}^{\text{ox}}(\text{ADP})_2$ to $\text{Fe}^{\text{red}}(\text{ADP})_2$ are the same (31). As a result, ATP/ADP exchange is iso-potential, and so the potential lowering upon nucleotide binding cannot contribute to the thermodynamic coupling between ET and ATP binding and hydrolysis.

The MoFe protein catalytic unit next binds to $\text{Fe}^{\text{red}}(\text{ATP})_2$ to form the ET-*active* [$\text{Fe}^{\text{red}}(\text{ATP})_2$, MoFe] complex (**Figure 5-5**, left, down). Structural differences between $\text{Fe}^{\text{red}}(\text{ADP})_2$ and $\text{Fe}^{\text{red}}(\text{ATP})_2$ must have thermodynamic consequences for the Fe cycle as the free energies for binding between the MoFe protein and Fe protein alone or Fe protein with bound ADP or ATP are different (1). The excess free energy for binding MoFe protein to $\text{Fe}^{\text{red}}(\text{ATP})_2$ relative to $\text{Fe}^{\text{red}}(\text{ADP})_2$ contributes to the thermodynamic coupling between ET and ATP binding/hydrolysis.

The $[\text{Fe}^{\text{red}}(\text{ATP})_2, \text{MoFe}]$ complex undergoes inter-protein “transport” of the electron, ATP hydrolysis, Pi release, and dissociation. In the absence of a known ordering of these steps, two alternative proposals have been considered to explain the coupling of ET to ATP binding and hydrolysis. In one, ATP *hydrolysis* itself provides the principal energy input for the conformational change(s) that drive $\text{Fe}^{\text{red}} \rightarrow \text{MoFe}$ protein ET; in the other, the bound ATP induces the formation of a reactive, “activated” conformation of the complex, and it is the free energy of ATP-activated protein-protein *binding* that drives ET. The present measurements of the rate constants for all of the key steps discriminates between these two alternatives, and in doing so sheds further light on the energy transduction through ATP hydrolysis: (i) That the ATP hydrolysis is temporally decoupled from and follows ET (**Figure 5-3**) shows that ET is not driven by the free energy of ATP hydrolysis, and that it must be the ATP-dependent free energy of protein-protein *binding* that drives ET. (ii) That ATP hydrolysis and Pi release occur as temporally separated steps, both of which precede the dissociation of the product $[\text{Fe}^{\text{red}}\text{ATP}_2, \text{MoFe}^{\text{red}}]$ complex (**Figure 5-4**) (13), demonstrates that *both* hydrolysis and Pi release are required to completely relax the conformationally activated complex, thereby inducing dissociation of the Fe protein from the reduced MoFe^{red} and completing the cycle.

Viewed in this way, the Fe protein thermodynamic cycle is analogous to the four-step thermodynamic cycle of the ABC (ATP-binding cassette) trans-membrane substrate transporters, in particular the exporter sub-class (27–30). These transporters catalyze substrate transport by a process dependent on conformational changes driven by ATP *binding*, with the system being reset for another cycle by ATP *hydrolysis*. The ABC

trans(ex)porter cycle begins with binding of the substrate to the protein, which triggers ATP binding (Step I); in nitrogenase the analogous step is ‘electron binding’ by $\text{Fe}^{\text{ox}}(\text{ADP})_2$ protein, namely reduction to $\text{Fe}^{\text{red}}(\text{ADP})_2$, followed by exchange of ADP by ATP. In the transporters, ATP binding free energy drives a sequence of conformational changes that results in an activated state that undergoes trans-membrane substrate transport (Step II); in nitrogenase, ATP binding free energy drives the formation of an activated $[\text{Fe}^{\text{red}}(\text{ATP})_2, \text{MoFe}]$ complex that undergoes deficit-spending $\text{Fe}^{\text{red}} \rightarrow \text{MoFe}$ electron transport. In the transporters, ATP hydrolysis to ADP and subsequent Pi release (Step III) elicit conformational relaxation (Step IV), thereby ‘resetting’ the transporter for another catalytic cycle; in nitrogenase, ATP hydrolysis and subsequent Pi release relax the complex, resulting in dissociation of the reduced MoFe protein, leaving the $\text{Fe}^{\text{ox}}(\text{ADP})_2$ protein ready for another Fe protein cycle. Thus, the concept of Fe protein as a “nucleotide switch” must be expanded to include the idea that the Fe protein-MoFe protein complex toggles between two conformational states – “activated” and “relaxed”-- in response to changes in nucleotide state, thereby driving nucleotide-dependent “electron transport”.

Nucleotide-Dependent Structural Changes. How do nucleotide-dependent changes in the conformation of the $[\text{Fe}; \text{MoFe}]$ complex drive ET? The X-ray structures of Fe-MoFe protein complexes with a suite of nucleotides (32), including nucleotide-free, ADP-bound, the ATP analogue β - γ -methylene ATP (AMPPCP)-bound, and the ATP-hydrolysis transition state represented by ADP- AlF_4 -bound complex, have suggested progressive changes in the structure of Fe protein accompanied by rearrangement at the protein-protein interface as a function of nucleotide state. We interpreted the osmotic-

pressure dependence of the observed $\text{Fe}^{\text{red}} \rightarrow \text{MoFe}$ ET process as reflecting motions of the Fe protein relative to MoFe (11), consistent with the crystallographic demonstration that changes in nucleotide state drive large changes in the buried protein-protein interface area (32). However, it must be that activation for ET includes conformational changes within the MoFe protein that have yet to be observed in crystal structures.

Neither the structure of the complex that binds the ATP analogue, AMPPCP, nor that of the complex that binds the analogue for the transition state of ATP hydrolysis, ADP-AlF₄, shows any significant perturbations within the MoFe protein relative to isolated MoFe protein. However, the ABC-transporter-like mechanism encapsulated in the cycle of **Figure 5-5** offers a possible resolution to this puzzle. As ATP hydrolysis/Pi release occurs only *after* ET, and thus ‘only’ contribute to relaxation of the ‘activated’ conformational state associated with the ATP complex, there is no requirement that the transition state for ATP hydrolysis be associated with a high-energy state within the MoFe protein.

Two further observations can be considered regarding the absence of changes within the MoFe protein in the structure of the AMPPCP-bound complex: (i) AMPPCP in fact is not a truly faithful ATP analogue in the nitrogenase system, as shown by the inability to promote proper ET and (ii) as the deficit-spending ET process is conformationally gated, it may well be that the anticipated state in which FeMo-cofactor and its environs are activated for substrate reduction are only formed by a conformational fluctuation and *never* exists in high occupancy for trapping and direct characterization.

Summary. By establishing the pre-steady state rate constant for ATP hydrolysis in nitrogenase catalysis, the order of sequential events in the nitrogenase cycle is finally

established to be: (i) conformationally gated ET, (ii) ATP hydrolysis, (iii) Pi release, and finally (iv) Fe protein dissociation from the MoFe protein. Establishing this order of events provide insights into the functions of ATP in the nitrogenase mechanism, revealing that it is the free energy of ATP binding and protein-protein association that control the ET events, rather than the free energy of ATP hydrolysis.

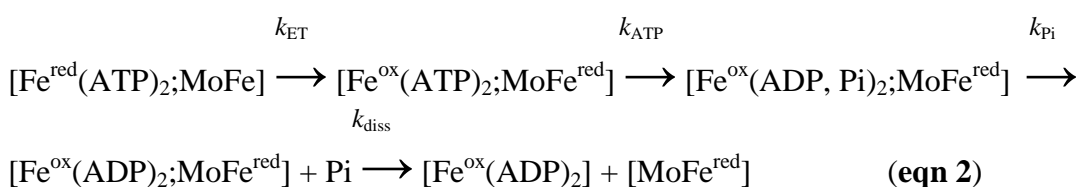
MATERIALS AND METHODS

Materials, Protein Purification and Activity Assays. All reagents, unless stated otherwise, were purchased from Sigma Aldrich Chemicals (St. Louis, MO). Nitrogenase proteins were expressed in *Azotobacter vinelandii* strain DJ995 (wild-type MoFe with His tag), and DJ884 (wild-type Fe protein) as described previously (33). The MoFe protein contained a seven-histidine tag near the carboxyl terminus of the α -subunit allowing purification using the previously described metal affinity chromatography method (33). Fe protein was purified using ion exchange and size-exclusion liquid chromatography (33, 34). Both proteins were greater than 95% pure based on sodium dodecyl sulfate-polyacrylamide gel electrophoresis separation followed by Coomassie blue staining. Manipulation of proteins was done in septum-sealed serum vials under argon atmosphere. All transfers of gases and liquids were done using gastight syringes.

Stopped-flow Spectrophotometry and the Oxidation of Fe Protein. Stopped-flow spectrophotometry was performed at 25°C with a Hi-Tech SF61 stopped-flow (SF) UV-visible spectrophotometer equipped with data acquisition software (Salisbury, Wits UK). The SF unit of the spectrophotometer was housed inside a nitrogen-filled glove box (< 5 ppm O₂). The temperature during the experiments was controlled by a circulating water bath housed outside the glove box (18). In these experiments, 75 μ M Fe and 20 μ M

MoFe protein were contained in one drive syringe while the other syringe contained 18 mM MgCl₂ and 10 mM ATP. Both syringes contained buffer [100 mM HEPES (pH 7.4) and 10 mM sodium dithionite]. Primary electron transfer from the Fe protein to the MoFe protein was monitored by an increase in absorbance at 430 nm that occurs as the [4Fe-4S] cluster of the Fe protein becomes oxidized during turnover within the [Fe^{red}(ATP)₂;MoFe] complex.

The data were fit using KinTech Explorer (Kintek Corp., Austin, TX) to a sequential A → B → C → D → E kinetic model (**eqn 2**).



In this model, k_{ET} , k_{ATP} , k_{Pi} and k_{diss} are the rates constants for ET, ATP hydrolysis, phosphate release, and [Fe^{ox}(ADP)₂;MoFe] complex dissociation, respectively. All steps of the ET process can be taken as irreversible except for ATP hydrolysis, and here the rate constant for the reverse reaction is so low that the reverse process can be ignored in the present experiments (1, 17). As a result the sequential model of **eqn 2** is appropriate (in the fitting process all reverse rate constants are fixed to a value of zero). To fit the ET data, the other rate constants were fixed at $k_{\text{ATP}} = 70 \text{ s}^{-1}$, $k_{\text{Pi}} = 16 \text{ s}^{-1}$, $k_{\text{diss}} = 6 \text{ s}^{-1}$.

Quench Flow Studies for ATP Hydrolysis. Pre-steady ATP hydrolysis assays were performed at 25°C on a rapid chemical quench-flow instrument (KinTek Corp, Austin, TX) housed in a nitrogen-filled glove box (< 5 ppm O₂). A 18 μL volume of 10 μM MoFe and 20 μM Fe (syringe A) was mixed with a 18 μL volume of 1 mM ATP with [α-

^{32}P]ATP (1.5 μCi) from syringe B, with varying times of reaction. Reactions were rapidly quenched with 45 μL of 0.5 M EDTA added from syringe C. Aliquots (0.9 μL) of the quenched reaction were spotted onto a thin layer chromatography (TLC) plate and developed in 0.6 M potassium phosphate buffer, pH 3.4 for 45 minutes. The [α - ^{32}P]ATP and the [α - ^{32}P]ADP were detected with a Storm PhosphorImager (Molecular dynamics, Sunnyvale, CA) and quantified using the ImageQuant software (Molecular Dynamics, Sunnyvale, CA). The data were fit to the kinetic model (**eqn 2**), with fixed values of $k_{\text{ET}} = 140 \text{ s}^{-1}$, $k_{\text{Pi}} = 16 \text{ s}^{-1}$, $k_{\text{diss}} = 6 \text{ s}^{-1}$.

Kinetics of Inorganic Phosphate Release. The time-course of phosphate release was determined in a stopped-flow (Auto SF-120, Kintek Corp, Austin, TX) using the coumarin (N-[2-(1-maleimidyl)ethyl]-7-(diethylamino) coumarin-3-carboxamide) labeled phosphate binding protein assay (MDCC-PBP) (22). Briefly, Pi binding to MDCC-PBP results in an increase in fluorescence (13, 22) ($\lambda_{\text{excitation}} = 430 \text{ nm}$, $\lambda_{\text{emission}} > 450 \text{ nm}$). The experiments were carried out at 25°C in SF-buffer (0.5 mM sodium dithionite and 25 mM HEPES; pH 7.4). Prior to each experiment, the stopped-flow syringes and flow lines were treated with a Pi-MOP (SF-buffer with 300 μM 7-methylguanine (7-meG), and 0.2 units/mL purine nucleoside phosphorylase (PNPase) for 15 min to remove contaminating Pi (22) and then rinsed with buffer. Two μM MoFe and 6 μM Fe was rapidly mixed with a solution of 10 μM PBP-MDCC, 20 mM MgCl_2 and 2mM ATP and the change in fluorescence was monitored over time. A control time course, conducted without nitrogenase, was used to correct for the presence of contaminating phosphate. PBP-MDCC fluorescence enhancement was converted to [Pi] after calibration in the stopped-

flow using $[\text{NaH}_2\text{PO}_4]$ standards as described (22). The Pi release data were fit to the sequential kinetic model (**eqn 2**) with $k_{\text{ET}} = 140 \text{ s}^{-1}$, $k_{\text{ATP}} = 70 \text{ s}^{-1}$, and $k_{\text{diss}} = 6 \text{ s}^{-1}$ fixed.

The Fe Protein-MoFe Protein Dissociation Rate Constant. The dissociation of the Fe protein from the MoFe protein was determined by following the release of the Fe protein from the MoFe protein in the stopped flow spectrophotometer. $\text{Fe}^{\text{ox}}(\text{ADP})_2$ is not reduced by dithionite within the $[\text{Fe}^{\text{ox}}(\text{ADP})_2;\text{MoFe}]$ complex. Thus, the rate constant for the dissociation of the $[\text{Fe}^{\text{ox}}(\text{ADP})_2;\text{MoFe}]$ complex was determined by measuring the decrease in absorbance at 430 nm during the reduction of Fe^{ox} to Fe^{red} by dithionite after $\text{Fe}^{\text{ox}}(\text{ADP})_2$ dissociates from the MoFe protein (14). Rate constants for dissociation were determined by fitting the data to a single-exponential equation (**eqn 3**)

$$A = e^{-k(\text{diss})t} \quad (\text{eqn 3})$$

where A is the amplitude of the absorbance change and k_{diss} is the rate constant for dissociation of the complex. Sodium dithionite was removed from the as-isolated MoFe and Fe proteins and exchanged into a 50 mM HEPES buffer with 200 mM NaCl, pH 7.4, by passage over a Sephadex G-25 column. Oxidized Fe protein was generated by adding increments of a 25 mM IDS solution to the Fe protein until a blue color remained. The excess IDS was removed by passing the sample over a Dowex ion-exchange resin and Sephadex G-25 column equilibrated with 50 mM HEPES buffer, pH 7.4. For each experiment, syringe A contained 40 μM Fe^{ox} protein, 40 μM MoFe protein, 5 mM MgADP in a 50 mM HEPES buffer, pH 7.4, and syringe B contained 200 μM Fe^{red} protein, and 20 mM sodium dithionite in 50 mM HEPES buffer, pH 7.4.

REFERENCES

1. Burgess BK, Lowe DJ (1996) Mechanism of molybdenum nitrogenase. *Chem Rev* 96:2983–3012.
2. Seefeldt LC, Hoffman BM, Dean DR (2009) Mechanism of Mo-dependent nitrogenase. *Annu Rev Biochem* 78:701–722.
3. Thorneley RN, Lowe DJ, Eady RR, Miller RW (1979) The coupling of electron transfer in nitrogenase to the hydrolysis of magnesium adenosine triphosphate. *Biochem Soc Trans* 7:633–636.
4. Hageman RV, Orme-Johnson WH, Burris RH (1980) Role of magnesium adenosine 5'-triphosphate in the hydrogen evolution reaction catalyzed by nitrogenase from *Azotobacter vinelandii*. *Biochemistry* 19:2333–2342.
5. Georgiadis MM, et al. (1992) Crystallographic structure of the nitrogenase iron protein from *Azotobacter vinelandii*. *Science* 257:1653–1659.
6. Kim J, Rees DC (1992) Structural models for the metal centers in the nitrogenase molybdenum-iron protein. *Science* 257:1677–1682.
7. Chan MK, Kim J, Rees DC (1993) The nitrogenase FeMo-cofactor and P-cluster pair: 2.2 Å resolution structures. *Science* 260:792–794.
8. Lancaster KM, et al. (2011) X-ray emission spectroscopy evidences a central carbon in the nitrogenase iron-molybdenum cofactor. *Science* 334:974–977.
9. Spatzal T, et al. (2011) Evidence for interstitial carbon in nitrogenase FeMo cofactor. *Science* 334:940.
10. Einsle O, et al. (2002) Nitrogenase MoFe-protein at 1.16 Å resolution: a central ligand in the FeMo-cofactor. *Science* 297:1696–1700.

11. Danyal K, Mayweather D, Dean DR, Seefeldt LC, Hoffman BM (2010) Conformational gating of electron transfer from the nitrogenase Fe protein to MoFe protein. *J Am Chem Soc* 132:6894–6895.
12. Danyal K, Dean DR, Hoffman BM, Seefeldt LC (2011) Electron transfer within nitrogenase: evidence for a deficit-spending mechanism. *Biochemistry* 50:9255–9263.
13. Lowe DJ, et al. (1995) Nitrogen fixation: Fundamentals and applications, *Current Plant Science and Biotechnology in Agriculture.*, eds Tikhonovich IA, Provorov NA, Romanov VI, Newton WE (Springer, Dordrecht, Netherlands), pp 103–108.
14. Thorneley RN, Lowe DJ (1983) Nitrogenase of *Klebsiella pneumoniae*. Kinetics of the dissociation of oxidized iron protein from molybdenum-iron protein: Identification of the rate-limiting step for substrate reduction. *Biochem J* 215:393–403.
15. Hageman RV, Burris RH (1978) Nitrogenase and nitrogenase reductase associate and dissociate with each catalytic cycle. *Proc Natl Acad Sci USA* 75:2699–2702.
16. Eady RR, Lowe DJ, Thorneley RNF (1978) Nitrogenase of *Klebsiella pneumoniae*: A pre-steady state burst of ATP hydrolysis is coupled to electron transfer between the component proteins. *FEBS Lett* 95:211–213.
17. Wilson PE, Nyborg AC, Watt GD (2001) Duplication and extension of the Thorneley and Lowe kinetic model for *Klebsiella pneumoniae* nitrogenase catalysis using a mathematica software platform. *Biophys Chem* 91:281–304.
18. Lanzilotta WN, Fisher K, Seefeldt LC (1996) Evidence for electron transfer from the nitrogenase iron protein to the molybdenum–iron protein without MgATP

- hydrolysis: characterization of a tight protein–protein complex. *Biochemistry* 35:7188–7196.
19. Imam S, Eady RR (1980) Nitrogenase of *Klebsiella pneumoniae*: reductant-independent ATP hydrolysis and the effect of pH on the efficiency of coupling of ATP hydrolysis to substrate reduction. *FEBS Lett* 110:35–38.
 20. Thorneley RN, Ashby G, Howarth JV, Millar NC, Gutfreund H (1989) A transient-kinetic study of the nitrogenase of *Klebsiella pneumoniae* by stopped-flow calorimetry. Comparison with the myosin ATPase. *Biochem J* 264:657–661.
 21. Ryle MJ, Seefeldt LC (2000) Hydrolysis of nucleoside triphosphates other than ATP by nitrogenase. *J Biol Chem* 275:6214–6219.
 22. Brune M, Hunter JL, Corrie JE, Webb MR (1994) Direct, real-time measurement of rapid inorganic phosphate release using a novel fluorescent probe and its application to actomyosin subfragment 1 ATPase. *Biochemistry* 33:8262–8271.
 23. Fisher K, Lowe DJ, Thorneley RN (1991) *Klebsiella pneumoniae* nitrogenase. The pre-steady-state kinetics of MoFe-protein reduction and hydrogen evolution under conditions of limiting electron flux show that the rates of association with the Fe-protein and electron transfer are independent of the oxidation level of the MoFe-protein. *Biochem J* 279:81–85.
 24. Lowe DJ, Thorneley RN (1984) The mechanism of *Klebsiella pneumoniae* nitrogenase action. The determination of rate constants required for the simulation of the kinetics of N₂ reduction and H₂ evolution. *Biochem J* 224:895–901.
 25. Rees DC et al. (2005) Structural basis of biological nitrogen fixation. *Phil Trans R Soc* 363:971–984.

26. Rees DC, Howard JB (1999) Structural bioenergetics and energy transduction mechanisms. *J Mol Biol* 293:343–350.
27. Linton KJ, Higgins CF (2007) Structure and function of ABC transporters: the ATP switch provides flexible control. *Pflugers Arch - Eur J Physiol* 453:555–567.
28. Locher KP (2009) Structure and mechanism of ATP-binding cassette transporters. *Phil Trans R Soc B* 364:239–245.
29. Goetz BA, Perozo E, Locher KP (2009) Distinct gate conformations of the ABC transporter BtuCD revealed by electron spin resonance spectroscopy and chemical cross-linking. *FEBS Lett* 583:266–270.
30. Rees DC, Johnson E, Lewinson O (2009) ABC transporters: The power to change. *Nat Rev Mol Cell Biol* 10:218–227.
31. Lanzilotta WN, Ryle MJ, Seefeldt LC (1995) Nucleotide hydrolysis and protein conformational changes in *Azotobacter vinelandii* nitrogenase iron protein: Defining the function of aspartate 129. *Biochemistry* 34:10713–10723.
32. Tezcan FA et al. (2005) Nitrogenase complexes: Multiple docking sites for a nucleotide switch protein. *Science* 309:1377–1380.
33. Christiansen J, Goodwin PJ, Lanzilotta WN, Seefeldt LC, Dean DR (1998) Catalytic and biophysical properties of a nitrogenase apo-MoFe protein produced by a *nifb*-deletion mutant of *Azotobacter vinelandii*. *Biochemistry* 37:12611–12623.
34. Burgess BK, Jacobs DB, Stiefel EI (1980) Large-scale purification of high activity *Azotobacter vinelandii* nitrogenase. *Biochim Biophys Acta* 614:196–209.

CHAPTER 6

UNCOUPLING NITROGENASE: CATALYTIC REDUCTION OF HYDRAZINE TO AMMONIA BY A MoFe PROTEIN IN THE ABSENCE OF Fe PROTEIN- ATP*

ABSTRACT

The catalytic reduction of hydrazine (N_2H_4) to ammonia by a β -98^{Tyr→His} MoFe protein in the absence of the Fe protein or ATP is reported. The reduction of N_2 or other substrates (e.g., hydrazine, protons, acetylene) by nitrogenase normally requires the transient association of the two nitrogenase component proteins, the Fe protein and the MoFe protein. The Fe protein, with two bound MgATP molecules, transfers one electron to the MoFe protein during each association, coupled to the hydrolysis of two MgATP. All substrate reduction reactions catalyzed by nitrogenase require delivery of electrons by the Fe protein coupled to the hydrolysis of MgATP. We report that when a single amino acid within the MoFe protein (β -98^{Tyr}) is substituted by His, the resulting MoFe protein supports catalytic reduction of the nitrogenous substrate hydrazine (N_2H_4) to two ammonia molecules when provided with a low potential reductant, polyaminocarboxylate ligated Eu^{II} (E_m -1.2 V vs. NHE). The wild-type and a number of other MoFe proteins with amino acid substitutions do not show significant rates of hydrazine reduction under these conditions, whereas the β -98^{His} MoFe protein catalyzes hydrazine reduction at rates up to 170 nmol NH_3 /min/mg MoFe protein. This rate of hydrazine reduction is 94 % of the rate catalyzed by the β -98^{His} or wild-type MoFe protein when combined with the Fe protein, ATP, and reductant under comparable conditions. The β -98^{His} MoFe protein

reduction of hydrazine in the absence of the Fe protein showed saturation kinetics for the concentration of reductant and substrate. The implications of these results in understanding the nitrogenase mechanism are discussed.

* Coauthored by Karamatullah Danyal, Dennis Dean, Brian M. Hoffman and Lance C. Seefeldt (2011) *Biochemistry* 50 (43), pp 9255-9263. Copyright 2011 American Chemical Society. Reprinted with Permission.

Reduction of N_2 to ammonia by the Mo-dependent nitrogenase requires the action of two component proteins called the Fe protein and the MoFe protein.¹ The MoFe protein contains the multimetallic FeMo-cofactor catalytic cluster [7Fe-9S-Mo-X-R-homocitrate] at which substrates bind, and the auxiliary P-cluster [8Fe-7S] that is proposed to mediate electron transfer from the Fe protein (**Figure 1**).² The Fe protein contains a [4Fe-4S] cluster and two MgATP binding sites.³ During catalysis by nitrogenase, the Fe protein transiently associates with the MoFe protein and a single electron is transferred from the Fe protein to the MoFe protein in conjunction with the hydrolysis of two MgATP molecules.⁴ The Fe protein-2MgADP then dissociates from the

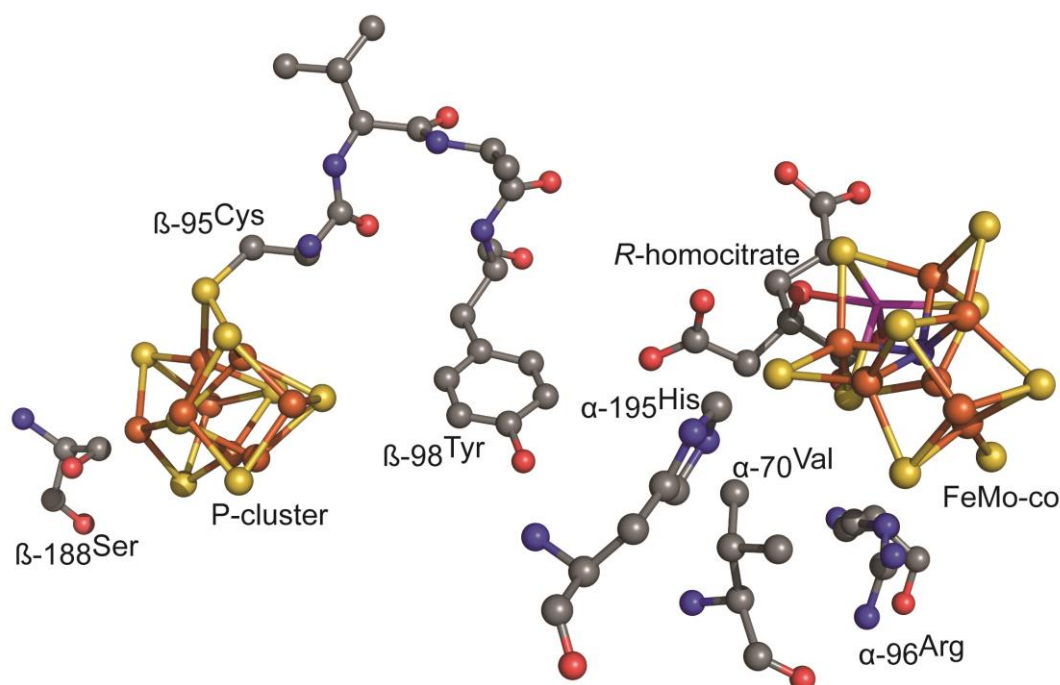


Figure 6-1: MoFe protein metal clusters and key amino acid residues are shown. The Fe protein association site is to the left outside of the view. Colors are Mo in magenta, Fe in rust, S in yellow, C in gray, O in red, and N in blue. Based on the protein data base file 1M1N.pdb.²

MoFe protein, allowing another reduced Fe protein-2MgATP to bind to the MoFe protein. This cycle is repeated to accumulate electrons in the MoFe protein to support substrate reduction. The Fe protein with bound ATP is the only known reductant of the MoFe protein that supports reduction of N₂ or any of a number of other small substrates.¹ Although several small electron transfer proteins (e.g. flavodoxin or ferredoxin) or electron mediators can donate electrons to oxidized metal clusters in the MoFe protein, none of these molecules can support substrate reduction.

These observations show that the Fe protein is more than a simple reductant of the MoFe protein, suggesting instead a specific task such as inducing conformational changes within the MoFe protein that allow substrate binding and/or electron transfer to FeMo-cofactor. This is supported by a recent report that electron transfer between the Fe protein and MoFe protein is conformationally gated, involving protein conformational changes.⁵ A number of X-ray structures of Fe protein-MoFe protein complexes have been solved in various nucleotide-bound states,⁶ yet no structural changes have been observed within the MoFe protein that might explain the role of the Fe protein/ATP.

In recent years, we have probed MoFe protein function by substituting specific amino acids for different amino acids and then characterizing the properties of the resulting MoFe protein variants.⁴ We reasoned that it might be possible to explore the putative Fe protein conformational change within the MoFe protein by means of amino acid substitution of residues near the P cluster, FeMo-cofactor, or in between these two clusters (**Figure 6-1**). Here, we report that when the β -98^{Tyr} residue, located within the MoFe protein between the P-cluster and FeMo-cofactor, is substituted by histidine, the

resulting MoFe protein (β -98^{His}) can reduce the nitrogenous substrate hydrazine (N_2H_4) to ammonia in the absence of the Fe protein and ATP, with electrons being supplied instead by a Eu^{II} -polyaminocarboxylate complex.

When electrochemically generated Eu^{2+} (reduction potential -0.36 V versus the standard hydrogen electrode (SHE) at pH 7.0) is mixed with a polyaminocarboxylate ligand (L) such as EGTA (ethylene glycol-bis(2-aminoethyl)-N,N,N',N'-tetraacetate-(4-)) or DTPA (diethylenetriamine-N,N,N',N'',N''-pentaacetate(5-)), it instantly forms a strong 1:1 complex that is a powerful and reactive one-electron reductant; the $\text{Eu}^{\text{III/II}}$ -EGTA and $\text{Eu}^{\text{III/II}}$ -DTPA redox couples have reduction potentials of -0.88 V and -1.14 V, respectively (pH 8.0).⁷

When the wild-type MoFe protein without Fe protein/ATP is mixed with Eu^{II} -EGTA or Eu^{II} -DTPA, no significant reduction of N_2 or hydrazine to ammonia is detected (**Figure 6-2, panel A**).⁸ We also examined a number of MoFe proteins with amino acid substitutions near the P cluster or FeMo-cofactor: α -70^{Val→Ala}, α -195^{His→Gln}, β -188^{Ser→Cys}, and α -70^{Val→Ala}/ α -96^{Arg→His} (**Figure 6-1**). Each of these residues in the MoFe protein has been previously implicated in some aspect of electron transfer or substrate reduction by the MoFe protein.⁴ When any one of these MoFe protein variants was mixed with Eu^{II} -DTPA, no significant reduction of hydrazine (**Figure 6-2, panel A**) or N_2 to ammonia was detected.

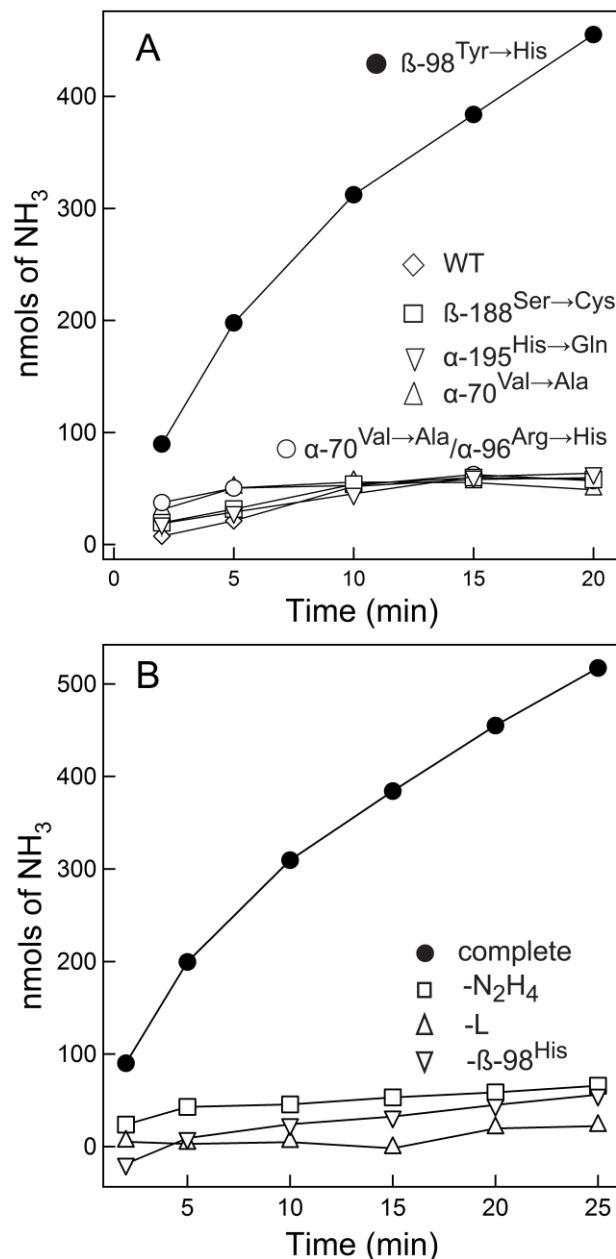


Figure 6-2: Hydrazine reduction to ammonia is shown as a function of time for different MoFe proteins (panel A) and for the β -98^{His} MoFe omitting each component of the assay (panel B). No Fe protein or ATP is added. Omission of Eu²⁺ resulted in no detection of ammonia. The concentration of hydrazine is 50 mM, the quantity of MoFe protein is 0.7 mg (2.8 nmol), and the concentration of Eu^{II}-DTPA is 0.5 mM (panel A) and 1 mM (panel B), with the pH = 7.0 and temperature = 25°C.

A prior study of a MoFe protein with β -98^{Tyr} substituted by histidine, which is located between the P cluster and the *R*-homocitrate end of FeMo-cofactor (**Figure 6-1**), implicated the tyrosine in electron transfer between the clusters.⁹ When the β -98^{His} MoFe protein was mixed with Eu^{II}-DTPA and hydrazine, a time-dependent production of ammonia was observed (**Figure 6-2, panel A**). The production of ammonia was dependent on the presence of the β -98^{His} MoFe protein, Eu²⁺, L, and hydrazine (**Figure 6-2, panel B**). After one minute of assay, a specific activity for hydrazine reduction of 170 ± 8 nmols NH₃/min/mg MoFe protein was determined. This rate is 94% of the rate measured for a fully functioning wild-type or β -98^{His} MoFe protein with Fe protein, MgATP and a MgATP regeneration system, and the reductant dithionite under the same conditions. The reduction of hydrazine by the β -98^{His} MoFe protein without Fe protein/ATP was found to continue over extended times (tested to 25 min), although the specific activity at longer times was lower (50 nmol NH₃/min/mg MoFe protein at 20 min) than at earlier times, suggesting that a component of the reaction was being depleted. Addition of more Eu^{II}-DTPA to an assay that had run for 20 min reactivated the reaction to near the initial rates, indicating that depletion of the reductant was the cause of declining rates over time. The rate of reduction of hydrazine depended on the concentration of Eu^{II}-DTPA and hydrazine, in each case showing saturation kinetics, with maximal rates observed at 1 mM Eu^{II}-DTPA and 50 mM hydrazine. Doubling the amount of MoFe protein doubled the rate of hydrazine reduction. The milder reductant Eu^{II}-EGTA was also examined and was found to support hydrazine reduction, albeit at lower rates (17 nmol NH₃/min/mg MoFe protein) when compared to Eu^{II}-DTPA.

Reduction of N_2 to ammonia by the β -98^{His} MoFe protein was not detected with either reductant even after extended reaction times. The Eu^{II} -DTPA and Eu^{II} -EGTA complexes catalyze H^+ and acetylene reduction in the absence of MoFe protein, so it was not possible to test these substrates in this reaction.

The reduction of N_2 by nitrogenase is a $6 e^-/6 H^+$ reaction that is likely to involve metal-bound partially reduced intermediates at the level of reduction of diazene (N_2H_2) and hydrazine.¹⁰ Hydrazine is reduced to ammonia by the fully functioning nitrogenase,¹¹ so it is reasonable to conclude that hydrazine joins late in the N_2 reduction pathway, requiring only $2e^-/2H^+$ for reduction.¹² Our observation of hydrazine reduction by the β -98^{His} MoFe protein, but not N_2 reduction, is consistent with the fact that hydrazine is easier to reduce than N_2 .¹³⁻¹⁴ The hydrazine reduction observed here cannot be catalyzed by FeMo-cofactor that has been released from the protein because isolated FeMo-cofactor does not catalyze this reaction¹⁵ and the β -98^{His} MoFe protein is stable.⁹ Further, we have determined that the β -98^{His} MoFe protein retains normal acetylene reduction activity¹⁶ when combined with Fe protein and ATP following removal of the Eu^{II} -L by gel filtration chromatography.

The results presented here demonstrate the catalytic reduction of hydrazine to ammonia by the β -98^{His} MoFe protein uncoupled from electron delivery by the Fe protein and ATP, instead using only a simple, but powerful, electron donor. How substitution of β -98^{Tyr} by histidine has activated the MoFe protein for hydrazine reduction without the Fe protein and ATP hydrolysis has yet to be established, but the results indicate that amino acid substitutions within the MoFe protein can partially mimic some of the conformational changes induced by the Fe protein/ATP that either activate electron

transfer from the P-cluster to FeMo-cofactor or allow substrate binding. The specific roles of the P-cluster and FeMo-cofactor in the Eu^{II} -L-dependent reduction of hydrazine observed here are under active investigation.

REFERENCES

- (1) Burgess, B. K.; Lowe, D. J. *Chem. Rev.* **1996**, *96*, 2983-3012.
- (2) Einsle, O.; Tezcan, F. A.; Andrade, S. L. A.; Schmid, B.; Yoshida, M.; Howard, J. B.; Rees, D. C. *Science* **2002**, *297*, 1696-1700.
- (3) Georgiadis, M. M.; Komiyama, H.; Chakrabarti, P.; Woo, D.; Kornuc, J. J.; Rees, D. C. *Science* **1992**, *257*, 1653-1659.
- (4) Seefeldt, L. C.; Hoffman, B. M.; Dean, D. R. *Annu. Rev. Biochem.* **2009**, *78*, 701-722.
- (5) Danyal, K.; Mayweather, D.; Dean, D. R.; Seefeldt, L. C.; Hoffman, B. M. *J. Am. Chem. Soc.* **2010**, *132*, 6894-6895.
- (6) Tezcan, F. A.; Kaiser, J. T.; Mustafi, D.; Walton, M. Y.; Howard, J. B.; Rees, D. C. *Science* **2005**, *309*, 1377-1380.
- (7) Vincent, K. A.; Tilley, G. J.; Quammie, N. C.; Streeter, I.; Burgess, B. K.; Cheesman, M. R.; Armstrong, F. A. *Chem. Commun.* **2003**, 2590-2591.
- (8) MoFe proteins were expressed and purified as described by Christiansen, J., Goodwin, P.J., Lanzilotta, W.N., Seefeldt, L.C., Dean, D.R. *Biochemistry* **1998**, *37*, 12611-12623. Hydrazine reduction assays were done at pH 7.0 and 25°C with ammonia detection as described by Barney, B.M., Igarashi, R.Y., Dos Santos, P.C., Dean, D.R., Seefeldt, L.C. *J. Biol. Chem.* **2004**, *279*, 53621-53624. Eu^{3+} was electrochemically reduced as described in (7).

- (9) Peters, J. W.; Fisher, K.; Newton, W. E.; Dean, D. R. *J. Biol. Chem.* **1995**, *270*, 27007-27013.
- (10) Pickett, C. J. *J. Biol. Inorg. Chem.* **1996**, *1*, 601-606.
- (11) Davis, L. C. *Arch. Biochem. Biophys.* **1980**, *204*, 270-276.
- (12) Hoffman, B. M.; Dean, D. R.; Seefeldt, L. C. *Acc. Chem. Res.* **2009**, *42*, 609-619.
- (13) Yandulov, D. V.; Schrock, R. R. *Science* **2003**, *301*, 76-78.
- (14) Pickett, C.J.; Ryder, K.S.; Talarmin, J. *J. Chem. Soc. Dalton Trans.* **1986**, 1453-1457.
- (15) Smith, B. E.; Durrant, M. C.; Fairhurst, S. A.; Gormal, C. A.; Grönberg, K. L. C.; Henderson, R. A.; Ibrahim, S. K.; Le Gall, T.; Pickett, C. J. *Coord. Chem. Rev.* **1999**, *185-186*, 669-687.
- (16) Acetylene reduction specific activity for the b-98^{His} MoFe protein with Fe protein and ATP was similar to that reported earlier (9). Hydrazine reduction specific activity with Fe protein and ATP was 180 nmol NH₃/min/mg MoFe protein at pH 7.0.

CHAPTER 7

SUMMARY AND FUTURE DIRECTIONS

During biological nitrogen fixation reduced Fe protein (bound to two ATP molecules) binds to the MoFe protein and undergoes conformational changes (Chapter 2).¹ These conformational changes allow an electron to be transferred from the P cluster to the M cluster, thereby generating a deficit of an electron at the P cluster. This deficit is in turn fulfilled by the [4Fe-4S] cluster of the Fe protein (Chapter 3).² Analysis of the conformational gating at lower temperatures shows that the mechanism of the electron transfer event is unaffected by temperature (Chapter 4).³ After the oxidation of the Fe protein (140 s^{-1}), hydrolysis of the two bound ATP molecules takes place (70 s^{-1}) followed by phosphate release and dissociation of the Fe protein from the MoFe protein (Chapter 5). The aforementioned conformational changes within the MoFe protein, induced by the Fe protein, serve as a gate to the electron transfer from the P to M cluster. Via site directed mutagenesis, this gate can be opened in variant forms of the MoFe protein allowing transfer of electrons to the M cluster from sources other than the Fe protein (Chapter 6).⁴

Based on research presented in this dissertation, the above statements can now be made about electron transfer and substrate reduction in nitrogenase. Though this knowledge increases our understanding of the mechanism of nitrogenase such as the order of events, the mechanism of ET, and the nature of conformational gating of intramolecular electron transfer within the MoFe protein, many core questions still remain. These will be discussed here in hopes for providing a guideline for future work.

Conformational Changes in Nitrogenase

Conformational changes occur in the two proteins in nitrogenase complex.^{1,5-7} Fe protein undergoes conformational changes upon the binding of two ATP molecules.^{8,9} This conformational change includes the movement of the [4Fe-4S] cluster of the Fe protein ~ 5 Å towards the surface of the protein.^{10,11} Upon complex formation, this conformational change aids in the electron transfer event by decreasing its distance from the P cluster.

Conformational changes in the Fe Protein of nitrogenase: In Chapters 2,3, and 4 of this dissertation we have presented evidence for conformational changes in the Fe protein related to the electron transfer event. The use of osmotic pressure has allowed us not only to understand that only ~ 800 Å² from the suggested ~ 2000 Å² area of conformational changes is involved in electron transfer event, but that these changes are involved in the electron transfer from the P cluster to the M cluster upon Fe protein binding.¹²

Questions still remain regarding the nature of the other events in the Fe protein cycle. Based on work presented in Chapter 5, we know that the ATP hydrolysis occurs after the electron transfer event. However, we are unaware of any conformational changes or gates between the electron transfer event and the ATP hydrolysis. Similar questions remain as gaps in our knowledge regarding both phosphate release and dissociation events. Studies conducted using the osmotic pressure effect of the viscogens used i.e. glycerol, sucrose, polyethylene glycol 300, 600, and glucose on the ATP hydrolysis, phosphate release and dissociation events might provide us insights into other conformational changes occurring in the Fe protein of nitrogenase.

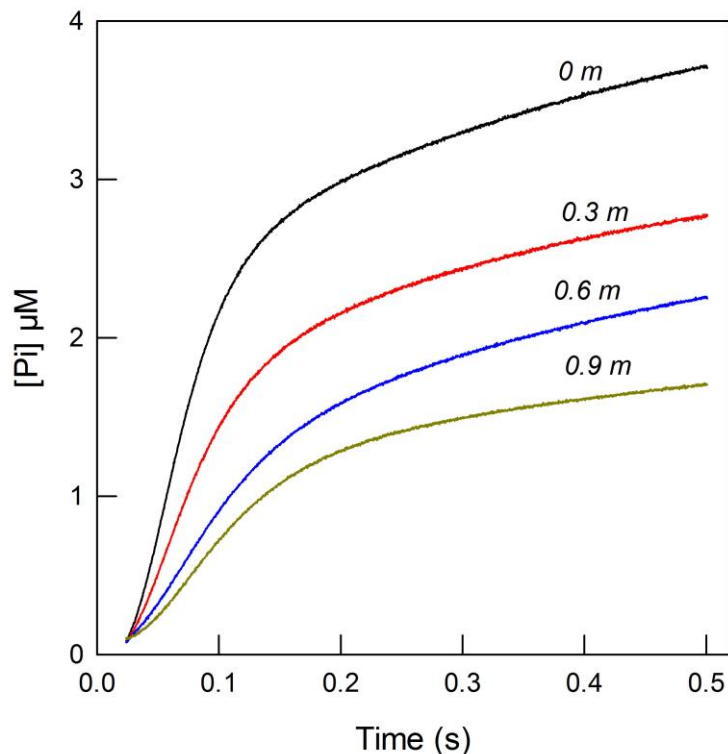


Figure 7-1: Osmotic pressure effects on phosphate release. Phosphate release is measured as an increase in fluorescence due to the binding of phosphate (Pi) to MDCC labeled phosphate binding protein. Each trace represents varying osmotic pressure (0-0.9 molal (*m*)) conditions in the system. The rate for each trace was calculated using the model described in Chapter 5.

Initial work towards understanding these conformational changes has already begun. Conformational changes related to the release of phosphate and dissociation are being studied. Based on initial results (Figure 7-1) we can say that the osmolytes e.g. sucrose shows that the phosphate release event is conformationally gated. The rates of the phosphate release event under differing osmotic pressure conditions have been analyzed (Figure 7-2) using the methodology described in Chapter 2. The slope of the change in rate of the phosphate release event is exactly double the slope of the change in rate of the

electron transfer event (Chapter 2). Based on these two osmolyte studies conducted thus far, we can say that $\sim 1600 \text{ \AA}^2$ area is involved from the complex formation to the release of phosphate from the Fe protein of nitrogenase.

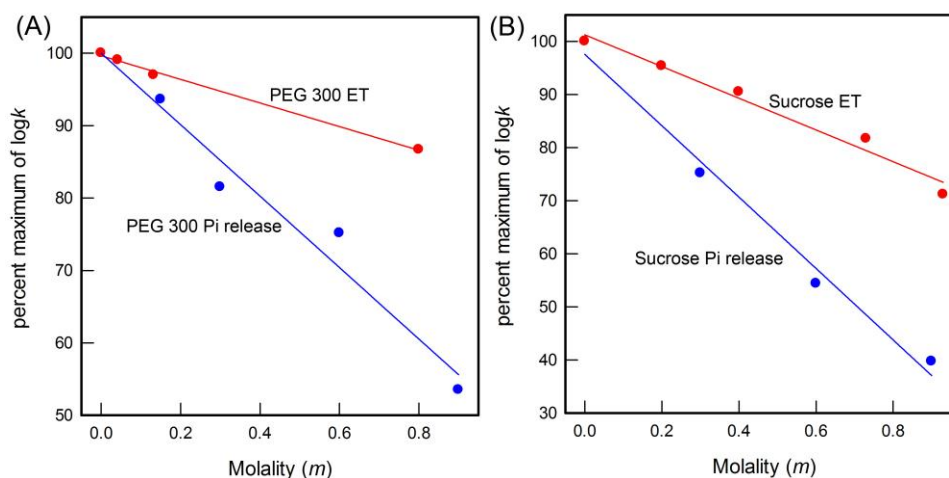


Figure 7-2: $\log k$ vs. molality of 1° ET vs. Pi release ($\log k_{\text{ET}}$ vs. $\log k_{\text{Pi}}$. Percent

maximum of $\log k$ vs. molality for phosphate release and 1° ET using polyethylene glycol and sucrose as osmolytes. The slope of $\log k$ vs. molality doubles in the case of each osmolyte for phosphate release indicating doubling of area for conformational change for the system.

The area involved in the complex formation to the primary electron transfer event ($\sim 800 \text{ \AA}^2$) includes any conformational changes that occur prior to the release of an electron from the Fe protein. Similarly, the area of conformational changes involved in the release of phosphate from the Fe protein involves all conformational changes prior to it. This includes the conformational changes involved in the electron transfer event. Thus, the area involved in the release of phosphate after the electron transfer event is ~ 700 - 800 \AA^2 .

The ability to differentiate the conformational changes occurring from one step in the Fe protein cycle to another highlights the importance of these osmolyte studies. Based on conformational changes from the electron transfer event to the phosphate release event we can deduce that the protein is undergoing a certain amount of changes after each event. This data is in agreement with the earlier crystallographic studies conducted with ATP analogues (Figure 7-3).^{12,13}

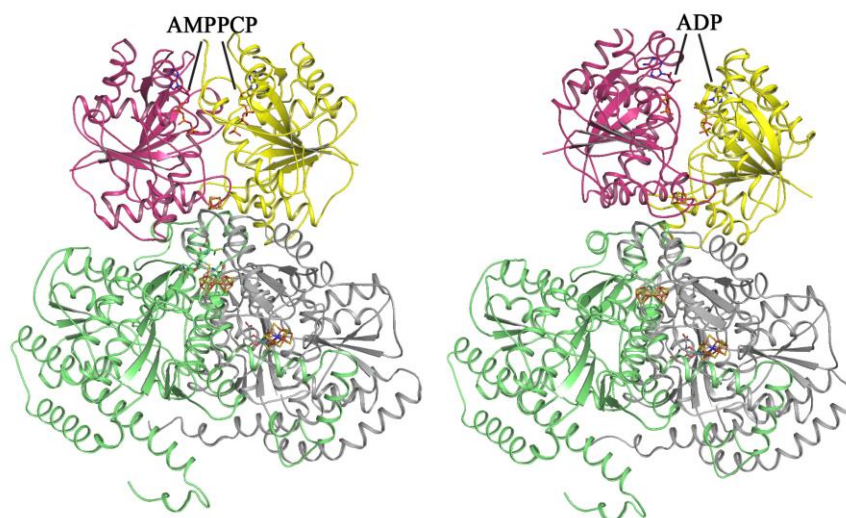


Figure 7-3: Protein-Protein docking geometries in AMPPCP and ADP bound Fe:MoFe complex. AMPPCP bound complex (left) (PDB ID 2AFK)¹² shows the interactions between the Fe protein (magenta and yellow) and the MoFe protein (grey and green) resulting in the smallest distance between the [4Fe-4S] cluster of the Fe protein and the P cluster of the MoFe protein. ADP bound complex (right) (PDB ID 1M34) shows an increased distance between the two clusters due to the motion of the Fe protein away from the MoFe protein.

The crystallographic studies on nitrogenase provide a picture of the different binding forms of the Fe protein to MoFe protein as analogues to different stages in the ATP hydrolysis events bound to the Fe protein.¹² However, these studies provide no

information on the dissociation event itself. Osmolytes could be used to determine the area of conformational change involved in the dissociation event. Two approaches, in conjunction with the osmolytes, could be used. Firstly flavodoxin (a biological reductant of the Fe protein) oxidation could be used to monitor the dissociation of the Fe protein from the MoFe protein.¹⁴ Secondly, since dissociation of the Fe protein from the MoFe protein is the rate limiting step, rate of substrate reduction (H^+ reduction to hydrogen) could be monitored with varying osmotic pressure to understand the conformational changes in the dissociation event.^{15,16} Both strategies have limitations and require proper controls. The use of flavodoxin as a reductant requires that its reduction of oxidized Fe protein is either not conformationally gated or is negligibly so. Similar questions need to be answered about product release.

In the crystallographic studies, no changes have been observed in the pre and post hydrolysis analogue (AMPPCP and ADP- AlF_4) bound complex of the Fe and MoFe protein.^{12,13} Moreover, though changes have been observed in the ADP bound complex, it is not known whether it is a state near or far from the phosphate release event. By performing osmotic pressure studies on the ATP hydrolysis event we can ascertain conformational changes that take place after the ATP hydrolysis event but prior to phosphate release. These studies could provide us with the complete picture of the different motions of the Fe protein on the surface of the MoFe protein during the Fe protein cycle.

Many surface residues on both Fe protein and MoFe protein have been studied in the past for their role in complex formation, electron transfer, and dissociation (e.g 100^{Arg} , 140^{Arg} on the Fe protein and α and β - 125^{Phe} on the MoFe protein) (Figure 7-4).¹⁷⁻

¹⁹ Osmotic pressure studies in combination with site directed mutagenesis could also be used in further understanding the role of these residues in each event during the Fe protein cycle.

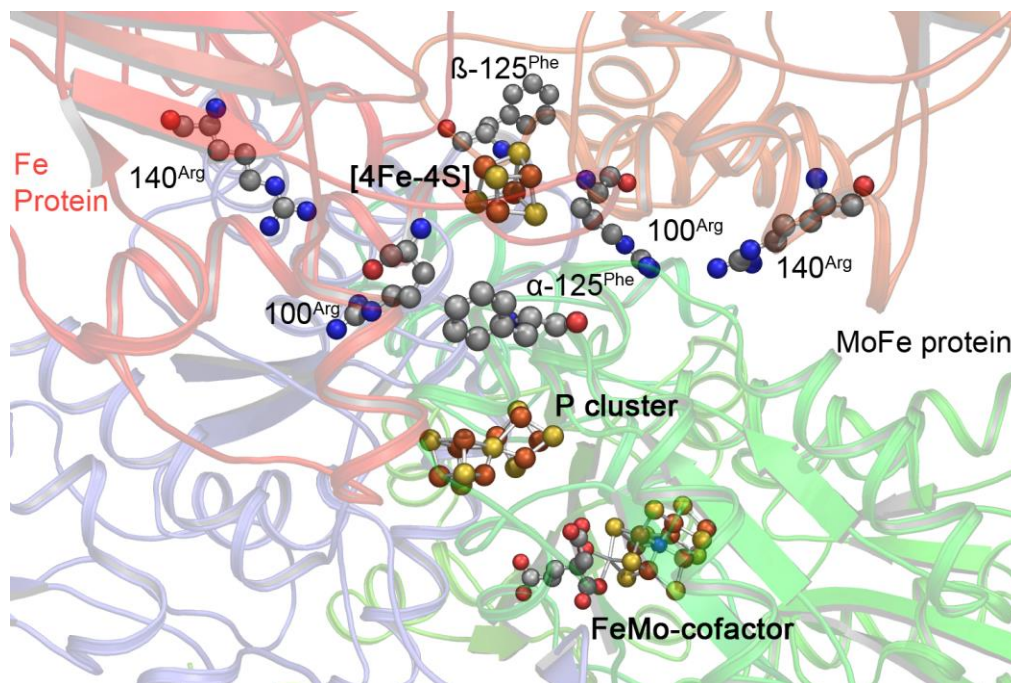


Figure 7-4: Interactions of surface residues between Fe and MoFe protein. Surface residues in the Fe protein (100 and 140^{Arg}) and α and β -125^{Phe} in the MoFe protein (β -subunit grey, α -subunit green) are shown in the AMPPCP complex crystal structure (PDB ID 2AFK).

Conformational changes in the MoFe protein: Conformational changes on the MoFe protein are much harder to visualize since no crystallographic evidence exists. In fact, crystal structures of the nitrogenase complex using ATP analogues i.e. AMPPCP, ADP+Pi analogue i.e. ADP+AlF₄, and ADP have been used to argue against significant conformational changes in the MoFe protein.¹² These arguments have been aided by the fact that all but one (2MIN: oxidized MoFe protein) of the crystal structures of the MoFe protein show no significant conformational changes.

A major evidence supporting the role of conformational changes in the MoFe protein in its reduction of substrate is presented in this dissertation (Chapter 7). This initial study suggests not only the occurrence of conformational changes in the MoFe protein, but also its importance in electron transfer to the M cluster and substrate reduction. This study shows that by making a single mutation on the MoFe protein between the P and M cluster, the MoFe protein is no longer dependent on the Fe protein as its sole reductant. The β -98^{Tyr-His} variant of the MoFe protein is capable of accepting electrons from a low potential reductant, polyaminocarboxylate ligated Eu^{II} (E_m -1.2 V vs. NHE), and of using these electrons to reduce hydrazine to ammonia.⁴

This initial result provides us evidence for the role of protein in facilitating electron transfer to the FeMo-cofactor. However, this does not provide us with the understanding of how the protein is facilitating this electron transfer. In order to understand this phenomenon, further analysis is needed. Survey studies using the Eu^{II} -ligand reductant need to be performed over a wide range of MoFe protein variants. Substrates other than hydrazine need to be tested for reduction using β -98^{Tyr-His} and Eu^{II} -L reductant. Crystallographic studies on the β -98^{Tyr-His} variant need to be performed. EPR analysis data needs to be gathered to further understand the electronic structure of FeMo-cofactor of the β -98^{Tyr-His} variant during a Eu^{II} -L based turnover event. More MoFe protein variants need to be made with mutations in the region between the P and M cluster.

Some initial work towards the goals described above has been accomplished. A small survey on some of the variant MoFe proteins available has been conducted and two other mutations lying between the P and M cluster have already been identified as similar

to β -98^{Tyr-His} variant of MoFe protein (Figure 7-5). These other two variant MoFe proteins α -64^{Tyr-His} and β -99^{Phe-His} have activities similar to that of the β -98^{Tyr-His} variant (Figure 7-6).

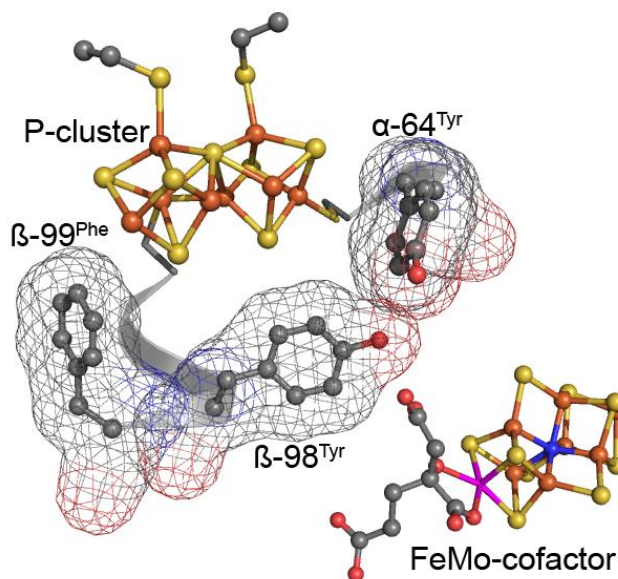


Figure 7-5: α -64^{Tyr}, β -98^{Tyr}, and β -99^{Phe} in mesh representation. The three amino acid residues relevant to the Fe independent reduction of the substrates (N_2H_4 , N_3^- and H_2) by the MoFe protein are highlighted in Mesh representation (PDB ID 3U7Q).

The specific activities, V_{max} , and K_m of all three variant MoFe proteins with Eu^{II} -L as the source of electron have been determined. The specific activities for the three MoFe variants at 100 mM hydrazine were 295 \pm 15, 198 \pm 3, and 110 \pm 2 nmols of ammonia per mg of protein per minute for α -64^{Tyr-His}, β -98^{Tyr-His}, and β -99^{Phe-His}, respectively. Varying hydrazine concentration was used to determine K_m and V_{max} for the three MoFe variants with Eu -L as the electron source. The data was fit to Michaelis Menten equation and K_m values of \sim 35, 21, and 89 mM hydrazine were found for α -64^{Tyr-His}, β -98^{Tyr-His}, and β -99^{Phe-His}, respectively. V_{max} values for α -64^{Tyr-His}, β -98^{Tyr-His},

and β -99^{Phe-His} were found to be ~424, 248, and 316 nmols of NH₃/min/mg of protein respectively (Figure 7-7).

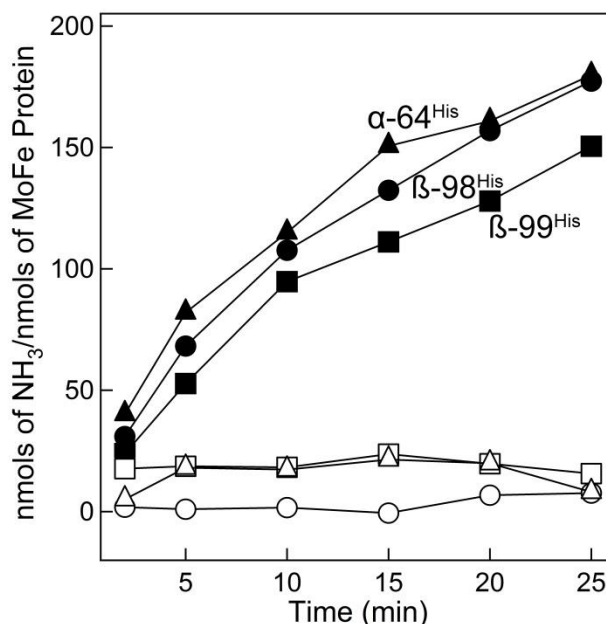


Figure 7-6: Time course analysis of the reduction of hydrazine to ammonia by ▲ α -64^{His}, ● β -98^{His}, and ■ β -99^{His} variant of the MoFe protein. The assays were performed by adding 1mM Eu^(II)DTPA to a solution containing 0.7 mg of MoFe protein and 100 mM hydrazine.

These initial results, though encouraging, are far from a complete picture of events inside the MoFe protein. The kinetic data highlights the need of further studies on variants between the P and the M cluster. It also highlights the need for combinations of mutations for α -64^{Tyr}, β -98^{Tyr}, and β -99^{Phe} residues.

Investigations into other substrates have yielded azide as a substrate for the α -64^{Tyr-His}, β -98^{Tyr-His}, and β -99^{Phe-His} proteins. Other substrates of nitrogenase are problematic with the Eu^{II}-L system since the reductant alone can reduce H⁺, acetylene and CN⁻ to hydrogen, ethylene and ammonia, respectively. Proton reduction has been

analyzed in greater detail by varying the polyaminocarboxylate ligand. Eu^{II} -EDTA does not generate detectable quantities of hydrogen in an aqueous system, however, it does generate some hydrogen with β -98^{His} variant of the MoFe protein. This opens up new avenues of future research in which reductants with more positive potentials than Eu^{II} -DTPA in combination with different and combinations of different mutations could be used to investigate these substrates.

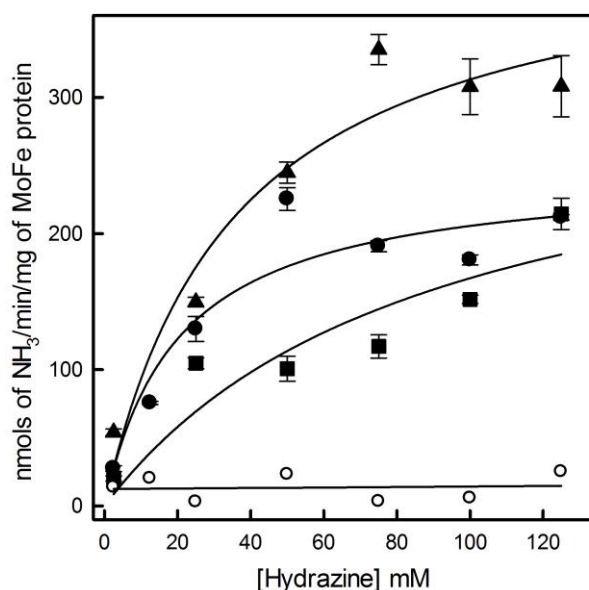


Figure 7-7: Reduction of hydrazine to ammonia by \blacktriangle α -64^{His}, \bullet β -98^{His}, and \blacksquare β -99^{His} variant of the MoFe protein with increasing hydrazine concentration. All assays were conducted for two minutes with 1mM Eu^{II} -DTPA and 100mM hydrazine concentration. The data was fit to Michaelis Menten equation.

Electron Transfer Events in Nitrogenase

Many advances in understanding the electron transfer event have been made in recent years and some are presented in this dissertation in Chapters 2,3,4, and 5 with the

order in electron transfer event discussed in Chapter 3. The electron transfer event in nitrogenase is a two-step process that is initiated after an iron protein, bound to two MgATP molecules, binds to the MoFe protein. First of the two steps is an electron transfer event from the P cluster to the M cluster of the MoFe protein. This event is triggered by the binding of the Fe protein to the MoFe protein and is conformationally gated ($k_{P \rightarrow M ET} = 140 \text{ s}^{-1}$). This electron transfer results in a deficit of electron at the P cluster which results in an electron transfer from the [4Fe-4S] (F) cluster of the Fe protein to the P cluster ($k_{F \rightarrow P ET} = 1700 \text{ s}^{-1}$).

The studies discussed in Chapter 3 show the electron transfer event from the Fe protein to the β -188^{Ser-Cys} variant of the MoFe protein studied using stopped flow UV-Vis spectrophotometry. This technique allows us to study the Fe protein without any interference from the MoFe protein. However, it also blinds us to events occurring on the MoFe protein. The rate of this direct electron transfer event is 1700 s^{-1} which makes it extremely fast. This represents a unique challenge in studying the events on the P and M cluster of nitrogenase in the β -188^{Ser-Cys} variant of the MoFe protein.

Rapid freeze quench EPR. As the rate of the first electron transfer event from the [4Fe-4S] cluster of the Fe protein to the P cluster of the MoFe protein variant β -188^{Cys} is fast (1700 s^{-1}), specialized techniques are needed for studying it. RFQ is a technique in which protein samples are mixed rapidly and quenched using a liquid nitrogen cooled isopentane bath. The frozen liquid is then packed inside an EPR tube and analyzed using an EPR spectrometer. Thus RFQ represents an attractive technique for early time point analysis.²⁰ However, this method is affected by a few problems. A major issue is the packing of the protein sample and quantification of this packed sample. In the past, RFQ

studies with nitrogenase have yielded some results though have failed to answer any of the major questions regarding electron transfer and substrate reduction in the different E states of nitrogenase.^{21,22} In order to overcome these problems, a novel technique for freeze quenching the nitrogenase enzyme in early time points after mixing was developed.

Viscogen freeze quench: Based on work conducted for chapters two and four of this dissertation we knew that osmolytes/viscogens could be used to slow down the electron transfer event in nitrogenase. We also knew that the addition of viscogens and lowering the temperature did not change the mechanism of electron transfer in nitrogenase. Based on this, a freeze quench technique was developed that takes into account the effect of high viscosity and low temperature in combination. At a temperature of $\sim 4^{\circ}\text{C}$ EPR samples of $\beta\text{-}^{188}\text{Cys}$ MoFe protein were made in highly viscous buffer ($\eta > 8$). A time course analysis was conducted by making individual samples at each time point.

Utilizing VFQ allowed us to study the EPR spectrum of the entire complex which in $\beta\text{-}^{188}\text{Ser-Cys}$ variant of the MoFe protein means being able to study all three clusters of nitrogenase.²³ The electron transfer from the F cluster of the Fe protein to the P cluster of the MoFe protein was thus observed. The resting state FeMo-cofactor EPR signal remained undisturbed during this event (Figure 7-9). If the electron had traveled to the resting state M cluster its signal would have begun to disappear. Instead, the EPR signal of the P cluster changed. The change in the EPR signal of the P cluster was found to be identical to the change in the signal for the Fe protein [4Fe-4S] cluster in the same

samples. This serves as evidence for the electron from the Fe protein being transferred to the P cluster of the MoFe protein in accordance with the deficit spending model.

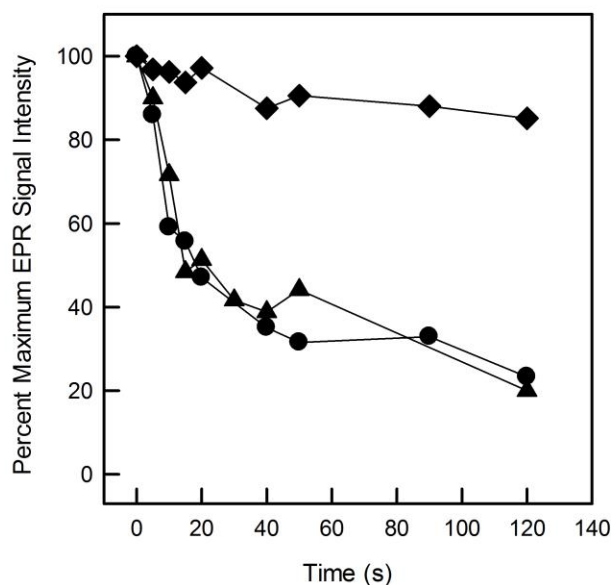


Figure 7-8: Percent maximum EPR signal intensity comparison of P cluster ●, M cluster ◆, and the [4Fe-4S] cluster of the Fe protein ▲. The data shows that the Fe protein oxidation is concurrent with the reduction of the P cluster.

However, since the β -188^{Ser-Cys} variant of the MoFe protein possesses a P^{ox} cluster in the dithionite reduced state, it serves as evidence for electron transfer to an artificially generated P^{ox} cluster. For deficit spending model of electron transfer to be proven, the P^{ox} species would have to be discovered during the primary electron transfer event. VFQ conducted with wild type MoFe protein with a P^N cluster does not show any evidence for a P^{ox} cluster. This is understandable due to the high rate of electron transfer from the F cluster to the P^{ox} cluster. Whereas in the β -188^{Ser-Cys}, with its P^{ox} cluster pre oxidized, binding of the iron protein is rate limiting during a VFQ experiment, in the wild type

protein P^{ox} is generated after the binding of the Fe protein and is thus unaffected by conditions generated due to high viscosity and lower temperature.

This emphasizes the need for further study in understanding the order of the electron transfer events in nitrogenase. Iron protein variants that can trigger the P to M electron transfer without allowing the backfill to P^{ox} are the most attractive avenues of future research since they allow the use of wild type MoFe protein. Variant forms of MoFe protein that are not in immediate vicinity of either the P or the M cluster but have an effect on the electron transfer and substrate reduction behavior e.g. β -98^{Tyr-His}, $\alpha\beta$ -125^{Phe-Ala}, α -281^{Tyr-His} could be good candidates for further exploration.^{18,24}

Exploration of substrate binding and E-states of FeMo-cofactor using VFQ: VFQ is an exciting new development in observing electron transfer to the MoFe protein. MoFe protein goes through eight successive electron transfer states in which it reduces substrates at varying E states (Figure 7-10).²⁵⁻²⁷

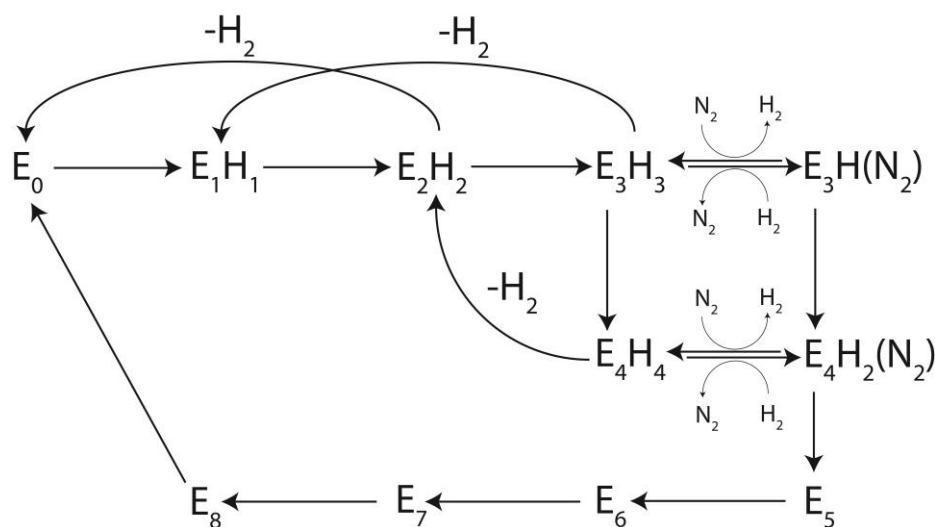


Figure 7-9: Lowe-Thorneley model of electron transfer and substrate binding in nitrogenase. Each successive state of FeMo-cofactor shows an E state.

VFQ can be used to study more than one electron transfer to the MoFe protein. Initial studies for these electron transfer events have already been conducted. Using α - $^{195}\text{His-Gln}$ variant of the MoFe protein, the binding of acetylene to the cofactor has been studied (Figure 7-11)^{28,29}. In Figure 7-11 (A) we can see the resting state (E_0) signal of the MoFe protein disappear over time into E_1 (EPR silent) followed by the $2e^-$ state E_2 in (B) which is identified by its unique EPR signal with this variant of the MoFe protein. Thus, here, VFQ allows us to follow the disappearance of E_0 and appearance of E_2 . The data presented in Figure 7-11(C) show earlier E states during nitrogenase reduction due to the high viscosity of the system. By varying the viscosity of the system, rate of accumulation of latter E states in nitrogenase can be enhanced allowing us to study different trapped states of nitrogenase. VFQ can thus be used to study the N_2 , propargyl alcohol, hydrazine, proton, and methyldiazene trapped states allowing us to map the route of the enzyme to a certain E state.³⁰⁻³³ The technique can further be used to study FeMo-cofactor interactions with multiple substrates. One of the most promising avenue of investigation here is understanding the relationship between N_2 and hydrazine (i.e. are they inhibitory towards each other).

Kinetic Isotope Effect in the Fe Protein cycle

Kinetic assays for the observation of product formation were conducted under H_2O and D_2O as a solvent for the enzyme. A kinetic isotope effect was observed in D_2O . The activity of the enzyme in D_2O dropped to 50% of the activity in H_2O .

In order to determine which step in the Fe protein cycle is affected by the change in solvent, electron transfer, ATP hydrolysis, phosphate release and dissociation of the Fe

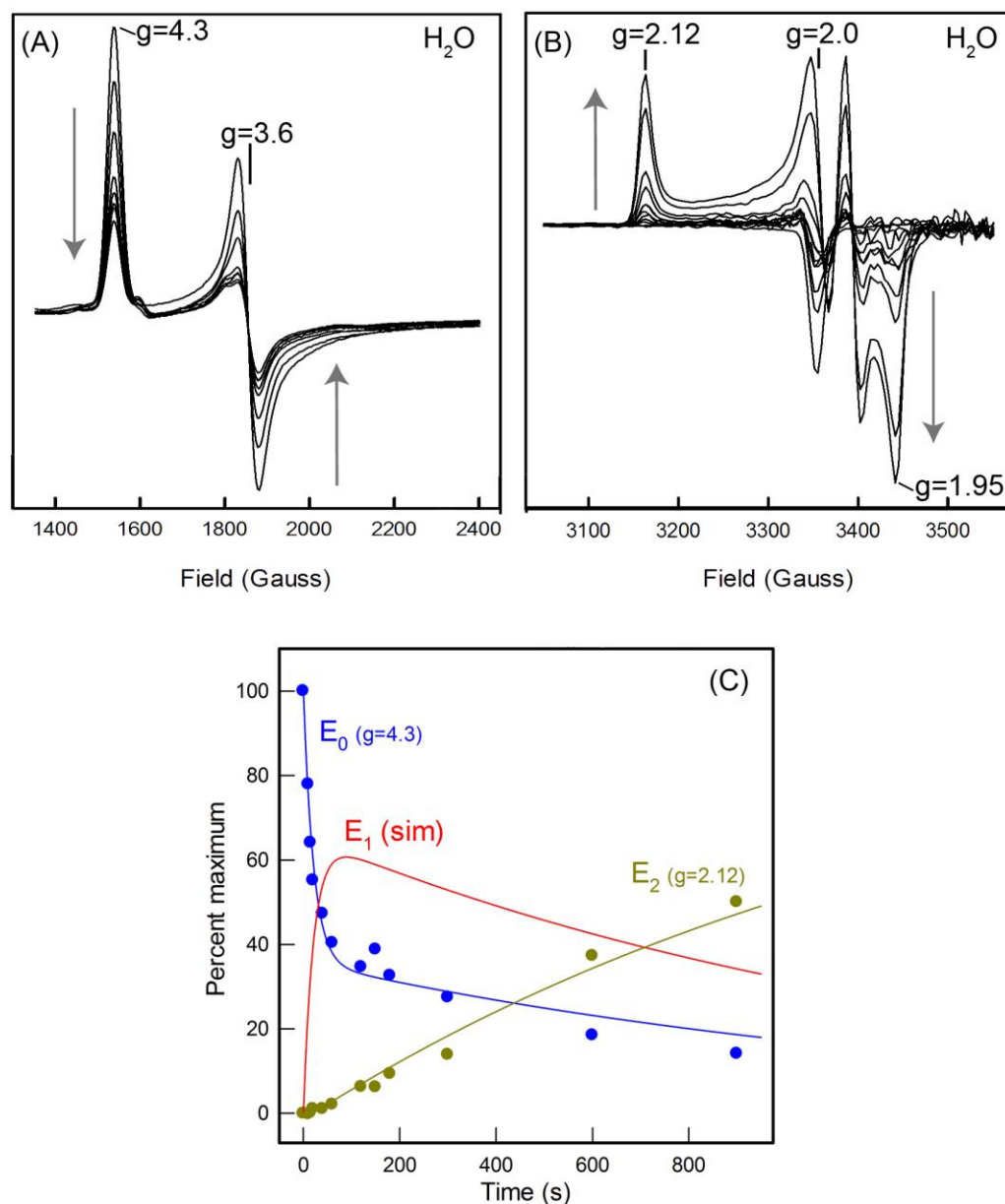


Figure 7-10: VFQ analysis of the early E states in α -195^{Gln} MoFe protein. (A) shows the disappearance of the resting state EPR signal into an EPR silent E₁ state. (B) shows the appearance of the E₂ state (EPR active, acetylene bound) from the EPR silent E₁ state. (C) shows the percent maximum EPR signal of each E state fitted with a sequential model developed in Kintek Global Explorer. The model can be used to simulate the amount of E₁ signal that accumulated between E₀ and E₁.

protein from the MoFe protein was analyzed in D₂O (Figure 7-12). The results of these experiments indicate that the phosphate release event slows down to $\sim 5 \text{ s}^{-1}$ in D₂O from 22 s^{-1} in H₂O. Since the rate of phosphate release in D₂O is nearly identical to the rate of dissociation, which is rate limiting at 6 s^{-1} and is unaffected by D₂O, it is not enough to account for the 50% decrease in rate of substrate reduction. The most likely explanation is that the Fe protein undergoes conformational changes after the release of phosphate but prior to the dissociation of Fe protein and these two steps (i.e. Pi release and dissociation) in combination result in the overall slowing of the enzyme in D₂O.

The use of VFQ in exploring the KIE: VFQ analysis on the accumulation of the acetylene trapped state was conducted with D₂O as a solvent. The kinetics of the first electron transfer event from the Fe protein to the MoFe protein in D₂O were identical to these kinetics in H₂O. However, marked differences were observed in the accumulation of the E₂ (2e⁻ transferred to FeMo-cofactor) state of the cofactor. In D₂O the E₂ state was not observed. After the electron transfer event from the Fe protein to the MoFe protein, ATP hydrolysis, phosphate release and dissociation occur. However, in D₂O, one of these events slows down to where the accumulation of E₂ in D₂O nearly halts (Figure 7-13). The VFQ data, thus, supports the hypothesis presented earlier in that the phosphate release event itself might not be the only step slowing the accumulation of E₂ and that it might be multiple steps that contribute to generate the D₂O effect.

The dissociation event in Figure 7-12 (D) is studied by poisoning the Fe protein in its oxidized state after phosphate release has occurred. The un-dissociated complex is then mixed with dithionite and the dissociation of Fe protein from the MoFe protein is

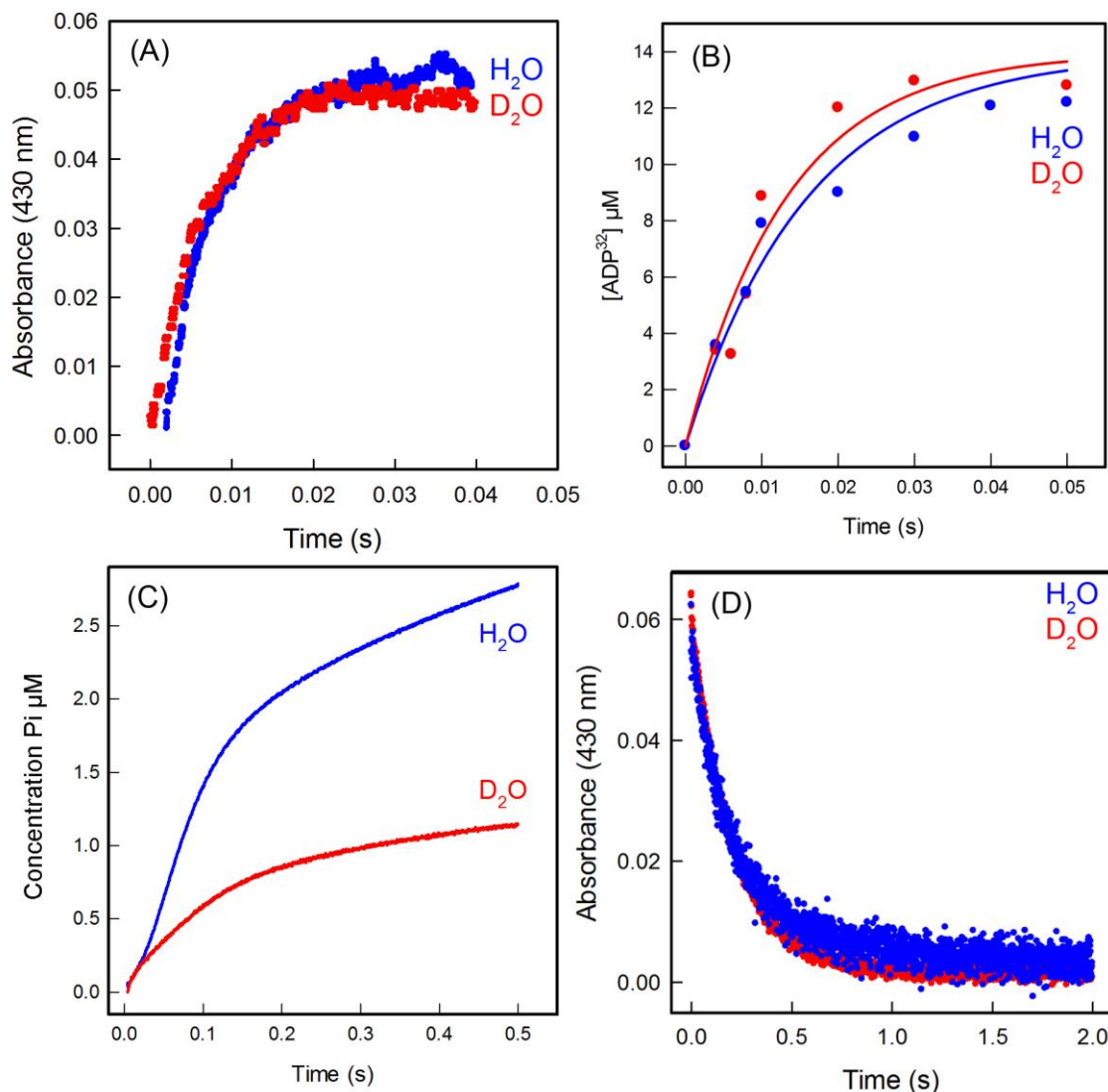


Figure 7-11: Kinetics of key nitrogenase catalytic steps in H₂O and D₂O at 25°C. (A)

The transfer of an electron is monitored as the change in absorbance at 430 nm as a function of time (Blue in H₂O and red in D₂O). (B) ATP hydrolysis is measured by monitoring the formation of α-³²P-ADP as a function of time. The data were fit to the kinetic model described in chapter 5 with a calculated k_{ATP} of $\sim 70 \text{ s}^{-1}$ for both H₂O and D₂O. (C) Phosphate (Pi) release is monitored by the increase in fluorescence from Pi binding to MDCC-PBP as a function of time. (D) Dissociation of Fe from the MoFe protein is monitored by the decrease in absorbance at 430 nm as a function of time.

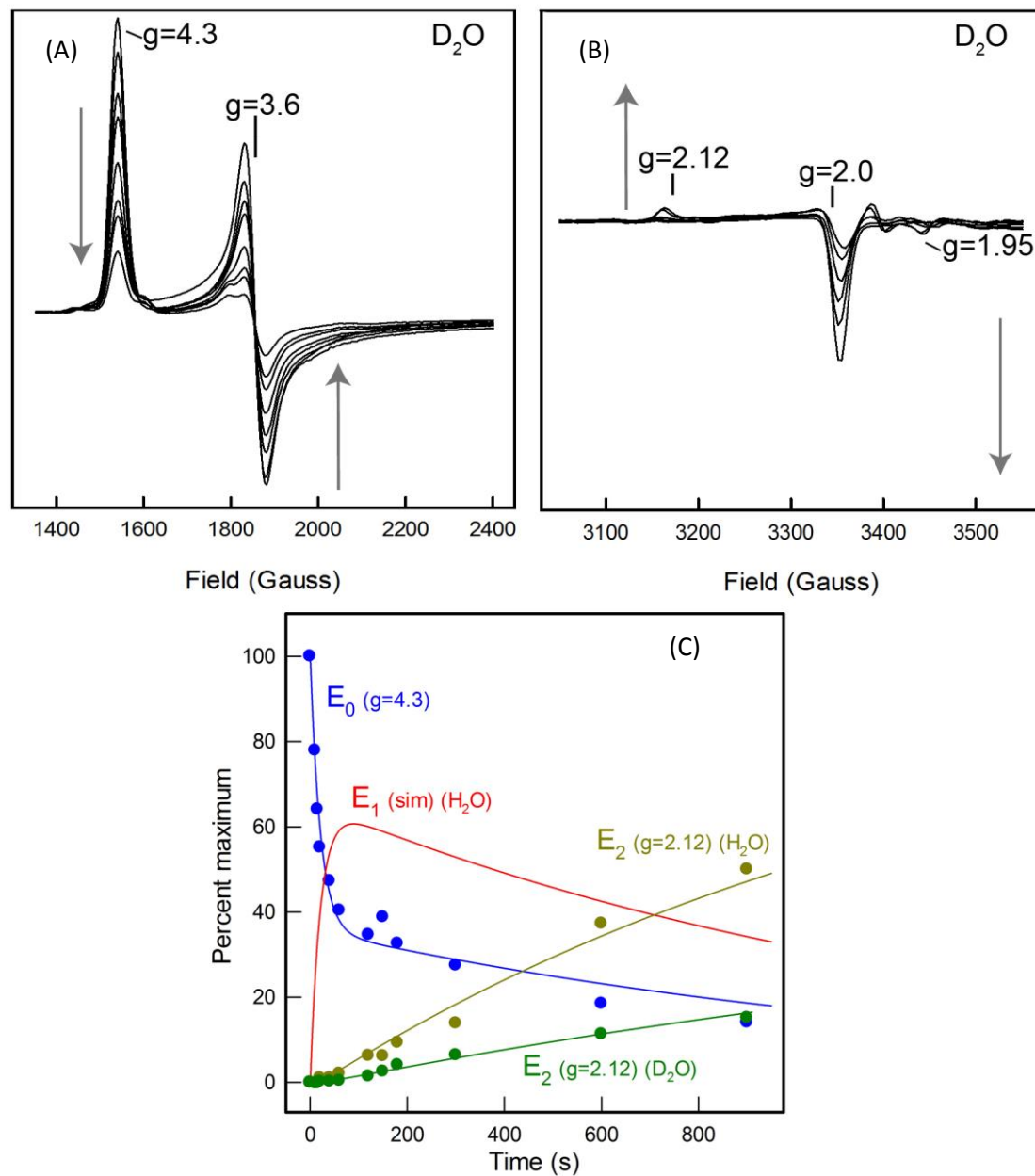


Figure 7-12: VFQ analysis of α -195^{Gln} MoFe protein with acetylene in D_2O . (A) shows the disappearance of the resting state EPR signal into an EPR silent E_1 state. (B) shows the lack of appearance of the E_2 state (EPR active, acetylene bound) from the EPR silent E_1 state. (C) shows the comparison between the E_2 states of H_2O vs. D_2O .

observed. This specific part of the dissociation at the end of a Fe protein cycle is unaffected by D_2O and no current method exists to study real time dissociation of the Fe protein from the MoFe protein (from complex formation to dissociation).

Studying the effect of osmotic pressure in the dissociation event as described earlier could provide an answer regarding the role of conformational changes in this D₂O effect. However, why the phosphate release event from the Fe protein slows down in D₂O remains unknown. Future phosphate release studies by utilizing variant proteins on both the MoFe protein (e.g. β -98^{Tyr-His}, β -188^{Ser-Cys} etc.) and the Fe protein (e.g. variants in the switch I and II region of the Fe protein)^{11,34-36} might be able to provide an insight into the effect of D₂O on the phosphate release event in the Fe protein cycle.

REFERENCES

- (1) Danyal, K., Mayweather, D., Dean, D. R., Seefeldt, L. C., and Hoffman, B. M. (2010) Conformational gating of electron transfer from the nitrogenase Fe protein to MoFe protein. *J. Am. Chem. Soc.* 132, 6894–6895.
- (2) Danyal, K., Dean, D. R., Hoffman, B. M., and Seefeldt, L. C. (2011) Electron transfer within nitrogenase: evidence for a deficit-spending mechanism. *Biochemistry.* 50, 9255–9263.
- (3) Mayweather, D., Danyal, K., Dean, D. R., Seefeldt, L. C., and Hoffman, B. M. (2012) Temperature invariance of the nitrogenase electron transfer mechanism. *Biochemistry* 51, 8391–8398.
- (4) Danyal, K., Inglet, B. S., Vincent, K. A., Barney, B. M., Hoffman, B. M., Armstrong, F. A., Dean, D. R., and Seefeldt, L. C. (2010) Uncoupling nitrogenase: catalytic reduction of hydrazine to ammonia by a MoFe protein in the absence of Fe protein-ATP. *J. Am. Chem. Soc.* 132, 13197–13199.

- (5) Lanzilotta, W. N., Parker, V. D., and Seefeldt, L. C. (1988) Electron Transfer in Nitrogenase Analyzed by Marcus Theory: Evidence for Gating by MgATP. *Biochemistry* 37, 399–407.
- (6) Burgess, B. K., and Lowe, D. J. (1996) Mechanism of molybdenum nitrogenase. *Chem. Rev.* 96, 2983–3012.
- (7) Peters, J. W., Stowell, M. H. B., Soltis, S. M., Finnegan, M. G., Johnson, M. K., and Rees, D. C. (1997) Redox-Dependent Structural Changes in the Nitrogenase P-Cluster. *Biochemistry* 36, 1181–1187.
- (8) Lanzilotta, W. N., Holz, R. C., and Seefeldt, L. C. (1995) Proton NMR investigation of the [4Fe-4S]¹⁺ cluster environment of nitrogenase iron protein from *Azotobacter vinelandii*: defining nucleotide-induced conformational changes. *Biochemistry* 34, 15646–15653.
- (9) Lanzilotta, W. N., Ryle, M. J., and Seefeldt, L. C. (1995) Nucleotide hydrolysis and protein conformational changes in *Azotobacter vinelandii* nitrogenase iron protein: defining the function of aspartate 129. *Biochemistry* 34, 10713–10723.
- (10) Chiu, H.-J., Peters, J. W., Lanzilotta, W. N., Ryle, M. J., Seefeldt, L. C., Howard, J. B., and Rees, D. C. (2001) MgATP-Bound and Nucleotide-Free Structures of a Nitrogenase Protein Complex between the Leu 127 Δ -Fe-Protein and the MoFe-Protein. *Biochemistry* 40, 641–650.
- (11) Igarashi, R. Y., and Seefeldt, L. C. (2003) Nitrogen fixation: the mechanism of the Mo-dependent nitrogenase. *Crit. Rev. Biochem. Mol. Biol.* 38, 351–384.

- (12) Tezcan, F. A., Kaiser, J. T., Mustafi, D., Walton, M. Y., Howard, J. B., and Rees, D. C. (2005) Nitrogenase complexes: multiple docking sites for a nucleotide switch protein. *Science* 309, 1377–1380.
- (13) Schmid, B., Einsle, O., Chiu, H.-J., Willing, A., Yoshida, M., Howard, J. B., and Rees, D. C. (2002) Biochemical and structural characterization of the cross-linked complex of nitrogenase: comparison to the ADP-AlF₄⁻-stabilized structure. *Biochemistry* 41, 15557–15565.
- (14) Shah, V. K., Stacey, G., and Brill, W. J. (1983) Electron transport to nitrogenase. Purification and characterization of pyruvate:flavodoxin oxidoreductase. The *nifJ* gene product. *J. Biol. Chem.* 258, 12064–12068.
- (15) Thorneley, R. N., and Lowe, D. J. (1983) Nitrogenase of *Klebsiella pneumoniae*. Kinetics of the dissociation of oxidized iron protein from molybdenum-iron protein: identification of the rate-limiting step for substrate reduction. *Biochem. J.* 215, 393–403.
- (16) Hageman, R. V., and Burris, R. H. (1978) Nitrogenase and nitrogenase reductase associate and dissociate with each catalytic cycle. *Proc. Natl. Acad. Sci. U.S.A.* 75, 2699–2702.
- (17) Wolle, D., Kim, C., Dean, D., and Howard, J. B. (1992) Ionic interactions in the nitrogenase complex. Properties of Fe-protein containing substitutions for Arg-100. *J. Biol. Chem.* 267, 3667–3673.
- (18) Christiansen, J., Chan, J. M., Seefeldt, L. C., and Dean, D. R. (2000) The role of the MoFe protein α -125Phe and β -125Phe residues in *Azotobacter vinelandii* MoFe protein-Fe protein interaction. *J. Inorg. Biochem.* 80, 195–204.

- (19) Seefeldt, L. C. (1994) Docking of nitrogenase iron-and molybdenum-iron proteins for electron transfer and MgATP hydrolysis: the role of arginine 140 and lysine 143 of the *Azotobacter vinelandii* iron protein. *Protein Sci.* 3, 2073–2081.
- (20) Krebs, C., Edmondson, D. E., and Huynh, B. H. (2002) Demonstration of peroxodiferric intermediate in M-ferritin ferroxidase reaction using rapid freeze-quench Mössbauer, resonance Raman, and XAS spectroscopies. *Meth. Enzymol.* 354, 436–454.
- (21) Fisher, K., Lowe, D. J., Tavares, P., Pereira, A. S., Huynh, B. H., Edmondson, D., and Newton, W. E. (2007) Conformations generated during turnover of the *Azotobacter vinelandii* nitrogenase MoFe protein and their relationship to physiological function. *J. Inorg. Biochem.* 101, 1649–1656.
- (22) Fisher, K., Newton, W. E., and Lowe, D. J. (2001) Electron paramagnetic resonance analysis of different *Azotobacter vinelandii* nitrogenase MoFe-protein conformations generated during enzyme turnover: evidence for $S = 3/2$ spin states from reduced MoFe-protein intermediates. *Biochemistry* 40, 3333–3339.
- (23) Chan, J. M., Christiansen, J., Dean, D. R., and Seefeldt, L. C. (1999) Spectroscopic evidence for changes in the redox state of the nitrogenase P-Cluster during turnover. *Biochemistry* 38, 5779–5785.
- (24) Peters, J. W., Fisher, K., Newton, W. E., and Dean, D. R. (1995) Involvement of the P Cluster in Intramolecular Electron Transfer within the Nitrogenase MoFe Protein. *J. Biol. Chem.* 270, 27007–27013.
- (25) Lowe, D. J., and Thorneley, R. N. (1984) The mechanism of *Klebsiella pneumoniae* nitrogenase action. The determination of rate constants required for the simulation of the kinetics of N_2 reduction and H_2 evolution. *Biochem. J.* 224, 895–901.

- (26) Thorneley, R. N., and Lowe, D. J. (1984) The mechanism of *Klebsiella pneumoniae* nitrogenase action. Simulation of the dependences of H₂-evolution rate on component-protein concentration and ratio and sodium dithionite concentration. *Biochem. J.* 224, 903–909.
- (27) Lowe, D. J., and Thorneley, R. N. (1984) The mechanism of *Klebsiella pneumoniae* nitrogenase action. Pre-steady-state kinetics of H₂ formation. *Biochem. J.* 224, 877–886.
- (28) Lee, H. I., Sørli, M., Christiansen, J., Song, R. T., Dean, D. R., Hales, B. J., and Hoffman, B. M. (2000) Characterization of an intermediate in the reduction of acetylene by the nitrogenase α -Gln¹⁹⁵ MoFe protein by Q-band EPR and ¹³C, ¹H ENDOR. *J. Am. Chem. Soc.* 122, 5582–5587.
- (29) Lee, H.-I., Sørli, M., Christiansen, J., Yang, T.-C., Shao, J., Dean, D. R., Hales, B. J., and Hoffman, B. M. (2005) Electron inventory, kinetic assignment (E_n), structure, and bonding of nitrogenase turnover intermediates with C₂H₂ and CO. *J. Am. Chem. Soc.* 127, 15880–15890.
- (30) Maskos, Z., Fisher, K., Sørli, M., Newton, W. E., and Hales, B. J. (2005) Variant MoFe proteins of *Azotobacter vinelandii*: effects of carbon monoxide on electron paramagnetic resonance spectra generated during enzyme turnover. *J. Biol. Inorg. Chem.* 10, 394–406.
- (31) Barney, B. M., Laryukhin, M., Igarashi, R. Y., Lee, H.-I., Dos Santos, P. C., Yang, T.-C., Hoffman, B. M., Dean, D. R., and Seefeldt, L. C. (2005) Trapping a hydrazine reduction intermediate on the nitrogenase active site. *Biochemistry* 44, 8030–8037.

- (32) Barney, B. M., Lukoyanov, D., Igarashi, R. Y., Laryukhin, M., Yang, T.-C., Dean, D. R., Hoffman, B. M., and Seefeldt, L. C. (2009) Trapping an intermediate of dinitrogen (N_2) reduction on nitrogenase. *Biochemistry* 48, 9094–9102.
- (33) Benton, P. M. C., Laryukhin, M., Mayer, S. M., Hoffman, B. M., Dean, D. R., and Seefeldt, L. C. (2003) Localization of a substrate binding site on the FeMo-cofactor in nitrogenase: trapping propargyl alcohol with an alpha-70-substituted MoFe protein. *Biochemistry* 42, 9102–9109.
- (34) Chiu, H.-J., Peters, J. W., Lanzilotta, W. N., Ryle, M. J., Seefeldt, L. C., Howard, J. B., and Rees, D. C. (2001) MgATP-bound and nucleotide-free structures of a nitrogenase protein complex between the Leu 127 Δ -Fe-protein and the MoFe-protein. *Biochemistry* 40, 641–650.
- (35) Lanzilotta, W. N., and Seefeldt, L. C. (1997) Changes in the midpoint potentials of the nitrogenase metal centers as a result of iron protein–molybdenum-iron protein complex formation. *Biochemistry* 36, 12976–12983.
- (36) Seefeldt, L. C., Morgan, T. V., Dean, D. R., and Mortenson, L. E. (1992) Mapping the site(s) of MgATP and MgADP interaction with the nitrogenase of *Azotobacter vinelandii*. Lysine 15 of the iron protein plays a major role in MgATP interaction. *J. Biol. Chem.* 267, 6680–6688.

APPENDIX



Karamatullah Danyal < danyal1980@gmail.com >

Request to reuse book chapter for my dissertation

Permissions Europe/NL < Permissions.Dordrecht@springer.com >

Thu, Jun 27, 2013 at 1:27 AM

To: Danyal <danyal1980@gmail.com>

Dear Sir/Madam,

With reference to your request to reprint material in which Springer Science and Business Media control the copyright, our permission is granted free of charge and at the following conditions:

Springer material

- represents original material which does not carry references to other sources (if material in question refers with a credit to another source, authorization from that source is required as well);
- requires full credit [Springer and the original publisher/journal title, volume, year of publication, page, chapter/article title, name(s) of author(s), figure number(s), original copyright notice] to the publication in which the material was originally published, by adding; with kind permission from Springer Science+Business Media B.V.;
- may not be altered in any manner. Abbreviations, additions, deletions and/or any other alterations shall be made only with prior written authorization of the author and/or Springer Science + Business Media.
- may not be republished in Electronic Open Access.

This permission

- a. is non-exclusive.
- b. includes use in an electronic form: provided it's password protected, or on intranet or university's repository, including UMI (according to the definition at the Sherpa website: <http://www.sherpa.ac.uk/romeo/>), or CD-Rom/E-book,
- c. is subject to a courtesy information to the author (address is given with the article/chapter).
- d. is personal to you and may not be sublicensed, assigned, or transferred by you to any other person without Springer's written permission.
- e. is valid only when the conditions noted above are met.

Permission free of charge on this occasion does not prejudice any rights we might have to charge for reproduction of our copyrighted material in the future.

Best regards,

Kind regards,

Nel van der Werf (Ms)
Rights and Permissions/Springer

Van Godewijkstraat 30 | P.O. Box 17
3300 AA Dordrecht | The Netherlands
tel +31 (0) 78 6576 298
fax +31 (0)78 65 76-377

Nel.vanderwerf@springer.com
www.springer.com

American Chemical Society's Policy on Theses and Dissertations

If your university requires you to obtain permission, you must use the RightsLink permission system. See RightsLink instructions at <http://pubs.acs.org/page/copyright/permissions.html>.

This is regarding request for permission to include **your** paper(s) or portions of text from **your** paper(s) in your thesis. Permission is now automatically granted; please pay special attention to the **implications** paragraph below. The Copyright Subcommittee of the Joint Board/Council Committees on Publications approved the following:

Copyright permission for published and submitted material from theses and dissertations

ACS extends blanket permission to students to include in their theses and dissertations their own articles, or portions thereof, that have been published in ACS journals or submitted to ACS journals for publication, provided that the ACS copyright credit line is noted on the appropriate page(s).

Publishing implications of electronic publication of theses and dissertation material

Students and their mentors should be aware that posting of theses and dissertation material on the Web prior to submission of material from that thesis or dissertation to an ACS journal may affect publication in that journal. Whether Web posting is considered prior publication may be evaluated on a case-by-case basis by the journal's editor. If an ACS journal editor considers Web posting to be "prior publication", the paper will not be accepted for publication in that journal. If you intend to submit your unpublished paper to ACS for publication, check with the appropriate editor prior to posting your manuscript electronically.

Reuse/Republishing of the Entire Work in Theses or Collections: Authors may reuse all or part of the Submitted, Accepted or Published Work in a thesis or dissertation that the author writes and is required to satisfy the criteria of degree-granting institutions. Such reuse is permitted subject to the ACS' "Ethical Guidelines to Publication of Chemical Research" (<http://pubs.acs.org/page/policy/ethics/index.html>); the author should secure written confirmation (via letter or email) from the respective ACS journal editor(s) to avoid potential conflicts with journal prior publication*/embargo policies. Appropriate citation of the Published Work must be made. If the thesis or dissertation to be published is in electronic format, a direct link to the Published Work must also be included using the ACS Articles on Request author-directed link – see <http://pubs.acs.org/page/policy/articlesonrequest/index.html>

* Prior publication policies of ACS journals are posted on the ACS website at <http://pubs.acs.org/page/policy/prior/index.html>

If your paper has **not** yet been published by ACS, please print the following credit line on the first page of your article: "Reproduced (or 'Reproduced in part') with permission from [JOURNAL NAME], in press (or 'submitted for publication'). Unpublished work copyright [CURRENT YEAR] American Chemical Society." Include appropriate information.

If your paper has already been published by ACS and you want to include the text or portions of the text in your thesis/dissertation, please print the ACS copyright credit line on the first page of your article: "Reproduced (or 'Reproduced in part') with permission from [FULL REFERENCE CITATION.] Copyright [YEAR] American Chemical Society." Include appropriate information.

Submission to a Dissertation Distributor: If you plan to submit your thesis to UMI or to another dissertation distributor, you should not include the unpublished ACS paper in your thesis if the thesis will be disseminated electronically, until ACS has published your paper. After publication of the paper by ACS, you may release the entire thesis (**not the individual ACS article by itself**) for electronic dissemination through the distributor; ACS's copyright credit line should be printed on the first page of the ACS paper.

CURRICULUM VITAE

Karamatullah Danyal

Department of Chemistry and Biochemistry
Utah State University
0300 Old Main Hill
Logan, UT 84322
690-9433

Work Phone: (435) 797-7392

Cell Phone: (208)

Education

Bachelor of Science in Chemistry and Biochemistry with a minor in English, Idaho State University, Pocatello, ID. Degree received May 2006. Cumulative GPA of 3.33

Associate of Science in Physics, Idaho State University, Pocatello, ID. Degree received May 2006. Cumulative GPA of 3.45

Research Experience

Research Assistant, Department of Chemistry and Biochemistry, Utah State University, Logan, UT. June 2009-Present.

Research Assistant/Teaching Assistant, Department of Chemistry and Biochemistry, Utah State University, Logan, UT. June 2006-2009.

Undergraduate Student Research, Department of Chemistry, Idaho State University, Pocatello, ID. January 2004-May 2006.

Undergraduate Student Research, Department of Biological Sciences, Idaho State University, Pocatello, ID. June 2002-December 2003.

Core Qualifications

Highly qualified with protein purification aerobically and anaerobically.

Experienced in activity assays utilizing various forms of product detection as well as spectrophotometric, fluorometric and spectroscopic methods for measurement of activity in both pre-steady state and steady state of the enzyme.

Understand the principle of molecular biology, including PCR, DNA analysis, expression vector construction and bacterial transformation

Highly experienced in bacterial growth and harvest methodologies.

Proficient in understanding and writing scientific literature

Proficient with the Microsoft Office Suite, IGOR Pro, Sigmaplot, KinTek explorer, Adobe creative Suite, and Pymol molecular visualizing system.

Professional Membership

Member of the American Chemical Society 2008-Present.

Awards and Honors

Journal of Heterocyclic Chemistry Undergraduate Research Grant 2005-2006.

World Cultures Celebration Outstanding Achievement Award 2005.

Pattie Family Scholarship 2005.

Biological Sciences Scholarship 2005.

Chemistry department Alumni Endowment Award 2003.

Teaching Experience

Teaching assistant for General, Organic and Biochemistry laboratory. Utah State University. Logan, UT. January 2007-May 2009

Presentations

Danyal, K. Keable, S. Inglet, B. Zadvornyy, O. Vincent, K. Peters, J. W. Dean, D.R. Hoffman, B.M. Seefeldt, L.C. Substrate reduction in nitrogenase using β -98^{His} variant of the MoFe protein in the absence of Fe protein and ATP. Poster Gordon Research Conference. June 2010.

Danyal, K. Barney, B.M. Lukoyanov, D. Dean, D.R. Hoffman, B.M. Seefeldt, L.C. Observing internal electron transfer in nitrogenase. Poster Gordon Research Conference. June 2010.

Danyal, K. Barney, B.M. Lukoyanov, D. Dean, D.R. Hoffman, B.M. Seefeldt, L.C. Observing internal electron transfer in nitrogenase. Poster 16th International Congress for Nitrogen Fixation. May 2009.

Danyal, K. Bateman, J. Rodriguez, R. Pak, J. Measurement of Emission Lifetimes of Ruthenium (II) Complexes for use in Solar Cell Research. Poster 61st Northwest Regional American Chemical Society meeting, June 2006

Danyal, K. Bateman, J. Rodriguez, R. Pak, J. Measurement of Emission Lifetimes of Ruthenium (II) Complexes Using Software developed in LabVIEW 7.0. Poster AMIS-ISU Research Symposium, AMIS Pocatello ID 2005.

Danyal, K. Kemper, B. Smith, R. Behavior of Small Male Beetles (*Nicrophorus*) In Mating with Females. Poster Idaho State University Undergraduate Research Symposium, Pocatello, ID, 2003.

Publications

Danyal, K. Mayweather, D. Dean, D.R. Seefeldt, L.C. Hoffman, B.M. Conformational Gating of Electron transfer from the Nitrogenase Fe protein to MoFe protein. *Journal of American Chemical Society*. (2010). **132** Pages 6894-6895.

Danyal, K. Inglet, B.S. Vincent, K.A. Barney, B.M. Hoffman, B.M. Armstrong, F.A. Dean, D.R. Seefeldt, L.C. Uncoupling Nitrogenase: Catalytic reduction of hydrazine to ammonia by a MoFe protein in the absence of Fe protein-ATP. *Journal of American Chemical Society*. (2010). **132** Pages 13197-13199.

Danyal, K. Dean, D.R. Hoffman, B. M. Seefeldt, L.C. Electron transfer within nitrogenase: Evidence of a deficit spending model. *Biochemistry*. (2011). **50** Pages 9255-9263.

Danyal, K. Yang, Z. Seefeldt, L.C. Mechanism of Mo-dependent nitrogenase. *Methods in Molecular Biology*. (2011). **766** Pages 9-29.

Yang, Z. Danyal, K. Seefeldt, L.C. Electron paramagnetic resonance spectroscopy. *Methods in Molecular Biology*. (2011). **766** Pages 191-205.

Mayweather, D. Danyal, K. Dean, D.R. Hoffman, B. M. Seefeldt, L.C. Temperature invariance of the nitrogenase electron transfer mechanism. *Biochemistry*. (2012). **51** Pages 8391-8398.

Moure, V. R. Danyal, K. Yang, Z. Wendroth, S. Muller-Santos, M. Pedrosa, F. O. Scarduelli, M. Gerhardt, E. C. M. Huerge, L. F. Souza, E. M. Seefeldt, L.C. The nitrogenase regulatory enzyme

dinitrogenase reductase ADP-Ribosyltransferase (DraT) is activated by direct interaction with the signal transduction protein GlnB. *Journal of Bacteriology*. (2013). **195** Pages 279-286.